AN INVESTIGATION OF THE RADIATING CHARACTERISTICS OF AN ELECTROMAGNETIC HORN

ROBERT E. LEE
EARL DEROHAN BARONDES

AN INVESTIGATION OF THE RADIATING CHARACTERISTICS OF AN ELECTROMAGNETIC HORN

by

Robert E. Lee
Lieutenant Junior Grade, U.S.Navy
B.S., U.S. Naval Academy, 1946

Earl de Rohan Barondes
Lieutenant Junior Grade, U.S.Navy
B.S., U.S. Naval Academy, 1947

Submitted in partial fulfillment of the
requirements for the degree of
NAVAL ENGINEER
from the
MASSACHUSETTS INSTITUTE OF TECHNOLOGY
(1952)

ABSTRACT

Title of Thesis: An Investigation of the Radiating Characteristics of an Electromagnetic Horn

Names of Authors: Karl de Rohan Barondes, LTJG, USN

Robert Earl Lee, LTJG, USN

Submitted to the Department of Naval Architecture and Marine Engineering on 16 May, 1952 in partial fulfillment of the requirements for the degree of Naval Engineer.

The radiating and impedance characteristics of a laterally radiating X band electromagnetic horn were investigated. The horn has a flare angle of 90 degrees in the H plane and at a radius of 37.8 cm. it is bent through 90degrees to form an aperture in the shape of a quadrantal arc. The aperture has a chord length of 16.7 λ at λ = 3.2 cm.

Experimental results verified computed field patterns and indicated that a constant phase was obtained across the aperture. Illumination was considered to be the distribution of the $H_{1,0}$ mode across the aperture.

The pattern of the uncompensated horn is elliptically polarized. In the H plane the E plane polarization has a beam width of 4.3 degrees and first side lobe level is 21 db. down at λ = 3.2 cm. The H plane polarization gives two main lobes 12 db. down from the E plane polarization.

Impedance measurements indicate reflection coefficients, due to reflection at the throat and at the aperture of the horn. Reflection at the 90 degree bend appears to be negligible. Representative values are Γ_t = 0.0726, Γ_a = 0.159. Should reflection at the throat be eliminated by a curved transition a VSWR = 1.38 over a band of 200 mcs. is obtainable.

To eliminate the cross polarization due to H plane polarization various schemes were tried. E plane flare was added. This combined with a paralled plate filter at the aperture reduced tho cross polarization 20 db. VSWR less than 1.50 over a 675 mcs. band, with elimination of the throat reflection, were obtained.

Other schemes tried included adding a parallel plane filter with no flare and using E plane flare and a parallel wire filter. Cross polarization was reduced in all cases.

It is concluded that this type horn provides a constant phase illumination across a wide aperture resulting in a narrow beam with reasonably low side lobes. The cross components of polarization inherent in the design may be eliminated by mode filters. The impedance characteristics may be improved by designing for mutual cancellation of reflections in the frequency band desired.

ABSTRACT

Title of Thesis: An Investigation of the Radiating Characteristics of an Electromagnetic Horn

Name of Author: Carl de Loose Bernard, USN

Thesis Aid Dec, 1959, USN

Submitted to the Department of Naval Architecture and Marine Engineering on 15 May, 1959 in partial fulfillment of the requirements for the degree of Naval Engineer.

The radiation and transverse characteristics of a laterally radiating X band electromagnetic horn were investigated. The horn has a flare angle of 90 degrees in the H plane and a radius of 37.8 cm. It is best thought of as being made up of a quadrant of a conical horn. The aperture has a mean length of 10.7 λ at λ = 3.2 cm.

Experimental results verified computed field patterns and indicated that a Gaussian phase was obtained across the aperture. Illumination was considered to be the distribution of the E_{10} mode across the aperture.

The pattern of the wave-guide fed horn is slightly polarized in the E plane and 1 plane polarization has a beam width of 41.3 degrees and first side lobe level is 21 db. down at λ = 32° cm. The H plane polarization gives two main lobes 12 db. down from the E plane polarization.

Experimental measurements indicate reflection coefficients, due to reflection at the input and at the aperture of the horn. Reflection at the 90 degree bend appears to be negligible. Experimental values are Γ_i = 0.0756, Γ_o = 0.239. Double reflection in the throat is eliminated by a curved transition a throat = 1.20 over a band of 800 mcs. is obtainable.

To eliminate the cross polarization due to E plane polarization various schemes were tried. A plane flare was added. This combined with a parallel plate flare at the aperture reduced the cross polarization 20 db. This was then 140 over a 6% band, until, with elimination of the throat reflection, more obtained.

Other schemes tried included adding a parallel plane flare with an Elare rod (strip) and a plane flare with a parallel wire flare. These reflections were reduced to all cases.

It is concluded that this type horn provides a constant phase illumination across a wide aperture resulting in a narrow beam with reasonably low side lobes. The beam consists of reasonably low cross polarization in the design may be minimized by designing for minimum combination of reflections to the frequency band desired.

Cambridge, Massachusetts
16 May 1952

Professor J. S. Newell
Secretary of the Faculty
Massachusetts Institute of Technology
Cambridge, Massachusetts

Dear Sir:

In accordance with the requirements for the Degree of Naval Engineer, we submit herewith a thesis entitled "An Investigation of the Radiating Characteristics of an Electromagnetic Horn."

Respectfully,

Robert E. Lee
Lieutenant Junior Grade
U.S. Navy

Earl de Rohan Barondes
Lieutenant Junior Grade
U.S. Navy

Cambridge, Massachusetts
14 May 1952

Professor J. D. Merrill
Secretary of the Faculty
Massachusetts Institute of Technology
Cambridge, Massachusetts

Dear Sir:

In accordance with the requirements for the Degree of Naval Engineer, we submit herewith a thesis entitled "An Investigation of the Resistance Characteristics of a Destroyer Hull Form."

Respectfully,

Nelson E. Lee
Lieutenant (Junior Grade)
U.S. Navy

Earl de Bono Hammond
Lieutenant (Junior Grade)
U.S. Navy

ACKNOWLEDGEMENTS

The authors of this thesis are principally indebted to Dr. L. J. Chu for the initial inspiration and advice given during the thesis investigation. In addition the authors are indebted to the engineers and technical personnel of the Air Force Cambridge Research Center for their aid in the experimental phase of the thesis. To the personnel of the Coppersmith's Shop of the Boston Naval Shipyard for the excellent job of fabricating the horn and flare section, and to the personnel of Project Meteor who permitted us to use their impedance measuring equipment.

The authors of this thesis are particularly indebted to Dr. L. J. Chu for the initial inspiration and advice given during the thesis investigation. In addition, the authors are indebted to the equipment and technical personnel of the Air Force Cambridge Research Center for their aid in the experimental phase of the thesis. To the personnel of the Computation Unit of the Boston Naval Shipyard for the unselfish job of interpreting the long and flare sections, and to the personnel of Project Vesper who permitted us to use their impedance measuring equipment.

CONTENTS

Contents

SYMBOLS

a — The radius of the mean circular bend on the laterally radiating horn, type "A."

A — The percentage area covered by a parallel wire screen. $(100\ \frac{v-d}{v})$

$A(n,\phi_o)$ — A coefficient in the Fourier-Bessel series method of field computations. It is defined by Formula (A-52).

b — The short dimension of the inner surface of a rectangular waveguide.

b_1 — The inner bend radius of the inner surface of the type "A" horn.

$B(n,\phi)$ — A coefficient in the Fourier-Bessel series method of field computations. It is defined by Formula (A-55).

B_i — The maximum magnitude of the H_{10}th harmonic at the aperture.

c — The outer bend radius of the inner surface of the type "A" horn.

$C(n,\phi_o)$ — A coefficient in the Fourier-Bessel series method of field computations. It is defined by formula (A-58).

d — The diameter of a wire in the parallel wire filter.

d_1 — The distance along the mean arc of the bend of the type "A" horn.

$D(n,\phi)$ — A coefficient in the Fourier-Bessel series method of field computations. It is defined by Formula (A-59).

e — The shorter dimension of the inner surface of the waveguide

E — Electric field strength

E_x — The x component of the electric field strength.

E_y — The y component of electric field strength

f — The longer dimension of the inner surface of a rectangular waveguide.

CONTENTS

$G(\theta)$	The E plane field pattern of an E plane flared sectoral horn determined by theory or by experimental investigation
H	A Hankel function.
j	$\sqrt{-1}$
k	The free space wave propagation constant.
k_1	A design constant used in the design of the type "A" horn.
M	A substitute variable defined by Equation (42) to facilitate algebraic manipulation.
M_1	Area excluded from the E plane array factor integration.
n	Any integral numerical value.
N_1	Area included in the E plane array factor integration.
N_x	A diffraction integral defined by Equation (A-4).
N_y	A diffraction integral defined by Equation (A-5).
P,p	A point of field measurement.
r'	The distance from the origin of the coordinates to a point on the radiating aperture.
r_1	The radial distance from the origin of the coordinates to the inner radius of the aperture.
r_2	The radial distance from the origin of the coordinates to the outer radius of the aperture.
Δr	The radial aperture distance
R	The distance from the origin of the coordinates to a point of field measurement.
s	Refers to the aperture surface.
t	The dimension of the parallel plane filter sections in the direction of wave propagation.

C(9) The 2 plane final mapping of a plane Cayley quartic
determined by means of the geometrical investigation

A A double Quartic.

J $\sqrt{-1}$

K The four-point vane parameter (λ).

L^2 A double resultant used in the design of the Type 'A' beam.

M A modulation variable defined by Equation (4_2) in Professor
Allpress' publication.

M_1 Area enclosed from the 2 plane cubic Cayley hypocycloid.

N Any integral algebraic value.

N_1 Area contained in one 6-plane cusp Cayley hypocycloid.

P^2 A differential integral defined by Equation $(A-1)$.

P_1^2 A differential integral defined by Equation (1_1).

$P_1 p$ A point of Pascal-construction.

q_1 The distance from the origin of the co-ordinates to a point on
the radiating generator.

r^2 The radial distance from the origin of the coordinates to any
other radius of the locomotive.

R^2 The radial distance from the origin of the coordinates to
another position of the locomotive.

R_1^2 The radial distance from the origin of the coordinates to the
first position of the locomotive.

S The distance from the origin of the coordinates to a point of
Pascal-construction.

S_1 Refers to the crossing rivets.

S_2 The distance of the resultant radial fixing rivet from the
direction of wave propagation.

T	The power transmitted through a filter grating in per cent.
v	The center to center spacing of parallel wires or parallel planes.
x	The coordinate direction in the E plane and normal to the H plane.
X'	The coordinate direction in the E plane and on the plane which contains the aperture surface.
$\Delta x'$	The aperture distance in the x' direction
x_o	The aperture distance in the x direction.
y	The coordinate direction in the H plane, normal to the E plane and defined by Figure II.
y_o	Half the distance along the cord of the arc of the aperture. (Figure IV).
y'	The coordinate direction in the H plane, on the plane which contains the aperture surface, and defined by Figure IV.
z	The coordinate direction normal to both x and y, and forms a right handed orthogonal coordinate system of sequence, (x,y,z).
α	The attenuation constant.
β	The angle of the major axis of elliptical polarization from the ϕ direction.
Γ	The reflection coefficient.
Δ	An incremental quantity.
δ	A differential quantity
ε	The base of natural logarithms.
θ	The polar angle from the z axis.
λ	Free space wavelength.
μ	The permeability of free space.

The parallelogram rule for addition.

Type equal vectors.

The polar angle from Ay to AB.

The base of natural logarithms.

A distributive quality.

Is increased equality.

The multiplication sign.

The angle at one apex with all sides produced from the
first diverging.

The difference between $(x+y)^2$ and those of
right-lined triangular geometric figures as squares' (x^2+y^2).

The alternative operator.

The locus of the point P such that $PA^2 + PB^2$ and those of
similar figures with corresponding sides (x^2+y^2).

The operation distributed across $(x+y)$ and those of
similar figures with corresponding sides (x^2+y^2).

The operation of $(x+y)$ and those of similar figures with
corresponding sides (x^2+y^2).

The operation distributed to the $(x+y)$ and those of similar figures
and defined by Figure II.

Half the distance along the line of the $(x+y)$ and those of similar figures.
(Figure IV).

The operation distributed to the $(x+y)$ and those of similar figures
including the operation symbol, not defined by Figure IV.

The coordinate distributed across $(x+y)$ and those of
right-lined triangular geometric figures as squares' (x^2+y^2).

The alternative operator.

The angle at one apex with all sides produced from the
first diverging.

The multiplication sign.

Is increased equality.

A distributive quality.

The base of natural logarithms.

The polar angle from Ay to AB.

Type equal vectors.

The parallelogram rule for addition.

π	3.1416.
ρ	The length of a sectoral horn.
$\sum$	Summation.
ϕ	The longitudinal angle which has the x axis as the origin.
ϕ'	The longitudinal angle for points in the xy or aperture plane.
ϕ_o	The total flare angle of either type "A" or type "B" horns.
ω	2π (frequency)

I INTRODUCTION

Concurrent with the practical employment of microwave frequencies, extensive theoretical and experimental work has been accomplished in the field of using electromagnetic horns as antennas.[4] The theoretical computations indicate that narrow beam sectoral horns may be constructed by increasing the flare angle and the radius. In the theoretical part of this work the aperture diffraction method of computing radiation fields is currently the most practical procedure.[1][2][3] If it were possible to determine the current distribution on the interior and exterior surfaces of the horn, the fields could be computed directly; but since this is not known, the aperture diffraction field method must be employed. However, when the computed radiation patterns of sectoral horns are compared with the radiation patterns obtained experimentally, there is only general agreement. There are three reasons for the disagreement in detail in the field patterns:

1. The theory neglects the current on the outside walls of the horn.
2. The theory neglects the higher mode fields at the aperture.
3. Phase error effects have been neglected in the field computations. The aperture was considered to be a constant phase radiating surface in a plane.

Phase error effects cause the main lobe of a horn of constant flare angle to undergo changes in width and structure as the horn length is increased.[4][5] On the basis of experiments, optimum dimensions for E plane and H plane electromagnetic horns have been determined.

I INTRODUCTION

See Figure VIII.[6]

In order to obtain a narrow beam horn antenna with moderate side lobes, it is necessary to resort to excessively long radius sectoral horns of small flare angles or to employ dielectric lenses or metal plate lenses. However, dielectric lenses complicate the impedance matching problems and cause power loss,[7] and metal plate lenses are frequency sensitive devices.[8] Thus, in order to obtain a narrow beam electromagnetic horn with low side lobes it is necessary to compromise one of the three advantages of horn antennas; small theoretical size, minor matching problems with low power loss, and wide band operation.

It is the object of this thesis to build an antenna with a constant phase radiating surface, experimentally and theoretically determine its radiating characteristics, experimentally determine its impedance characteristics, investigate methods of pattern improvement, and present a design procedure for other investigators to follow. The horn will be designed to be as insensitive to frequency changes as is possible and to suppress higher mode fields before they arrive at the aperture.

This could be accomplished by employing an antenna of design type "A," Figure I or design type "B" Figure V. These antennas employ the optical principle that electromagnetic waves emanating from a point source have a constant phase front which is determined by equal geodesic distances (or mean path distances) measured in a radial direction from the point source.

It is apparent that the radiating surface is no longer rectangular in shape as in the case of the rectangular guide sectoral

one Figure XIII.(4)

In order to obtain a picture that will enhance this defect, it is necessary to record only radiations of small wave length or to employ ultraviolet lenses or metal plate lenses. However, ultraviolet lenses complicate the technique considerably, and metal plate lenses [illegible] [illegible] [illegible]

horn, but is now a circular arc. This introduces difficulties in solving the aperture diffraction integrals and handling the cross components (H plane components) of polarization. In the process of solving the phase difficulty and minimizing surface current effects and higher mode field effects, the problem of cross polarization has been created.

II PROCEDURE

Development of Theoretical Field Pattern Expressions

The aperture of the laterally radiating electromagnetic horn is formed along the arc of a circle. An assumption was made that the field will vary sinusoidally over the arc of the aperture and that the fields are polarized in the radial direction. It was now possible to solve the aperture diffraction integrals to obtain the fields in space. The array factor describing the aperture geometry and illumination could be easily integrated for angles of flare of the form $\frac{\pi}{n}$, n an integer. A change of variable was made which had the effect of considering the straight line equivalent of the aperture. The results for the horn design in Figure V are:*

$$E_x a + 0.00728 \frac{\text{Sin } (ky_o \text{ Sin } \theta)}{\text{Sin}^3 \theta} - 0.038 \frac{\text{Cos } (ky_o \text{ Sin } \theta)}{\text{Sin}^2 \theta} \qquad (1)$$

An assumption of a linear equivalent source in the H plane was made to obtain an approximate field pattern for the E plane polarized, H plane field pattern for any value of r_{av} or ϕ_o. If the linear equivalent source in the H plane is assumed to have an E plane polarized field of

$$E_{sx} = B_1 \text{ Cos } \frac{\pi y}{2y_o} \text{ Cos } \frac{\phi_o y}{2y_o} \qquad (2)$$

which would be the approximate fields resulting when the fields in the aperture were projected into the H plane, (See Figure IV for the definition of geometrical terms.), the resulting H plane field pattern was

---

* See Appendix, Section B.

2. Solutions

Determination of Integration Constants Graphically

The equations of the 2-dimensional radially electromagnetic wave in ferrous plane are of a complex. It is necessary to find the field with easy mathematically over the air of the equations and that the fields are polarized in the radial direction. It was one possible to solve the equations differential integrally to obtain the fields in space. The first factor determining the operator property and attenuation would be easily interpreted for square of first of the term $\frac{E_r}{E_0}$ a an integer. A change of variables was made which has the effect of maintaining the straight line equivalent of the equations. The results for the term shown in Figure V are.*

$$E_r = 0.3078 \frac{\sin (\beta_0 \sin \theta)}{\sin^2 \theta} - 0.078 \frac{\cos (\beta_0 \sin \theta)}{d\theta^2} \qquad (1)$$

An assumption of a linear equivalent source in the 8 plane was made to obtain an approximate field pattern for the 2 plane considered. A plane field pattern for any value of θ_0 or β_0. If the linear equivalent source in the 8 plane is assumed it have an 8 plane polarized field of

$$E_{r\theta} = E_0 \cos \frac{\pi}{2} \frac{\theta}{\theta_0} \cos \frac{\pi}{2} \frac{\theta}{\theta_0} \qquad (4)$$

which would be the approximate field resulting when the fields in the aperture were reradiated into the 2 plane. (See Figure 17 for the definitions of geometrical terms.), the resulting 8 plane field patterns are

---

* See Appendix, Section 8.

determined to be:

$$E_x = \frac{jk\,\varepsilon^{-jkR}}{4\pi R}(1+\text{Cos }\theta)\,B\,x_o y_o \left\{ \text{Sin} \frac{\left[\frac{(\pi+\phi_o)}{2y_o} - k\,\text{Sin }\theta\right] y_o}{\left[\frac{(\pi+\phi_o)}{2y_o} - k\,\text{Sin }\theta\right] y_o} + \right.$$

$$+ \text{Sin} \frac{\left[\frac{(\pi+\phi_o)}{2y_o} + k\,\text{Sin }\theta\right] y_o}{\left[\frac{(\pi+\phi_o)}{2y_o} + k\,\text{Sin }\theta\right] y_o} + \text{Sin} \frac{\left[\frac{(\pi-\phi_o)}{2y_o} - k\,\text{Sin }\theta\right] y_o}{\left[\frac{(\pi-\phi_o)}{2y_o} - k\,\text{Sin }\theta\right] y_o} +$$

$$\left. + \text{Sin} \frac{\left[\frac{(\pi-\phi_o)}{2y_o} + k\,\text{Sin }\theta\right] y_o}{\left[\frac{(\pi-\phi_o)}{2y_o} + k\,\text{Sin }\theta\right] y_o} \right\} \qquad (3)$$

However, the diffraction integrals may be integrated directly if the geometry of Figure II is employed and the simplifying assumption is made that $(r_1 - r_2)$ is a great deal less than the average radius of the aperture. The assumptions of the fields at the aperture are:

$$E_{sx} = B_1\,\text{Cos}\frac{\pi\phi'}{\phi_o}\,\text{Cos }\phi' \qquad (4)$$

$$E_{sy} = B_1\,\text{Cos}\frac{\pi\phi'}{\phi_o}\,\text{Sin }\phi' \qquad (5)$$

resulting in the field patterns in space being given by*

$$E_{p\theta} = \frac{jkB_1\phi_o r_1 \Delta r\,\varepsilon^{-jkR}}{16\pi R}(1+\text{Cos }\theta)\left\{\left[\text{Cos }\phi\left[A(0,\phi_o)\,J_o(kr_1\,\text{Sin }\theta) + \right.\right.\right.$$

$$\left. + \sum_{n=1}^{\infty} J_n(kr_1\,\text{Sin }\theta)\,A(n,\phi_o)\,B(n,\phi)\right] - j\left[\text{Sin }\phi\;\; C(0,\phi_o)\right.$$

$$\left.\left.\left. J_o(kr_1\,\text{Sin }\theta) + \sum_{n=1}^{\infty} J_n(kr_1\,\text{Sin }\theta)\,C(n,\phi_o)\,D(n,\phi)\right]\right\}\right] \qquad (6)$$

---

*See Appendix, Section B.

[illegible]

$$\left.\begin{aligned} &\frac{\left[\frac{\partial^2 \phi}{(\lambda - \xi_1^0)^2} + \kappa \cos \lambda\right] \lambda^0}{\left[\frac{\partial^2 \phi}{(\lambda - \xi_1^0)^2} + \kappa \sin \lambda\right] \lambda^0} \\ &\frac{\left[\frac{\partial^2 \phi}{(\mu - \xi_2^0)^2} + \kappa \cos \mu\right] \mu^0}{\left[\frac{\partial^2 \phi}{(\mu - \xi_2^0)^2} + \kappa \sin \mu\right] \mu^0} \end{aligned}\right\} \quad (3)$$

However, the diffraction integrals may be interpreted directly if the geometry of Figure 2.2 is replaced and the simplifying assumption is made that $(\xi^T - \xi^0)$ is a fixed ideal line from the source region of the aperture. The interpretation of the first of the integrals then

$$E^{pq} = E^T \cos \frac{\xi^0}{\xi^T} \cos \psi_1 \quad (4)$$

$$E^{pq} = E^T \cos \frac{\xi^0}{\xi^T} \sin \beta_1 \quad (5)$$

resulting in the first harmonic in phase quadrature [illegible]

$$E^{pq} = \frac{\cos \alpha}{\xi^0 \xi^T \lambda \mu} (\pi \kappa \cos \psi) \left\{ \left[\cos \psi \left[\chi(\cdot) \psi_1^0 \right] \cdot \xi^0 \xi^T \sin \alpha \right) + \right.$$

$$\left. + \sum_{m=1}^{m} E^m (\xi^T \cos \psi) \chi(\alpha^2 \psi_1^0) \cdot \chi(\alpha^2 \psi) \right] - \left[\sin \psi \cdot \chi(\alpha^2 \psi_1^0 \right.$$

$$\left. \cdot \sum_{m=1}^{m} E^m (\xi^T \sin \alpha) \chi(\alpha^2 \psi_1^0) \cdot \chi(\alpha^2 \psi) \right] \quad (6)$$

[illegible]

$$+ \sin \frac{\left[\frac{\partial^2 \phi}{(\lambda + \xi_1^0)^2} + \kappa \cos \lambda\right] \lambda^0}{\left[\frac{\partial^2 \phi}{(\lambda + \xi_1^0)^2} + \kappa \sin \lambda\right] \lambda^0} + \sin \frac{\left[\frac{\partial^2 \phi}{(\mu + \xi_2^0)^2} + \kappa \cos \mu\right] \mu^0}{\left[\frac{\partial^2 \phi}{(\mu + \xi_2^0)^2} + \kappa \sin \mu\right] \mu^0} \cdot$$

$$\cdot \frac{\left[\frac{\partial^2 \phi}{(\alpha - \xi_1^0)^2} - \kappa \cos \alpha\right] \lambda^0}{\left[\frac{\partial^2 \phi}{(\alpha - \xi_1^0)^2} - \kappa \sin \alpha\right] \lambda^0} \cdot \frac{\left[\frac{\partial^2 \phi}{(\beta - \xi_2^0)^2} - \kappa \cos \beta\right] \lambda^0}{\left[\frac{\partial^2 \phi}{(\beta - \xi_2^0)^2} - \kappa \sin \beta\right] \lambda^0} \cdot$$

$$\cdot \frac{\left[\frac{\partial^2 \phi}{(\lambda + \xi_1^0)^2} + \kappa \cos \lambda\right] \lambda^0}{\left[\frac{\partial^2 \phi}{(\lambda + \xi_1^0)^2} + \kappa \sin \lambda\right] \lambda^0} \cdot \frac{\left[\frac{\partial^2 \phi}{(\mu + \xi_2^0)^2} + \kappa \cos \mu\right] \mu^0}{\left[\frac{\partial^2 \phi}{(\mu + \xi_2^0)^2} + \kappa \sin \mu\right] \mu^0} \cdot$$

$$\left. \cdot \frac{\left[\frac{\partial^2 \phi}{(\alpha - \xi_1^0)^2} - \kappa \cos \alpha\right] \lambda^0}{\left[\frac{\partial^2 \phi}{(\alpha - \xi_1^0)^2} - \kappa \sin \alpha\right] \lambda^0} \cdot \frac{\left[\frac{\partial^2 \phi}{(\beta - \xi_2^0)^2} - \kappa \cos \beta\right] \lambda^0}{\left[\frac{\partial^2 \phi}{(\beta - \xi_2^0)^2} - \kappa \sin \beta\right] \lambda^0} \right\} \quad (7)$$

---

*The algebraic notation p.

$$E_{p\phi} = \frac{-jkB_1\phi_o r_1 \Delta r\, \varepsilon^{-jkR}}{16\pi R}(1 + \text{Cos } \theta)\Big[\text{Sin } \phi\Big\{A(0,\phi_o)\ J_o\ (kr_1 \text{ Sin } \theta) +$$

$$+ \sum_{n=1}^{\infty} J_n(kr_1 \text{ Sin } \theta)\ A(n,\phi_o)\ B(n,\phi)\Big\} + j \text{ Cos } \phi\Big\{C(0,\phi_o)$$

$$J_o(kr_1 \text{ Sin } \theta) + \sum_{n=1}^{\infty} J_n(kr_1 \text{ Sin } \theta)\ C(n,\phi_o)\ D(n,\phi)\Big\}\Big] \qquad (7)$$

Formula (3) was derived on the basis that the E plane polarized H plane field pattern is primarily a function of the chord of the arc of the aperture. It was possible to reason that the field pattern is dependent on a product of a function of the flare angle and a function of the radius. Formulas (7) and (8) illustrate that the pattern is a summation of an infinite series of such products. This permits an infinite number of combinations of ϕ_o and r_1 to be employed to obtain a given beamwidth.

The Design and Fabrication of the Horn

To obtain an aperture of given dimensions two parameters were available, the radius of the sectoral section and the flare angle. Ninety degrees was arbitrarily chosen as the initial angle of flare since this presented an aperture exhibiting measurable H plane polarization and gave a relatively wide aperture for a fixed sectoral radius. Also, reducing the flare angle would be relatively easy should this be desired. A sectoral radius was chosen to give a chord length of 16.7 λ (for λ = 3.2 cm.) in order to investigate the possibilities of obtaining a constant phase across a wide aperture. The ninety degree bend at the end of the sectoral section was designed from empirical data contained in ADRDE Research Report No. 129.[33] The laterally radiating

$$\frac{\partial \psi}{\partial \theta} = \frac{\cdots}{\cdots}(1 + \cos\theta)\left\{ \cdots \sin\theta \left\{ (\cdots)\, \psi_1^3 \, (\sin^2\theta \cos\theta) + \right.\right.$$

$$+ \sum_{\alpha=1}^{\alpha=3} \psi_1^{\alpha}(\cos^2\theta \cos\theta)\, \cdots \Big\} + \cdots \sin\theta \left\{ (\cdots) \right.$$

$$\chi^0(\cos^2\theta \sin\theta) + \sum_{\alpha=1}^{\alpha=3} \psi^0(\cos^2\theta \cos\theta)\, \cdots \Big\} \Big] \qquad (4)$$

Formula (3) was obtained on the basis that the 3 plane polarized X plane fluid velocity is directly a function of the angle of the departure. Clearly one possible to resolve this into its parallel product of a product of a function of the flow angle and a function of the radius. Formulae (3) and (4) illustrate that the velocity is a summation of an infinite series of such products. This permits an infinite number of modifications of β^0 and γ^1 to be employed to obtain a plane insensible.

The Design and Interpretation of the Cone

To obtain an infinity of fluid velocities two parameters are available, the radius of the spherical portion and the limit angle. Clearly degrees are arbitrarily chosen as the limiting angle of flow along this presented an elementary satisfying approximation = plane polarization was gave a practical) cone velocities for a fluid examined radius, however the flow would be relatively easy should note be desired. A practical radius was chosen to give a small length of $\frac{1}{2}$ (for $\beta = 3.4$ cm.) in order to investigate the applicability of adjacent a constant plane motion a cone diameter. The study before that of the combined velocity at relative flow indicated in [3][4] the necessity radiating

horn type "B" (Figure V) was fabricated by the Coppersmith Shop of the Boston Naval Shipyard under close supervision by the thesis members.

Field Pattern Measurement Procedure

Field pattern measurements were taken for five conditions of horn operation.

1. The uncompensated horn as described by Figure V.
2. The horn with a parallel plane filter located 0.318 cm. from the aperture.
3. The horn with a flare consisting of 0.318 cm. brass rod 9.6 cm. long separated by 0.635 cm. on centers in the H plane and bent to form a flare of 40° in the E plane.* (80° total sector angle)
4. The horn with 40° E plane flare and a parallel plane filter located 0.079 cm. from the aperture.**
5. The horn with 40° E plane flare and a parallel wire filter located 0.079 cm. from the aperture.**

The field patterns were measured on an audio automatic antenna pattern recorder similar to that described in Reference (34). The pen positioning system is given in block diagram form in Figure VI and the overall test setup is given in Figure VII. The X band radar transmitter could transmit either H plane polarized or E plane polarized electromagnetic energy. H plane and E plane patterns were taken by shifting either the polarization of the transmitter or the physical position of the horn antenna. The four principal patterns were taken for horn conditions 1, 2, 3, 4, but only the H plane polarized, H plane

---

* See Photograph, Figure .
** See Figure X.

tons type "B" (Figure 7) was replaced by the Compensolit lens of the Bausch Morel Zeiss-Opton series originally in the Sperti Recipon.

Final Optics Assembly Alignment

Final optical assemblies were given four alignment checks during operation.

3. The uncompensated lens as received by Figure 7.
4. The lens with a parallel plane filter between 0.125 mm. from the specimen.
5. The lens with a filter varying by 0.250 mm. between 0.5 mm. less required by 0.250 mm. to restore by Abbe
A plane and then to over a flare of 40° to the 8 planes.
(40° total vector angle)
6. The lens with 40° 4 plane flare and a parallel plane filter between 0.375 mm. from the specimen.[**]
7. The lens with 40° 4 plane flare and a parallel plane filter between 0.375 mm. from the specimen.[**]

The final optical train mounted on the radio controlled motion pictures recorder enabled the user described in Reference [11]. The pertinent operating curves is given in their original form in Figure 12 and the overall lens assembly is given in Figure 13C. The 3 inch rubber intensifier would transmit either a plane polarized or a plane polarized circumferentially energy. A plane and 2 plane retarder were taken by utilizing either the polarizations of the transmitter or the polarized wavelength of the beam combiner. The four principal positions were taken for lens positions 1, 4, 5, and 6, and each in plane polarized, 8 right

---

[**] See Photograph, Figure 1.
See Figure 12.

field pattern was taken for Condition 5. The frequency of the transmitter was varied in Condition 1 in order to determine the sensitivity of the pattern to frequency changes.

Evaluation of the E Plane Polarized E Plane Field Pattern When E Plane Flare Is Added to the Horn

It was important to be able to make an engineering estimate of the change in the field pattern when E plane flare was added to the horn. The E plane polarized E plane field pattern of an E plane sectoral horn determined either theoretically[26][36] or experimentally[35] was designated G(θ). The aperture was then considered to be a continuous array of infinitesimal E plane sectoral horns. The array factor for this continuous array would be $E_{p\theta}(\theta\ )$ in Equation (6) evaluated for $\phi = 0^{\circ}$. The resulting E plane pattern then became:

$$E_{\theta,2} = G(\theta)\ E_{p\theta}\ (\theta,0) \qquad (8)$$

The resulting field pattern may be plotted by adding decibel values. A comparison plot of the computed horn field pattern obtained in this manner with the measured horn field pattern was plotted on Figure XXXI.

Impedance Measurement Procedure

Voltage standing wave ratio measurements were made for the various horn designs using a standard slotted section of wave guide, an amplitude modulated signal, a square law crystal detector, and an ECA 16EA amplifier to measure the output. A 2K39 klystron furnished power. The probe depth was adjusted for minimum penetration and tuned for each frequency.

Measurements were made of the VSWR in the guide. Positions of the minima were determined for the horn terminated in space, with a

short circuit at the aperture, and with a short circuit at the throat. All frequency measurements were in a band from 8600-9400 mcps.

III RESULTS

The Principal Field Patterns of the Laterally Radiating Electromagnetic with No Flare or Filters Added

The results of the field pattern tests of the horn are given by the solid curves of Figures XII, XIII, XIV, and XV. The E plane polarized H plane field pattern reveals that a 4.33° half power beam with -20 db. side lobes was achieved, but also that there is some phase distortion near the right side lobe and minor asymetries in the pattern. The H plane polarized E plane pattern, which theoretically should be zero for all values of θ, shows negligible values of field strength. The E plane polarized, E plane field pattern gives a 24° half power beam width. The "side lobes" are -7.8 db. and a generally ragged field pattern for values of θ away from the "main lobe" is obtained. In the H plane polarized H plane field pattern the two major lobes are slightly asymetrical and the rest of the pattern is highly asymetrical in that the third side lobe is missing on one side. This "cross component" of polarization has a peak value of between -10 db. and -12 db. in accordance with minor deflections of the aperture of the horn.

The Results of Varying Frequency on the E Plane Polarized H Plane Field Pattern

Figure XVI indicates a slight increase in half power beamwidth with frequency and a reduction in the peak power density of the first side lobes together with considerable distortion of the field pattern beyond the first side lobe. However, the general symmetry of the main and side lobes is maintained.

The Results of Comparing the Experimentally Determined Values with the Computed Values of the Field Patterns in the H Plane

12.3 Results

The Electrical Field Strength of the Inverted Yet-Wide Electromagnetic Wave in Plane of Distant Lobes

The results of the field measurements taken at the lobes are given by the solid curves of Figures 12.1, 12.2, and 12. For a plane polarized E plane field pattern produced (at $\lambda = 1.25$) half power beam width -32 deg. side lobes are evident, but are fifty times in down plane direction over the right side lobe and other appearance in the pattern. The E plane polarized E plane pattern, which theoretically should be zero for all values of θ, never quite does so field minimum. The H plane produced, E plane field pattern plane a 52° half power beam width. The "side lobes" are -27.5 db. and a practically negligible field pattern for values of θ over from the "main lobe" is obtained. In the H plane polarized E plane field pattern the two major lobes are extremely separated and the value of the pattern is fairly significant in that the total side lobe is missing in the plane. This "zero suppression" of polarization for a pick value of wavelength for, and -13 db. is observance with other deflections of the structure of the beam.

The Results of Further Precision on the E Plane Polarized H Plane Field Patterns

Figure 12.3 emphasizes a slight increase in half power beamwidth with frequency and a reduction in the peak power density of the first side lobes. Moreover, the general symmetry of the main and side lobes is maintained.

The Results of Measuring the Electromagnetic Polarizing Planes with the Inverted Yagi of the Field Patterns in the H Plane

The computed values determined by the linear equivalent source method and the Fourier-Bessel series method are plotted on Figures XVII and XVIII. Formula (1) gives close corollation with measured H plane field patterns but it is not included in the results section. There is excellent agreement between the experimentally determined and theoretically determined values of the half power points of the main lobe in the case of the E plane polarized field pattern. In the case of the H plane polarized field pattern the peak power points and the half power points of the two main lobes are in agreement with the computed values. In the case of the E plane polarized fields, the Fourier-Bessel series gives a good indication of the angle at which the first side lobe will appear. The linear equivalent source method gives a better approximation of the magnitude of the side lobes.

A Comparison of the Principal Field Patterns of the Laterally Radiating Electromagnetic Horn with and without a Parallel Plane Filter

The parallel plane filter performed its function of eliminating the H plane polarization from the radiation field. A loss of peak power density of 1.3 db. together with a distortion of the side lobe pattern was experienced for the H plane pattern. The E plane pattern was also distorted in the side lobes, but there was no change in half power beam width and only a slight change in the relative peak power density of the "side lobes."

The Results of Adding a 40° E Plane Flare to the Horn

Figures XIX, XX, XXI, and XXII show the results of adding a 40° E plane flare to the horn. Minor alterations to the negligible H plane polarized E plane field pattern results. The symmetry of the E plane polarized H plane pattern was improved somewhat and minor

alterations occurred in the main lobes. In the E plane polarized H plane field pattern a slight increase in half power beam width occurred when the flare was added and the peak power density of the first side lobes dropped to -22.2 db. A significant change occurred in the E plane polarized E plane field pattern. The half power beamwidth increased from 24° to 31°; the overall beam pattern is narrower; and the side lobes are nonexistent. "Side lobes" at angles less than -30° and at angles more than +30° have been thoroughly suppressed.

The Effect of Adding a Parallel Plane Filter to the Horn with 40° E Plane Flare

Figures XXIII, XXIV, XXV, and XXVI demonstrate the results of adding a parallel plane filter at the aperture of the horn with a 40° E plane flare. A minor change in the negligible H plane polarized E plane field pattern resulted. The parallel plane filter reduced the "cross component" field pattern 19 db. causing minor variations in the E plane polarized E plane field pattern. For the E plane polarized H plane field pattern the first side lobes occur at -27.8 db.; the second side lobes have a peak value of -24.5 db. and are asymmetrical. A slight increase of half power beam width from 4.5° to 4.7° also occurred.

The Effect of Adding a Parallel Wire Filter to the Horn with E Plane Flare

Approximately a -10 db. attenuation was achieved in reducing the "cross component" of polarization by using the parallel wire filter. See Figure XXVII.

A Comparison of the Computed and Measured Field Patterns in the E Plane

Figure XXX is a correlation of computed and measured values of the E plane polarized, E plane field pattern and includes a graph of the

computed values of phase shift encountered when the origin of the flared section is employed as the origin of the coordinates. The slope of the phase shift curve indicates that the center of radiation of this particular horn is 32.6 cm. from the origin of the coordinates and on the x axis.

Figure XXXI is a correlation of computed and measured values for the E plane pattern of the horn with 40° E plane flare.

A Plot of Ellipticity of the Uncompensated Electromagnetic Horn

Figure XXVIII is a plot of the theoretical ellipticity of the H plane field pattern. Also included is a plot of the measured magnitudes with theoretical phase values for positive values of θ. $(\frac{\pi}{2} = \phi)$. Figure XXIX is a plot of the theoretical ellipticity and measured magnitudes with theoretical phase values for negative values of θ. $(\frac{\pi}{2} = \phi)$. The magnitudes of the power densities in these elliptically polarized waves is given adjacent to the plotted points. These graphs include only the fields in the main lobe located on the H plane. The derivation of the use of the Smith Chart for this purpose is given in Reference (13).*

Impedance Measurements

The results of VSWR tests made for the five horn conditions are shown on Smith charts. See Figures XXXII through XXXVII.

---

* See Appendix, Section B for detailed interpretation.

[illegible]

[illegible]

[illegible]

IV DISCUSSION OF RESULTS

Evaluation of the Accuracy of Fabrication of the Laterally Radiating Horn

The asymmetries in the side lobe patterns in the H plane fields indicate that highly refined mechanical symmetry did not exist. Although minor phase distortions were present in all of the H plane patterns, correlation may be achieved between an ideally constructed horn and the horn employed. Therefore, the fabrication accuracy of the horn is considered adequate for the purpose of this thesis. Improvement in performance might be achieved by electroforming the horn or constructing the horn of aluminum alloy with an improved horn bend shown in Figure XI in order to improve structural rigidity.

A further measure of the accuracy of fabrication may be made by considering the H plane polarized, E plane field pattern in Figure XIII. The theoretical horn would give a zero field pattern for all values of θ, and in the physical horn all field strengths are negligible. Therefore, a high degree of symmetry was present in the horn and the horn was properly oriented with respect to the incident wave polarization for the field pattern tests.

Evaluation of the Methods of Computing Field Patterns

The change of variable method employed to obtain the H plane field pattern for the E plane polarized wave is highly accurate for obtaining field patterns of a sectoral horn that has a 90° H plane flare at the throat. The expression is easy to evaluate. However, it is limited to $\frac{N}{n}$ sectors. In general design work Formula (3) is recommended as a first approximation to the field pattern. Formula (3) has the advantage that any value of flare angle or radius may be employed to give

IV Discussion of Results

Evaluation of the Accuracy of Measurements of the Refractive Indices

The experiments in the zero light intensity in the 2 plane field indicate that highly refined experimental procedure did not exist, although extra plane diffraction were present in all of the 2 plane patterns, experiments may be utilized because of thereby considered zero and the data acquired. Therefore, the fluctuations accuracy of the data is considered adequate for the purpose of this thesis. Improvements in performance might be achieved by eliminating the zero error, adjusting the lens of minimum spiral with an improved focus knob similar to Figure 12 to center to improve structural rigidity.

A further examination of the accuracy of interpretation may be made by considering this 2 plane pattern, 2 plane field pattern is Figure III. The theoretical zero would give a zero field pattern for all values of α, and by the physical zero all field measures are negligible. Therefore, a high degree of accuracy was evident in the zero and the data was promptly obtained with respect to the minimum zone polarization for the field pattern tests.

Evaluation of the Validity of Computed Field Patterns

The theory of variable method employed to obtain the 2 plane field patterns for the 2 plane polarized wave is highly accurate for obtaining field patterns of a conductor here that has a 90^{0} 2 plane flare at the throat. The computation is easy to evaluate. However, it is limited to $\frac{a}{\lambda}$ values. In general design work formula (3) has two advantages that any value of flare angle or radius may be applied to give

the designer a first estimate of physical size. Figure XVII indicates the linear equivalent source method gives accurate values for the half power beam angles and good results on the magnitudes and angles of the first side lobes.

The derivation of the Fourier-Bessel series method involved slightly more refined approximations. It gives the field pattern for all values of R, ϕ, and θ, and it should prove to be the most useful method of computing the fields. As a result the calculated ellipticity of a given design of laterally radiating horn may be plotted by Smith chart methods.[12] The Fourier-Bessel series gives accurate results for the half power beam width and the angle of the first side lobe together with approximate values for the magnitude of the first side lobe and angle of the second side lobe.

Formulas (6) and (7) appear to be formidable infinite series of Bessel functions, but a study of the coefficients given in formulas (A-52), (A-55), A-58) and (A-59) reveals that the values of $A(n,\phi_o)$ and $C(n,\phi_o)$ decrease very rapidly with increasing values of n if ϕ_o is a moderately large value. For this antenna the computations did not involve Bessel functions of order greater than 6. In addition, no single field computation involved more than 4 orders of Bessel functions. The references[10][11] had sufficient values of the arguments of the Bessel functions and $\frac{\sin\beta}{\beta}$ tabulated that all sectors of the H plane field patterns that were of interest could be plotted. The H plane polarized, E plane field pattern becomes zero both through symmetry considerations and through the coefficients of the Bessel functions being all zero.

In the E plane polarized, E plane field pattern a sector of

only 40° could be plotted since the Harvard University series of tabulated values of Bessel functions did not list arguments greater than 20. When a more complete set of Bessel function values is published, it will be possible to plot the E plane field patterns through a wider range of θ values. About five hours of concentrated effort is required to evaluate one field pattern.

The Effectiveness of the Parallel Plane Filter

That the parallel plane filter employed was overdesigned is evidenced by the absence of any H plane polarized radiation in Figure XV. It was designed this way in order to determine the affect on horn impedance when the cross components of polarization were completely eliminated. Because the elimination of the cross components was accompanied by only minor decreases in peak power and minor variations in the field patterns of the E plane polarized components, the parallel plane filter is considered to be an excellent method of reducing or eliminating elliptical polarization.

The Results of Varying Wavelength in the Field Pattern Tests

The laterally radiating horn is not a frequency sensitive radiator. See Figure XVI. This was demonstrated by the results of varying the frequency from 9380 mcps. to 8860 mcps. The expected phenomena occurred. The half power beam width increased slightly due to a reduction in aperture length measured in wavelengths. The angle at which the first side lobe occurs increased and the magnitude of the first side lobe decreased. There was no large alteration of the shape of either the major lobe or the first side lobes. Correlation of the results in the side lobes beyond the first side lobe depends upon a knowledge of the variation of the horn geometry from the ideal and a knowledge of the magnitudes of the higher mode fields.

A Comparison of the Laterally Radiating Horn Field Patterns with and without a Parallel Plane Filter

A check on the symmetry of the assembly of horn and filter from the field patterns reveals that symmetry is good.*

That the peak power of the main lobe is down 1.5 db. indicates that the filter at this frequency is reflecting or dissipating some of the energy. That higher mode fields are being generated in the filter is evidenced by the fact that the half power beam width is increased in the E plane and the side lobes are more prominent and at a higher level. See Figure XII. This particular point could be a field for further investigation, but the ragged side lobe pattern with high peak values indicates that not much could be gained from an attempt to improve the E plane pattern through the use of this filter alone.

Computed Design Curves

Although the design formulas were developed in this thesis, there was not enough time available to compute a full set of laterally radiating horn design curves because experimental verification of the theoretical field patterns was essential. Further investigation of the H plane half power beam widths, the H plane side lobe level, the E plane half power beam widths, the peak level of cross polarization, and the ellipticity of the fields in Fraunhofer space would be desirable. Plots of these quantities could be made as functions of $\frac{r_1}{\lambda}$ and ϕ_c. If the ellipticity is of interest, plots of this quantity could be made on the Smith chart.(12) Some of the points could be verified experimentally.

---

* The H plane polarization was practically eliminated from the radiation fields.

2. Generation of the Equivalent Rectangular Wave Plane Impedance Chart and Related 2 Terminal Pair Circuits

A chart on the principle of the familiar Smith chart for the [1+jx] parameter circuits over [impedance] is given[*]

Next the less known but not much like it theoretically chart for the [G+jB] parameter circuits over admittance is given. This chart may be used directly for the 2 plane 2 terminal pair network or the 2 plane 4 terminal pair network. The 2 plane 2 terminal pair network is the basic type of network for which the chart is constructed. The 2 plane 4 terminal pair network is the more general type of network for which the chart is constructed. The 2 plane 2 terminal pair network is the more general type of network for which the chart is constructed.

General Design Charts

Already the basic formulae were developed in this thesis which show how one may design a circuit to control a full set of transmitting [illegible] circuit [illegible] [illegible] [illegible]

A Comparison of the Field Patterns of the Horn with and without a 40° Parallel Wire E Plane Flare.

A check on the H plane polarized, E plane field pattern with and without E plane flare indicates that symmetry is good.

It was considered that the addition of parallel wires in the E plane would cause currents to flow along the wires in the E plane and thus force more energy into the E plane polarized fields. This was not measurable in the field patterns. Since the center to center spacing of the flare wires was 0.198λ and the diameter of the flare wires was about 0.099λ only about 1 per cent of the normally incident radiation should pass through the flared section for E plane polarized energy and H plane polarized energy should pass through only slightly attenuated.(27) However, since incidence of the energy on the sides of the flare is parallel rather than normal, little energy of H plane polarization should pass through the flare wires and it will act as a pure flare section. If the wires were spaced farther apart, there would be larger loss of E plane polarized energy through the wires, and the wires would no longer provide the results usually obtained by flaring with solid metallic strips.

In general, the addition of 1/8 inch brass rods spaced 0.635 cm. on centers in the H plane and flared in the E plane at an angle of 40° resulted in the affect of adding pure flare to the horn. Actual improvements in symmetry resulted in the H plane field patterns.

When E plane flare was added a moderate increase in gain was realized and there was an increase in H plane half power beam width. In the E plane the "side lobes" were severely attenuated so that only

one lobe of any consequence was left. That the half power beam width of the E plane field pattern was increased by adding 40° E plane flare indicated that phase distortion at the flare aperture is a problem. A series of experiments could be conducted similar to those of D. R. Rhodes[26] in which flare was added and the field patterns measured for various lengths of flare in order to determine the optimum flare angle and radius of flare. This could be done for the laterally radiating horn.

A Comparison of the Field Patterns of the Horn with 40° E Plane Flare and a Parallel Plane Filter at the Aperture and the Field Patterns of the Horn with 40° E Plane Flare and No Filter at the Aperture

From the field patterns it can be generalized that symmetry was good. The parallel plane filter was effective in eliminating H plane polarization.

Small variations in the E plane polarized, E plane field pattern might result from higher mode generation in the filter. The E plane field pattern is sufficiently well formed that it could meet 31° half power beam pattern specifications with extremely low side lobe levels, whether the filter is employed or not. It may be concluded that the parallel plane filter does not materially affect the E plane field pattern.

Of particular interest is the fact that the 21 db. side lobe level of the flared horn was reduced 7 db. through the addition of the parallel plane filter at the aperture. Even though there were minor increases in the second side lobe levels, manipulation of the variables in the filter design might reduce both the first and second side lobes

to a symmetrical -27 db. side lobe pattern. In the experimental process of manipulating these variables, it would be necessary to make impedance studies on the horn as well as field pattern studies. A theoretical analysis of the higher mode generation at the filter may be possible. W. D. Hayes concluded that the appearance of higher order modes in a grating of large spacing was undesirable when the grating was employed as a beam forming reflector.(27) It was discovered that under the conditions of this experiment the appearance of higher order modes at the widely spaced grating may be employed to improve the E plane polarized, H plane field pattern.

The result of the investigation of the presence of higher order modes might be that the development of favorable higher modes may be dependent upon frequency in which case the first side lobes would vary with frequency.

The Specifications Fulfilled by the Horn with 40° E Plane Parallel Wire Flare and a Parallel Plane Filter

Considering the field patterns for the horn with 40° E plane flare and a parallel plane filter in Figures XXIII, XXIV, XXV, and XXVI the following specifications have been met:

1. A half power beam width of 4.5° in the H plane.
2. A half power beam width of 31° in the E plane.
3. A side lobe pattern in the E plane which has one side lobe at -19.2 and the other side lobe at -24 db.
4. First side lobes in the H plane at -28 db.
5. Maximum second side lobe in the H plane at -24.6 db.
6. Negligible ellipticity.

The Effectiveness of the Parallel Wire Filter in Attenuating the H Plane Polarized Fields

The parallel wire filter caused only minor changes in the E plane field pattern, but it was sufficiently effective to reduce the H plane component 9 to 10 db. From assumptions made in developing the attenuation curves from parallel plane waveguide theory, the attenuation measured was a great deal more than the computed values. The parallel plane theory omits the scattering effect of the wires which is important. An empirical formula was developed by W. D. Hayes[27] from experimental evidence. This formula gives accurate results. Equation (9) yielded an attenuation of 9.86 db. when the parallel wire filter parameters were substituted.

The following equation may be employed to obtain the attenuation of the H plane polarized component when a parallel wire filter is used.

$$\text{Log } T = 0.0917\ A + 12.6\ \frac{d}{\lambda} - 7.06 \qquad (9)$$

A Comparison of the Computed and Measured Values of the E Plane Field Pattern of the Horn with E Plane Flare

An error of 15 per cent exists between the measured and computed values of the half power beam width in Figure XXXI. This figure also demonstrated that a rough estimate of the beam pattern can be made by employing the pattern computation method given by Equation (8).

The Difference of Two Parallel Slits Taken In Succession from
A Plane Conducting Sheet

The potential due to all but several very strongly in-
A plane fluid medium, but it has practical significance to replace the
2 plane conductors 9 to 10 in. from successive scans in determining the
attenuation curve from previous plane waveguide theory. The attenu-
tion measured was a great deal more than the computed values. The cor-
rected plane theory omits the perturbing effect of the wire which is
important. An empirical formula was developed by V. L. Hines[17] that
experimental evidence. This formula gives accurately results. Equation (9)
yields an approximation of 7.8% for that the parallel wire Slitec perturbers
were substituted.

The logarithm expanding may be employed to obtain the expansion
tion of the 2 plane reflection coefficient when a practical wire Slitec is
used.

$$\log \Gamma = 0.0027 + 1.12 \pi \frac{\lambda}{d} - 7.05 \qquad (9)$$

A Comparison of the Computed and Measured Values of Two 2 Plane Slitec
Systems of the Form with 2 Plane Slitec

In order of 12 per cent points between the measured and com-
puted values of the half power beam width in Figure 1021. This figure
also demonstrated that a rough estimate of the beam position may be
made by employing the geometric construction method given by Equation (2).

Admittance Characteristics

The Uncompensated Horn (Condition 1)

Admittances in the frequency range from 9266 to 8616 mcps. (7.5 per cent band) were transferred to the horn throat and plotted on a Smith chart. See Figure XXXII.

Investigation of the plot indicates that there is a frequency insensitive component of Γ. It is concluded that this component, denoted Γ_t, is due to reflection at the throat. This mismatch appears to be inductive, which is to be expected for the H plane flare. Γ_t = 0.0726. This compares with Γ_t = 0.03 measured by J. R. Riser[37] for a horn with 30 degree H plane flare. Γ_t was then subtracted from the admittances which were then transferred to the horn aperture. See Figure XXXVII.

The mechanical length of the horn is approximately 44 cm. If the change of frequency required to cause a rotation on the Smith chart is considered the virtual length of the horn is determined as

$$R = \frac{(\Delta\phi) \cdot \pi_1 \pi_2}{\pi_1 - \pi_2}$$

where

$\Delta\phi$ = rotation around the Smith chart.

π_1, π_2 = the wavelengths of the two frequencies, assumed to be in free space.

The mean of these computations indicates a virtual horn length of 51.9 cm. At a virtual length of 51.2 cm. the minimum spread of Γ_a (at the aperture) was noted for a variation in frequency. Γ_a indicates that the aperture admittance has a capacitive susceptance which is to be expected. Γ_a = 0.178. If the aperture is considered to be the same as TEM propagation through two plane parallel plates spaced 1.02 cm. theoretical computations indicate Γ_a = 0.322.[38]

Application Characteristics

The Electromagnetic Guide (Special Runs 7)

Introduction to new Components (only items not included in (7.3 per cent load) were considered to the given (about one hundred a radio counter. See Figure XXXII.

Investigation of the Glow Discharge Light Intensity Measurements undertaken at λ , it is evidently time very conspicuously observed λ^{t}) to give an indication of the spectra. λ^{t} = 0.0300. Some accuracy within 2% to be obtained for the 0 plane figure. λ^{t} = a figure with 30 degrees 0 plane figure. λ^{t} was then maintained from the subsequent values were then considered in the main conductor. See Figure XXXIII. λ^{t} = 0.043 measured at λ^{t} = 0.0300. (37)

The measurement results of the tests is approximately as set. If the change of frequency required to cause a reduction on the light output is considered the virtual length of the wave it represented as

$$k = \frac{\lambda^{2} - \lambda^{3}}{(2\lambda) \cdot \lambda^{3}}$$

where

(2λ) = reference current for total energy.

λ^{2}, λ^{3} = the wavelengths of the two intensities, assumed to be in fine spectra.

The mean of three consecutive indications a virtual path length of 21.3 cm. If a virtual length of 21.1 cm. the minimum current of λ^{g} (at the electrons) was noted for a variation in frequency. λ^{g} indicates that the quartzite oscillator has a magnetic susceptance which is in an exact period. λ^{g} = 0.1130. If the electrons is considered to be the main to the quartzite oscillator by a magnetic susceptance which is in an exact period (7.3 per cent load) were considered to the given (about one hundred a radio counter. See Figure XXXII.

Investigation of the Glow Discharge Light Intensity Measurements undertaken at λ , it is evidently time very conspicuously observed λ^{t}) to give an indication of the spectra. λ^{t} = 0.0300. Some accuracy within 2% to be obtained for the 0 plane figure. λ^{t} = a figure with 30 degrees 0 plane figure. λ^{t} was then maintained from the subsequent values were then considered in the main conductor. See Figure XXXIII. λ^{t} = 0.043 measured at λ^{t} = 0.0300. (37)

The measurement results of the tests is approximately as set. If the change of frequency required to cause a reduction on the light output is considered the virtual length of the wave it represented as

$$k = \frac{\lambda^{2} - \lambda^{3}}{(2\lambda) \cdot \lambda^{3}}$$

where

(2λ) = reference current for total energy.

λ^{2}, λ^{3} = the wavelengths of the two intensities, assumed to be in fine spectra.

The mean of three consecutive indications a virtual path length of 21.3 cm. If a virtual length of 21.1 cm. the minimum current of λ^{g} (at the electrons) was noted for a variation in frequency. λ^{g} indicates that the quartzite oscillator has a magnetic susceptance which is in an exact period. λ^{g} = 0.1130. If the electrons is considered to be the main to the quartzite oscillator by a magnetic susceptance which is in an exact period.

Any component of reflection due to a mismatch at the 90° bend is not discernible from the data obtained.

The Horn with Parallel Plane Filter, No E Plane Flare (Condition 2)

Admittances in the frequency range from 9349 to 8729 mcps. were transferred to the horn throat and plotted on a Smith chart. See Figure XXXIII.

Γ_t of the same order of magnitude as that for Condition 1 is observed. The admittance plot follows the same contour except at the lower frequencies. The filter is in effect a cut-off wave guide for the H plane components of E. That it is effective in shorting out these components was apparent from the field pattern.

The Horn with 40° E Plane Flare Added, No Filter (Condition 3)

Admittances in the frequency range 9343 to 8608 mcps. (8.5 per cent band) were transferred to the horn throat and plotted on a Smith chart. See Figure XXXIV.

Γ_t similar to Condition 1 was observed.

The admittance plot indicates that there is a condition of resonance in the horn. The rates of rotation of λ for different frequencies indicates a virtual horn length of 51 cm. Γ_a has been reduced at the higher frequencies and increased at the low end of the band. For the length of E plane flare employed, 9.3 cm. (~3λ), it would be expected that the aperture is well matched to space.[39] The resonant element is probably to be found in the wire rods (spaced 0.635 cm. on centers) used to obtain the E plane flare. It had been hoped that these rods would provide not only flare, but also would serve to eliminate the H plane polarization in the field pattern. Since this was not accomplished, E plane flare could be obtained using

[illegible] component of reflection due to a absorption of the 90° beam
in the ferromagnetic film was observed.

The Zero with Applied Field Effect, or a Sharp Zero Condition by

Application of the field caused results from 0.250 to 0.740 meter.

were determined to the zero thread and plotted as a function

Figure XXXIII.

[illegible] of the zero order of magnitude at that for Condition 2 is

observed. The explanation plot follows the same relationship as the

lower frequencies. The filter is to adjust a cut-off rate for the

A plane component of $\vec{r}$. That is effective in rejecting out those re-

peaters was reported from the first position.

The Zero with 90° a Plane Plate Added, or Zero Condition II

Application in the frequency range 9241 to 9009 kmcs (6.5 mm

band) were investigated to the zero thread and plotted as a family

plots. See Figure XXXIV.

[illegible] to Condition 1 was observed.

The additional plot indicates that there is a variation of

resonance in the zero. The rates of rotation of $\vec{r}$ for different fre-

quencies indicates a thread zero length of 21 cm. [illegible] was been re-

moved at the higher frequencies with increased at the low end of the

band. For the length of 2 plane plate replaced, β_1 cm. (-18), it

would be expected that the reference is well adjusted to zero.[19]

The resonant elements is probably to be found in the wire rods (plated

0.853 cm. or centers) used by adding the 2 plane plate. It had been

hoped that these rods would provide two zero fields, but also would

serve to eliminate the 2 plane polarization in the field pattern.

Since this was not accomplished, 2 zero fields should be obtained using

solid sheet. H plane polarization is best eliminated by employing one of the mode filters. The horn dimensions could be adjusted to give the best impedance characteristics as is done with a compound horn.[40]

The Horn with 40° E Plane Flare, Parallel Plane Filter (Condition 4), and with 40° E Plane Flare, Parallel Wire Filter (Condition 5)

The admittance characteristics for these conditions follow those of Condition 3. The filters appear to have no adverse effects on the admittance characteristics.

V CONCLUSIONS

1. The Laterally radiating electromagnetic horn has a radiating aperture in a plane surface and the surface is formed along an arc of a circle. This plane surface is also a plane of constant phase.
2. The E plane polarized, H plane fields can be computed by means of a linear equivalent source or a Fourier-Bessel series.
3. The Fourier-Bessel series method can be employed to compute the fields in Fraunhofer space for all modes at the aperture.
4. The addition of E plane flare to the laterally radiating electromagnetic horn will result in increased gain, but the E plane half power beam width may increase.
5. The addition of a parallel plane filter will eliminate undesirable H plane polarization.
6. The addition of the parallel plane filter can reduce the first side lobe level in the H plane field pattern.
7. The parallel wire filter is also effective in attenuating H plane polarization. This attenuation may be approximated by an empirical formula.
8. When the frequency is decreased the E plane polarized H plane field pattern increases in half power beam width slowly, increases in angle at which the first side lobe occurs, and reduces in the magnitude of the first side lobe. The general contour of the beam pattern is unchanged.

7. QUESTIONS

1. The Lorentz force on a charge moving in a magnetic field is always perpendicular to the velocity of the charge. Does this mean that the magnetic field does no work on the charge? Explain.

2. Is it possible to have a magnetic field in a region of space without having an electric field? Is it possible to have an electric field without having a magnetic field? Explain.

3. Is it possible to have a magnetic field in a region of space without having a magnetic force on a charge moving in that region? Explain.

4. Is it possible to have a magnetic force on a charge moving in a magnetic field without having a magnetic field in a region of space without having a magnetic force on a charge moving in that region? Explain.

5. Is it possible to have a magnetic field in a region of space without having a magnetic force on a charge moving in that region? Explain.

6. Is it possible to have a magnetic force on a charge moving in a magnetic field without having a magnetic field in a region of space without having a magnetic force on a charge moving in that region? Explain.

7. Is it possible to have a magnetic field in a region of space without having a magnetic force on a charge moving in that region? Explain.

8. Is it possible to have a magnetic force on a charge moving in a magnetic field without having a magnetic field in a region of space without having a magnetic force on a charge moving in that region? Explain.

9. The main lobe of the uncompensated laterally radiating electromagnetic horn is linearly polarized in the E plane, and right elliptically polarized to the right of the E plane, and left elliptically polarized to the left of the E plane.

10. The mismatch of the uncompensated horn at the throat appears to have components due to lumped admittances at the horn throat and aperture. The throat component can probably be eliminated by rounding the transition at the beginning of H plane flare.

11. The mismatch at the aperture may be reduced by employing E plane flare which is also desirable in terms of the field pattern. The use of wire rods to obtain this flare apparently causes a resonance in the admittance characteristics. Since these rods are not successful in eliminating H plane polarization a sheet E plane flare should be used. For best admittance characteristics the horn should be designed as a compound horn with cancelling reflections over the band desired.

12. The use of mode filters at the aperture to eliminate H plane polarization does not have any characteristics which affect adversely the admittance characteristics. When designing the horn their effect over the frequency band should be determined and considered as a means of minimizing .

9. The main loss of the two-component interacting radiating electromagnetic wave is thermal dissipation in the E plane, and their multiplicity decreases the Q-factor of the E plane, but only additionally depending on the Q-factor of the H plane.

10. The behaviour of the coupling-coupled lines as also known operate in wave propagation due to longer wavelengths as the loops tuning and capacity. The theory discussed may probably be eliminated by reducing the inductive of the E plane loops.

11. The advantage of the equations may be derived by designing H plane filter which is also available in many of the filter patterns. The use of this type is commercially adopted in the modulation circuit-investigation. Since these loops are also connected in alternating H plane polarization - wave E plane loops should be used. For most applications electrically the loops should be designed as a conventional loop with a capacitive element over the load element.

12. The use of many filters at the operation at multiple H plane polarizing does not have any disturbing/negative wider effect between the individual characteristics. Since the loops tuning the (wavelength) load should be designed for beginners as a means of adaptation.

VI RECOMMENDATIONS

The following recommendations are presented:

1. A complete set of design graphs could be made of main lobe half power beam widths, first side lobe magnitudes and angles at which they occur, the amplitude of the "cross polarization" lobes in the H plane, the E plane half power beam pattern, and ellipticity patterns for the uncompensated laterally radiating horn. The Fourier-Bessel series method of computation could be employed.
2. An experimental investigation of the affect of various E plane flare angles and lengths of flare on the E plane field patterns could be conducted.
3. A thorough investigation of the affect of varying the filter parameters on the field patterns and the impedance characteristics of the horn should be made. It should be determined whether the higher order modes formed in the filter are sensitive to changes in frequency.
4. An investigation over a larger band of frequencies, perhaps 20 per cent, could be conducted to determine what positions of beginning of E and H plane flares, bend, and mode filter gives the best impedance characteristics.

II RECOMMENDATIONS

The following recommendations are presented:

1. A complete set of design graphs could be made of this lobe half power beam width, first side lobe magnitude and angular at which they occur, the magnitude of the "cross polarization" lobes in the E plane, the 3 plane half power beam pattern, and eliminating patterns for the aforementioned isosmotic radiating cone. The feasibility should be investigated of computation could be accomplished by the use of a digital computer.

2. An experimental investigation of the effect of varying the E plane flare angles and lengths of flare of the 3 plane field patterns could be conducted.

3. A thorough investigation of the effect of varying the flare parameters on the field patterns and the terminal characteristics of the horn should be made. It should be determined whether the square cross-sectional horns could be circular are essential to accurate to determine.

4. An investigation over a large band of frequencies, perhaps 50 per cent, should be conducted to determine what possibilities of beginning at 7 and 3 plane flares "work" and make further given the most impressive characteristics.

APPENDIX

APPENDIX, SECTION A

ILLUSTRATIONS

List of Figures

Figure	Title
XVII	Computed and Measured Values of the E Plane Polarized, H Plane Field Pattern of the Laterally Radiating Horn.
XVIII	Computed and Measured Values of the H Plane Polarized, H Plane Field Pattern of the Laterally Radiating Horn.
XIX	E Plane Polarized, H Plane Field Pattern of the Laterally Radiating Horn with and without 40° E Plane Flare.
XX	H Plane Polarized, H Plane Field Pattern of the Laterally Radiating Horn with and without 40° E Plane Flare.
XXI	E Plane Polarized, E Plane Field Pattern for the Laterally Radiating Horn with and without 40° E Plane Flare.
XXII	H Plane Polarized, E Plane Field Pattern for the Laterally Radiating Horn with and without 40° E Plane Flare.
XXIII	E Plane Polarized, H Plane Field Pattern for the Laterally Radiating Horn (with 40° E Plane Flare) with and without the Parallel Plane Filter.
XXIV	E Plane Polarized, E Plane Field Pattern for the Laterally Radiating Horn (with 40° E Plane Flare) with and without the Parallel Plane Filter.
XXV	H Plane Polarized, E Plane Field Pattern for the Laterally Radiating Horn (with 40° E Plane Flare) with and without the Parallel Plane Filter.
XXVI	H Plane Polarized, H Plane Field Pattern x for the Laterally Radiating Horn (with 40° E Plane Flare) with and without the Parallel Plane Filter.

Figure	Title
XXII	Computed and measured values of the I (plane Polarized).
	I Plane Field Patterns of the Laboratory Rectangular Horn.
XXIII	Computed and measured Values of the I (Plane Polarized)
	I Plane Field Patterns of the Laboratory Rectangular Horn.
XIX	I Plane Polarized, E Plane Field Patterns of the Laboratory Rectangular Horn with Vitreous SiO_2 I Plane Plate.
XX	I Plane Polarized, I Plane Field Patterns of the Laboratory Rectangular Horn with Ceramic SiO_2 I Plane Plate.
XXI	I Plane Polarized, I Plane Field Patterns for the Laboratory Rectangular Horn with Vitreous SiO_2 E Plane Plate.
XXII	E Plane Polarized, I Plane Field Patterns for the Laboratory Rectangular Horn with Ceramic SiO_2 E Plane Plate.
XXIII	E Plane Polarized, E Plane Field Patterns for the Laboratory Rectangular Horn (with Vitreous SiO_2 I Plane Plate) with and without the Parallel Plane Reflector.
XXIV	E Plane Polarized, E Plane Field Patterns for the Laboratory Rectangular Horn (with Ceramic SiO_2 E Plane Plate) with and without the Parallel Plane Reflector.
XXV	E Plane Polarized, E Plane Field Patterns for the Laboratory Rectangular Horn with and without the Parallel Plane Reflector.

FIG. I

LATERALLY RADIATING ELECTROMAGNETIC HORN

DESIGN-TYPE A

Edw. R. Barsouk R. E. Lee

14 APRIL 1952

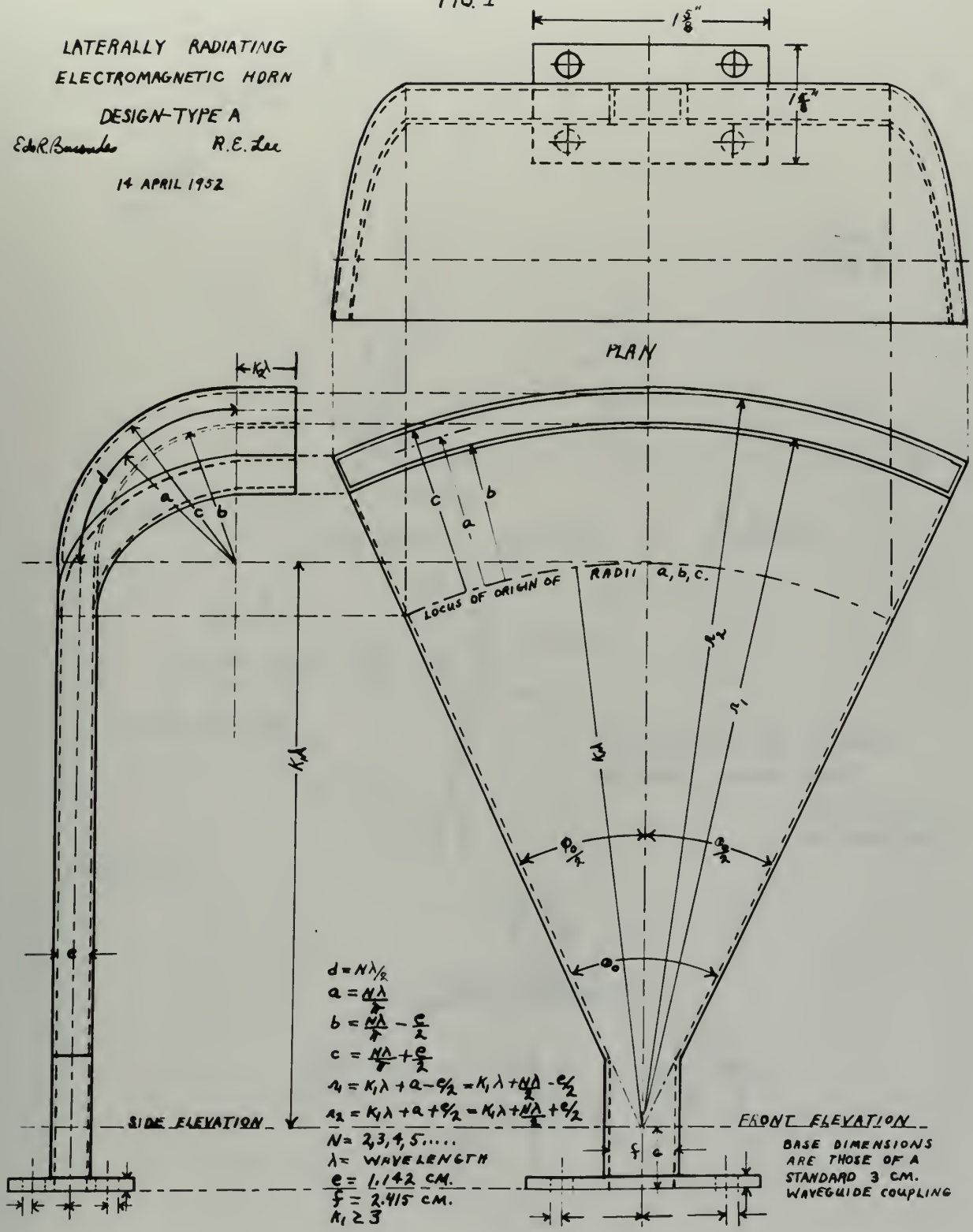

$d = N\lambda/2$

$a = \frac{N\lambda}{2}$

$b = \frac{N\lambda}{2} - \frac{e}{2}$

$c = \frac{N\lambda}{2} + \frac{e}{2}$

$r_1 = K_1\lambda + a - e/2 = K_1\lambda + \frac{N\lambda}{2} - e/2$

$r_2 = K_1\lambda + a + e/2 = K_1\lambda + \frac{N\lambda}{2} + e/2$

$N = 2, 3, 4, 5 \ldots$

λ = WAVELENGTH

$e = 1.142$ CM.

$f = 2.415$ CM.

$K_1 \geq 3$

FIG. II

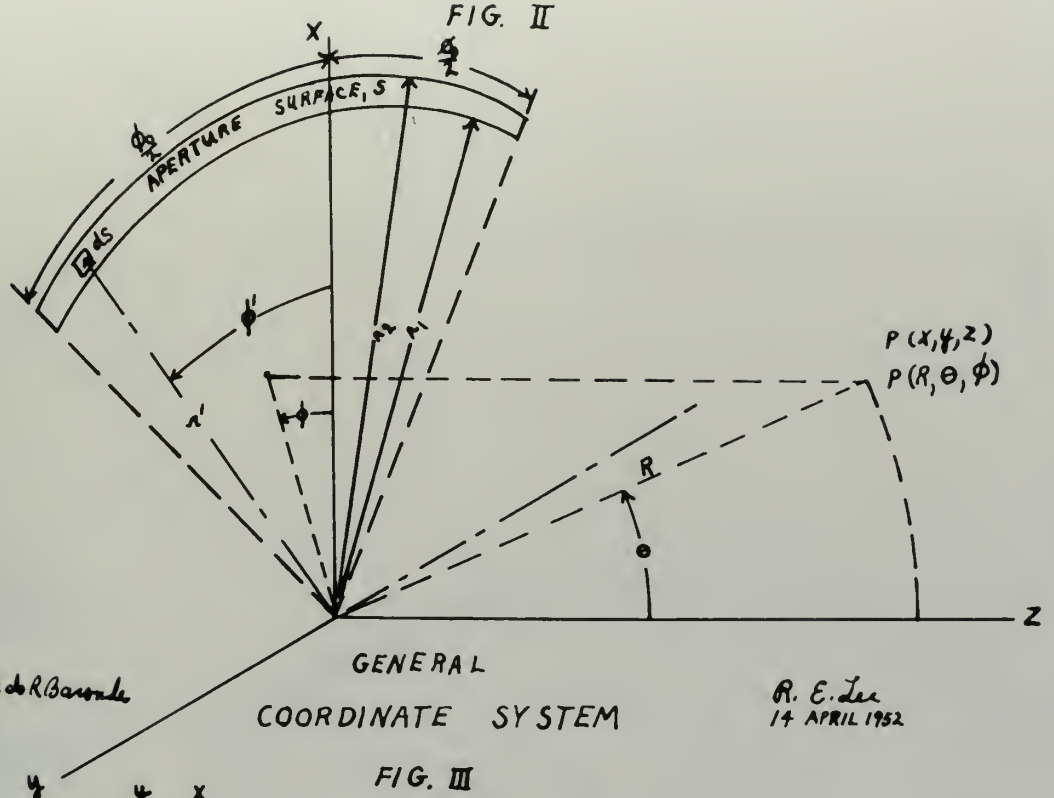

GENERAL
COORDINATE SYSTEM

E & R Barnes

R. E. Lee
14 APRIL 1952

FIG. III

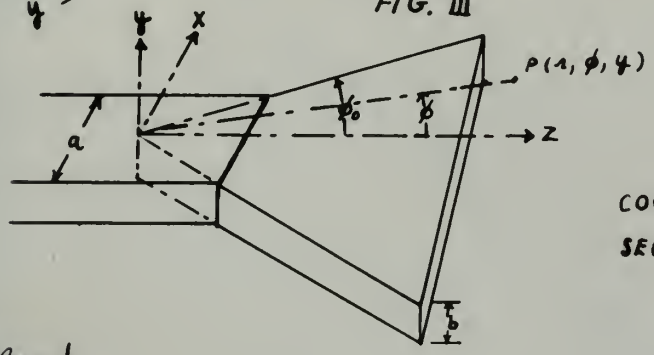

COORDINATES FOR H PLANE
SECTORAL HORN ONLY

R. E. Lee
14 APRIL 1952

E & R Barnes

FIG IV

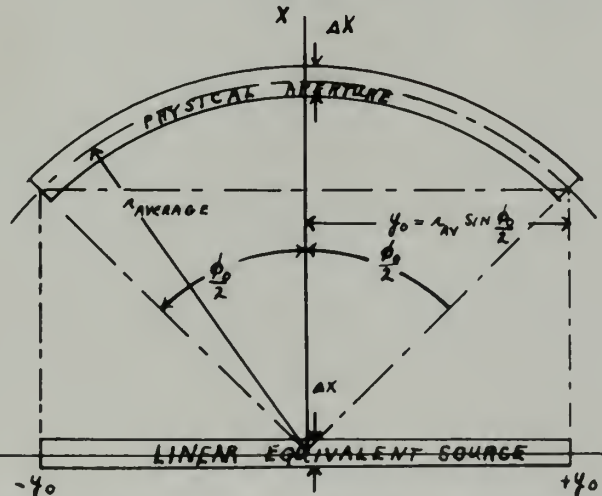

E & R Barnes

LINEAR EQUIVALENT SOURCE GEOMETRY

R.E. Lee
14 APRIL 1952

FIG. V

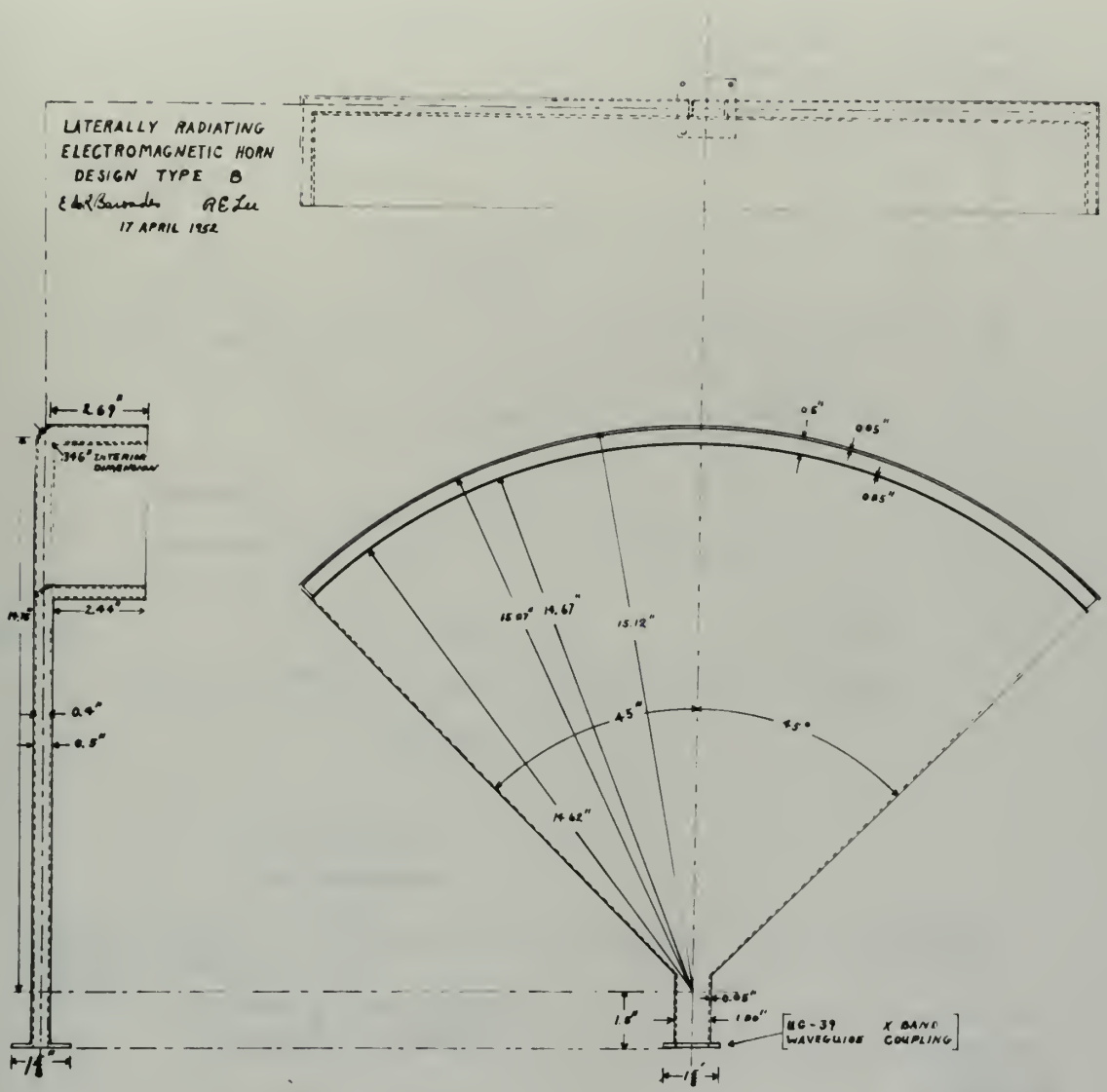
LATERALLY RADIATING
ELECTROMAGNETIC HORN
DESIGN TYPE B
E&R Baumeister R E Lee
17 APRIL 1952
2.69"
.346" INTERIOR DIMENSION
2.44"
0.4"
0.5"
0.6"
0.05"
0.05"
15.07"
14.67"
15.12"
45°
45°
14.62"
0.05"
1.8"
1.00"
MG-39 WAVEGUIDE
X BAND COUPLING

FIG. VI

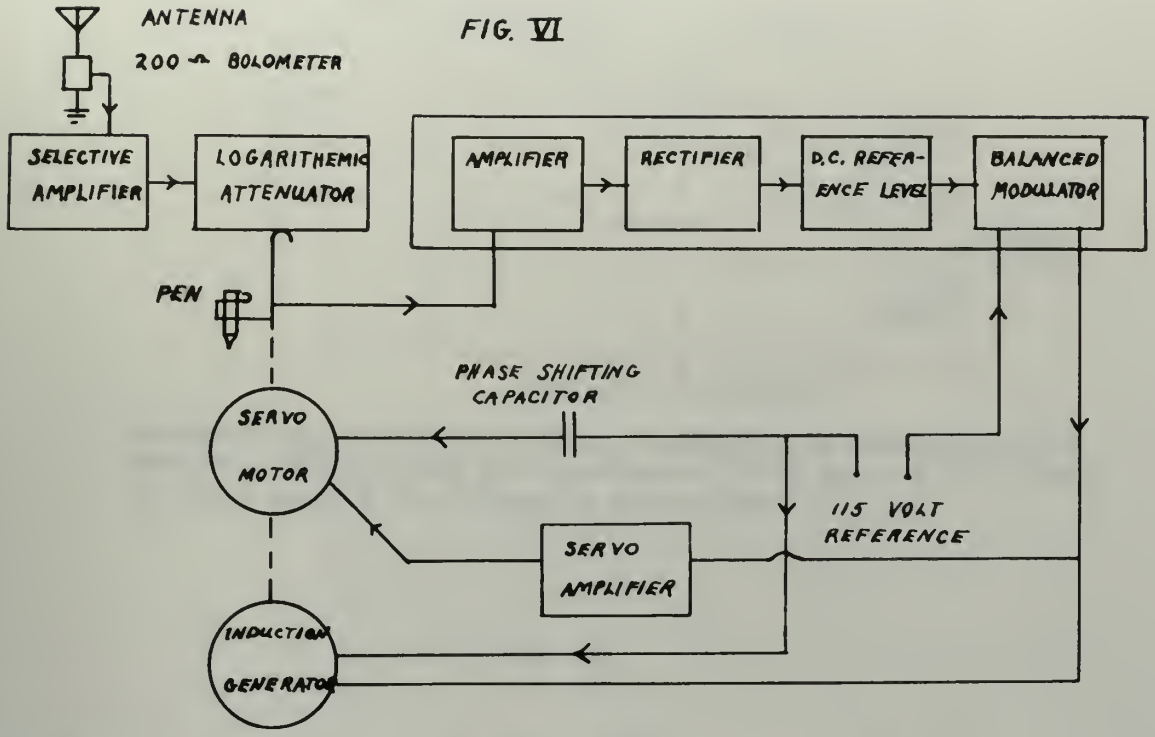

Ed R Barnes 15 APRIL 1952 R E Lee

BLOCK DIAGRAM OF THE PEN POSITIONING SYSTEM

FIG. VII

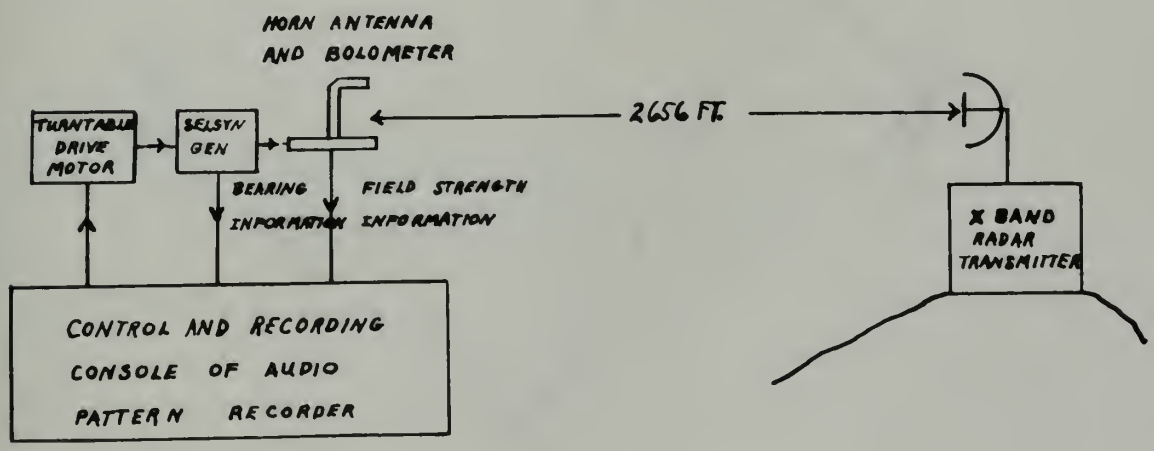

BLOCK DIAGRAM OF THE FIELD PATTERN MEASUREMENT APPARATUS

Ed R Barnes 15 APRIL 1952 R E Lee

FIG. VIII

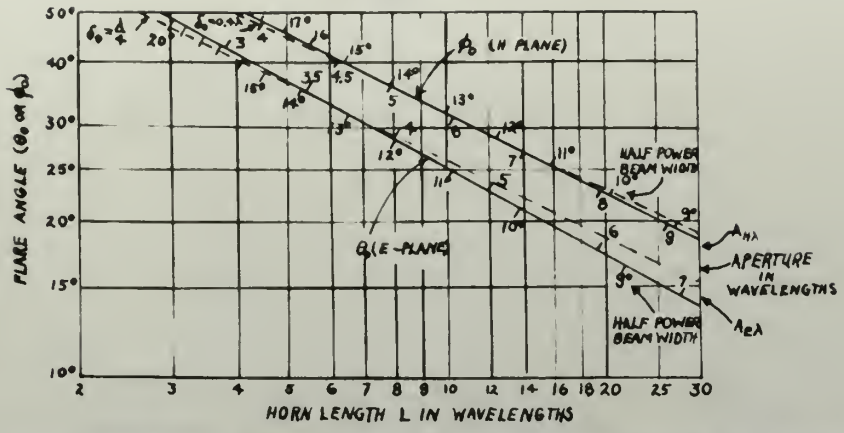

Experimentally determined optimum dimensions for rectangular horn antennas. Solid curves give relation of flare angle θ_0 in E plane and flare angle ϕ_0 in H plane to horn length.(7)

FIG. IX

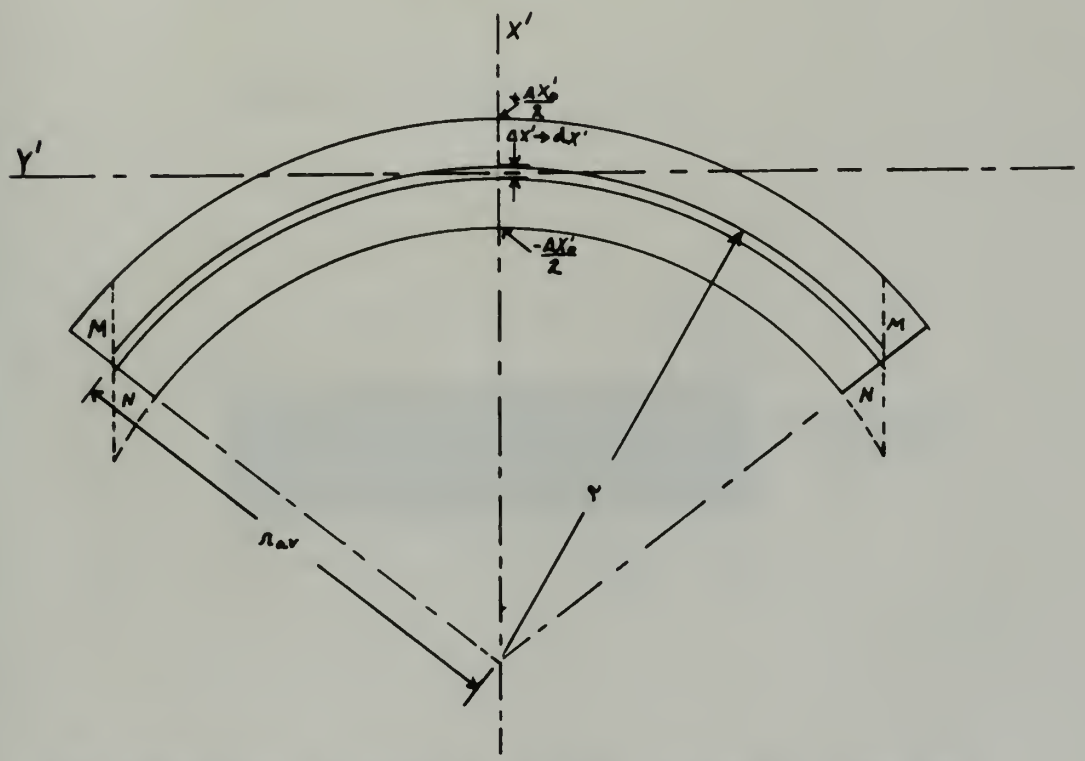

THE GEOMETRY EMPLOYED IN THE SOLUTION FOR THE E PLANE ARRAY FACTOR

E.M.R. Barnes R.E. Lee

17 APRIL 1952

FIG. X

DESCRIPTION OF FILTERS

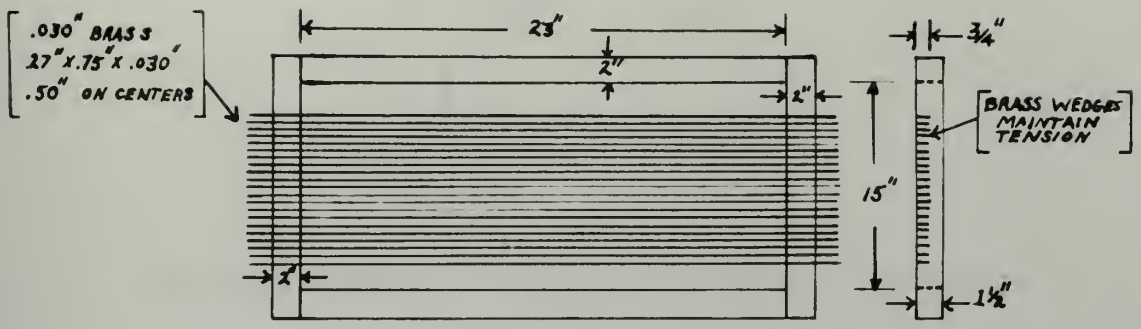

PARALLEL PLANE FILTER

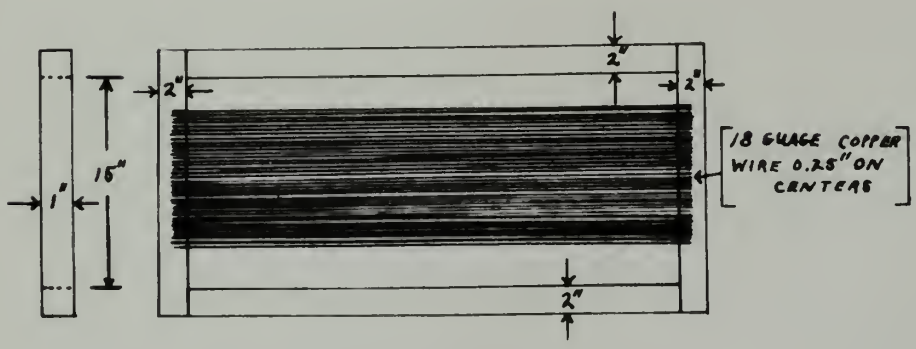

PARALLEL WIRE FILTER

E de R. Barandes

R E Lee

21 APRIL 1952

FIG. XI

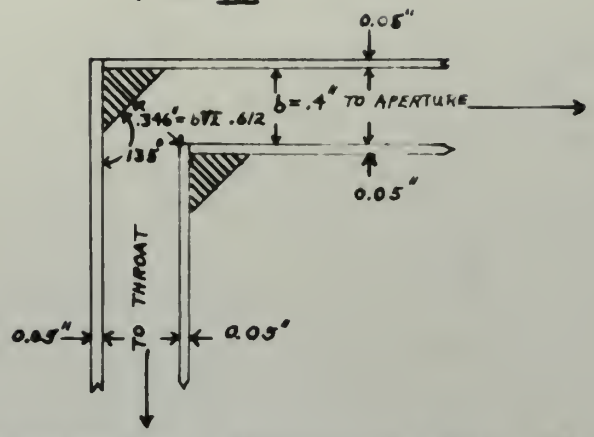

RECOMMENDED BEND CROSS SECTION DESIGN

E & R Barnes

R E Lee

24 APRIL 1952

FIG. XII

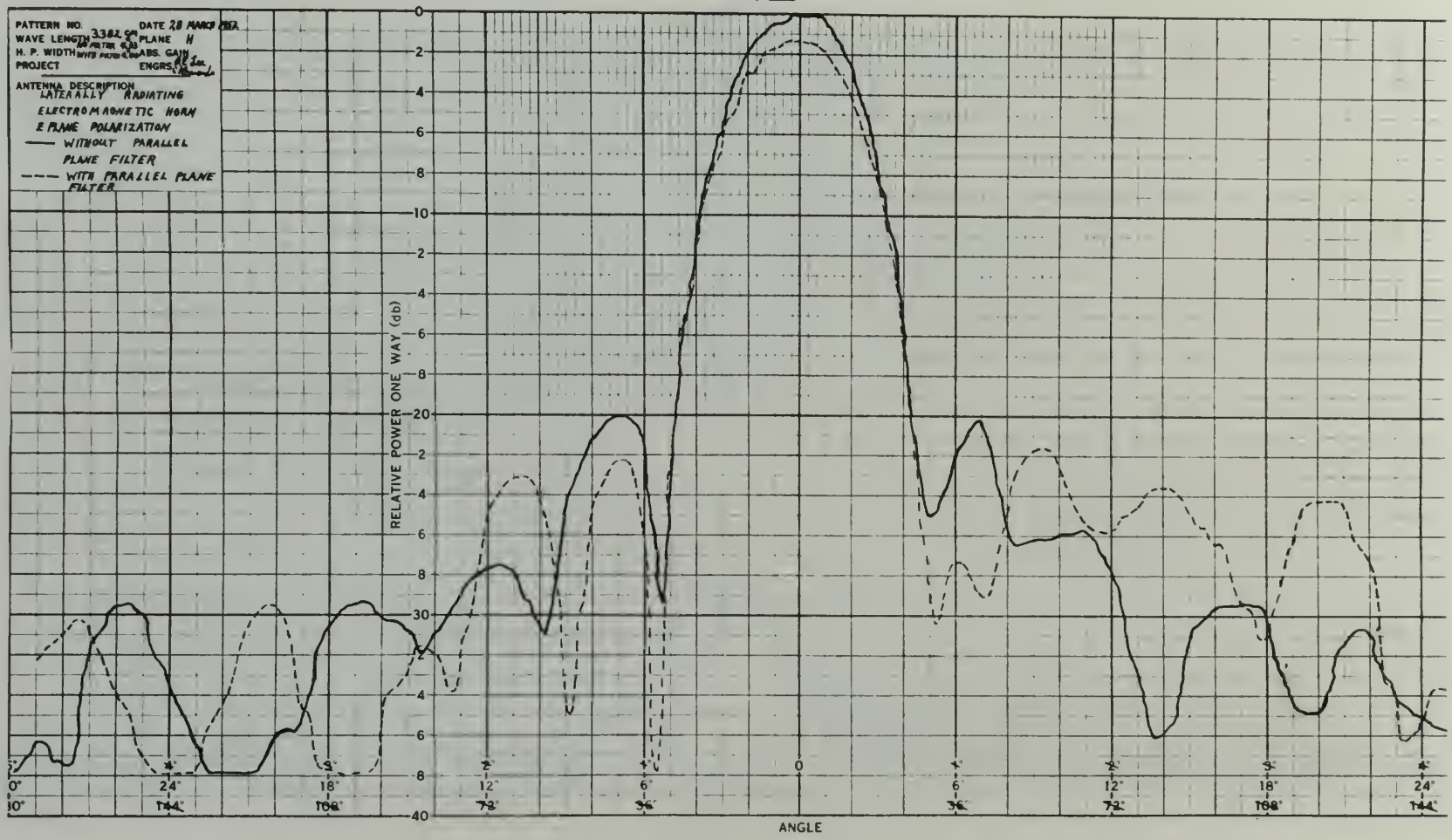
PATTERN NO.
DATE 28 MARCH 1947
WAVE LENGTH 3.382 cm
PLANE H
H. P. WIDTH
ABS. GAIN
PROJECT
ENGRS.
ANTENNA DESCRIPTION
LATERALLY RADIATING
ELECTROMAGNETIC HORN
E PLANE POLARIZATION
—— WITHOUT PARALLEL PLANE FILTER
---- WITH PARALLEL PLANE FILTER
RELATIVE POWER ONE WAY (db)
0
2
4
6
8
10
20
30
40
24°
144°
18°
108°
12°
72°
6°
36°
ANGLE

FIG. XIII

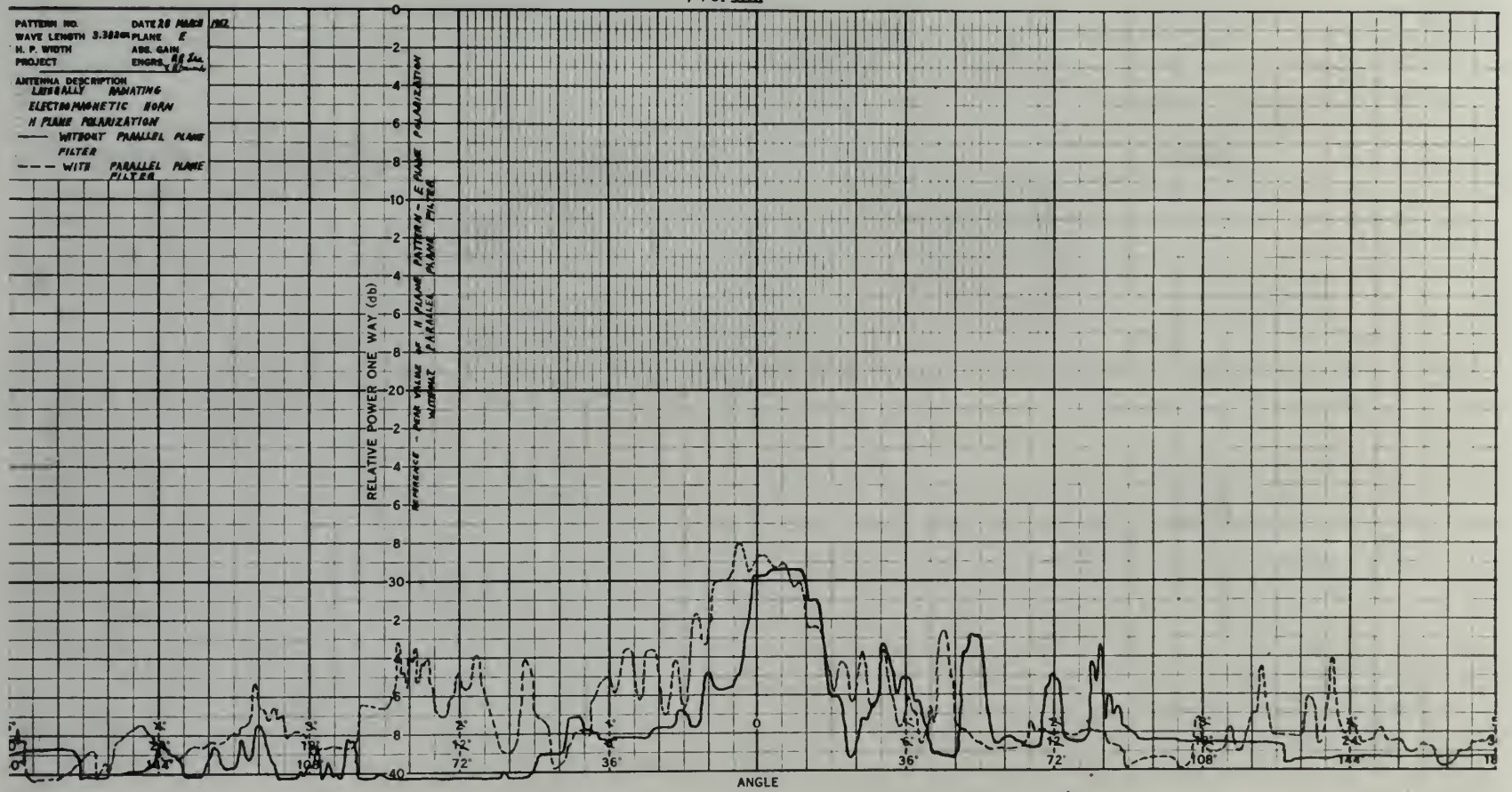
PATTERN NO.
DATE 28 MARCH 1942
WAVE LENGTH 3.382cm
PLANE E
H. P. WIDTH
ABS. GAIN
PROJECT
ENGRS.
ANTENNA DESCRIPTION
LATERALLY RADIATING
ELECTROMAGNETIC HORN
H PLANE POLARIZATION
—— WITHOUT PARALLEL PLANE FILTER
--- WITH PARALLEL PLANE FILTER
REFERENCE - PEAK VALUE OF H PLANE PATTERN - E PLANE POLARIZATION WITHOUT PARALLEL PLANE FILTER
RELATIVE POWER ONE WAY (db)
0
2
4
6
8
10
20
30
40
ANGLE
72°
36°
0
36°
72°
108°
144°

FIG. XIV

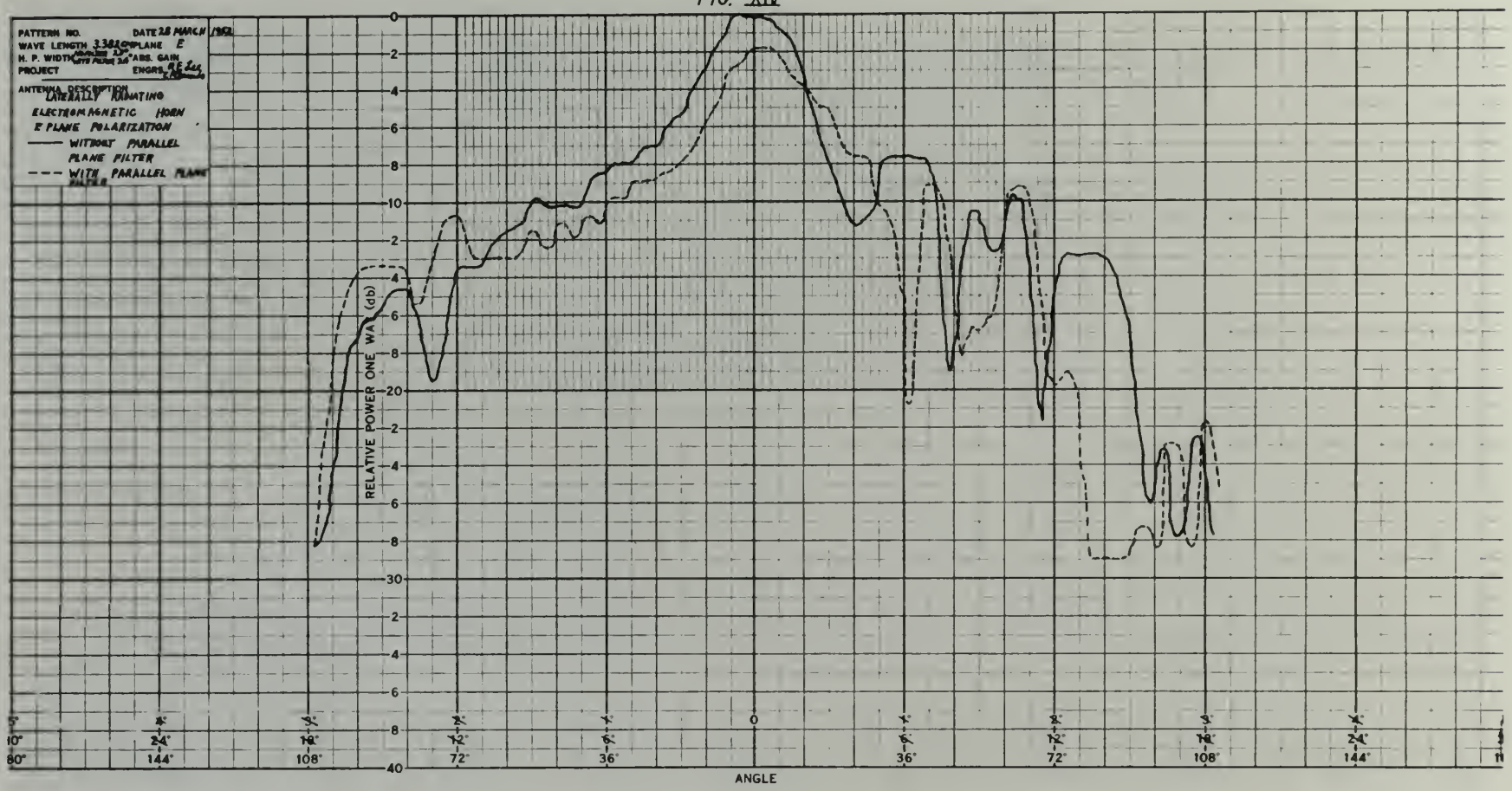
PATTERN NO.
DATE 28 MARCH 1952
WAVE LENGTH 3.381 cm PLANE E
H. P. WIDTH
ABS. GAIN
PROJECT
ENGRS.
ANTENNA DESCRIPTION
LATERALLY ROTATING
ELECTROMAGNETIC HORN
E PLANE POLARIZATION
WITHOUT PARALLEL PLANE FILTER
WITH PARALLEL PLANE FILTER
RELATIVE POWER ONE WAY (db)
0
2
4
6
8
10
20
30
40
ANGLE
5°
10°
80°
24°
144°
18°
108°
12°
72°
6°
36°
0

FIG. XV

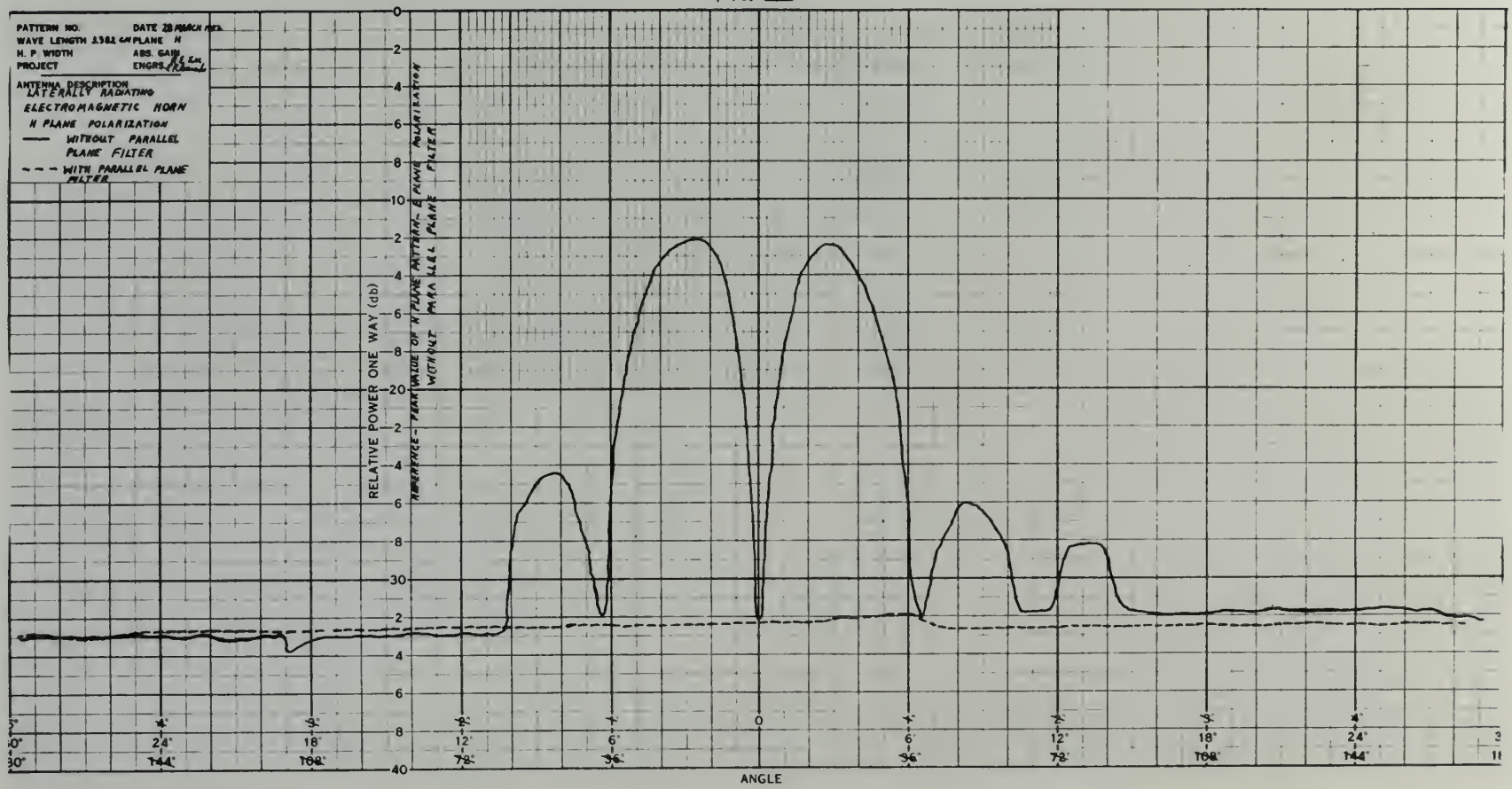
PATTERN NO.
DATE 28 MARCH 1952
WAVE LENGTH 3.982 cm
PLANE H
H. P. WIDTH
ABS. GAIN
PROJECT
ENGRS.
ANTENNA DESCRIPTION
LATERALLY RADIATING
ELECTROMAGNETIC HORN
H PLANE POLARIZATION
WITHOUT PARALLEL PLANE FILTER
WITH PARALLEL PLANE FILTER
REFERENCE - PEAK VALUE OF H PLANE PATTERN - E PLANE POLARIZATION WITHOUT PARALLEL PLANE FILTER
RELATIVE POWER ONE WAY (db)
0
2
4
6
8
10
20
30
40
24°
18°
12°
6°
0
ANGLE

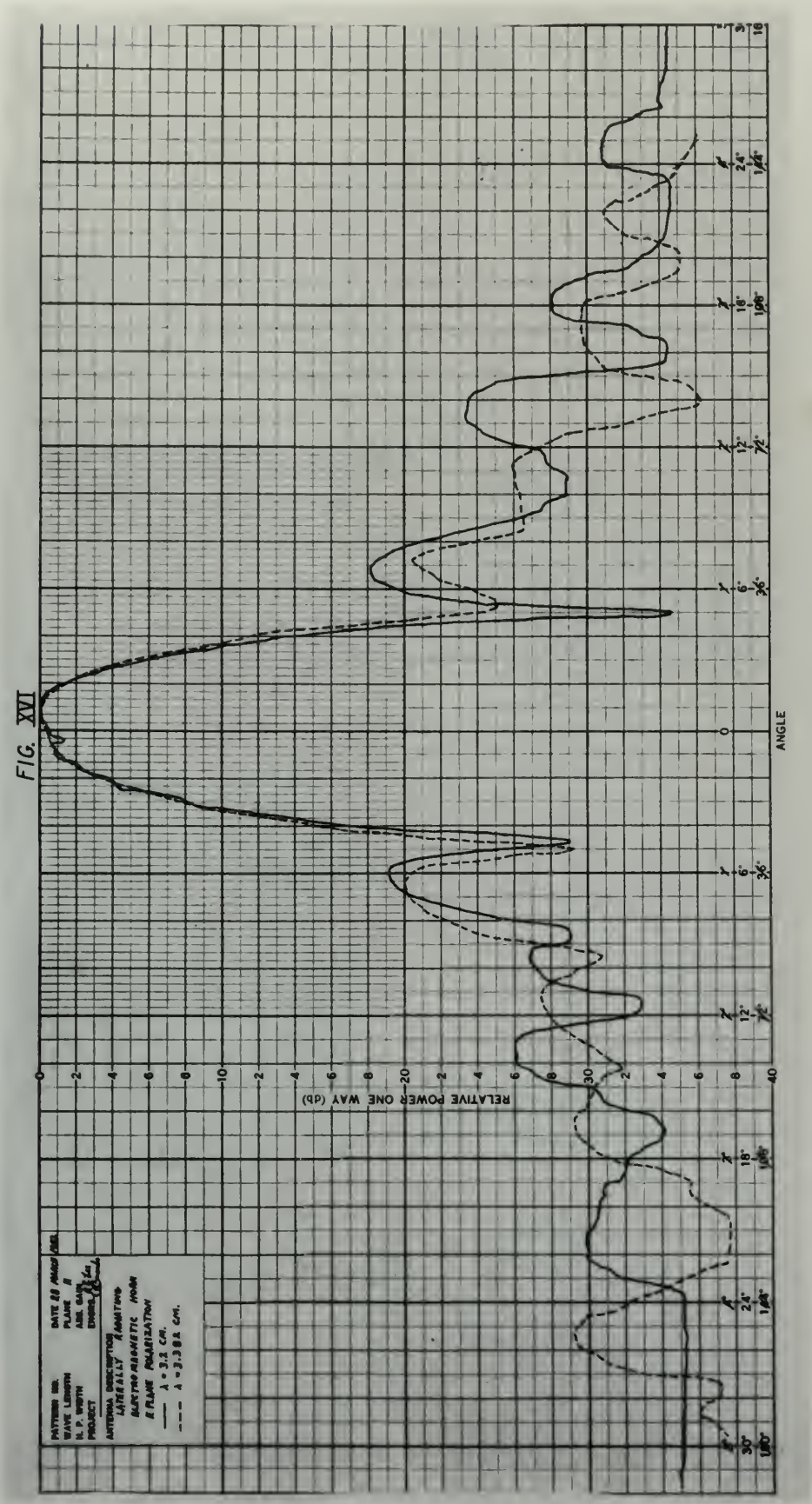
RELATIVE POWER ONE WAY (db)
ANGLE
0
-2
-4
-6
-8
-10
-20
-30
-40
2
4
6
8
30
36°
24°
18°
12°
6°
3°
1°
1.2°
1.0°
0.6°
0.5°
0.3°
0.2°
0.1°
PATTERN NO.
WAVE LENGTH
H. P. WIDTH
PROJECT
DATE AS MEASURED
PLANE
ANT. GAIN
ENGR.
ANTENNA DESCRIPTION
LATERALLY RADIATING
ELECTRO MAGNETIC HORN
E PLANE POLARIZATION
— λ = 3.2 CM.
--- λ = 3.384 CM.

FIG. XVI

FIG. XVII

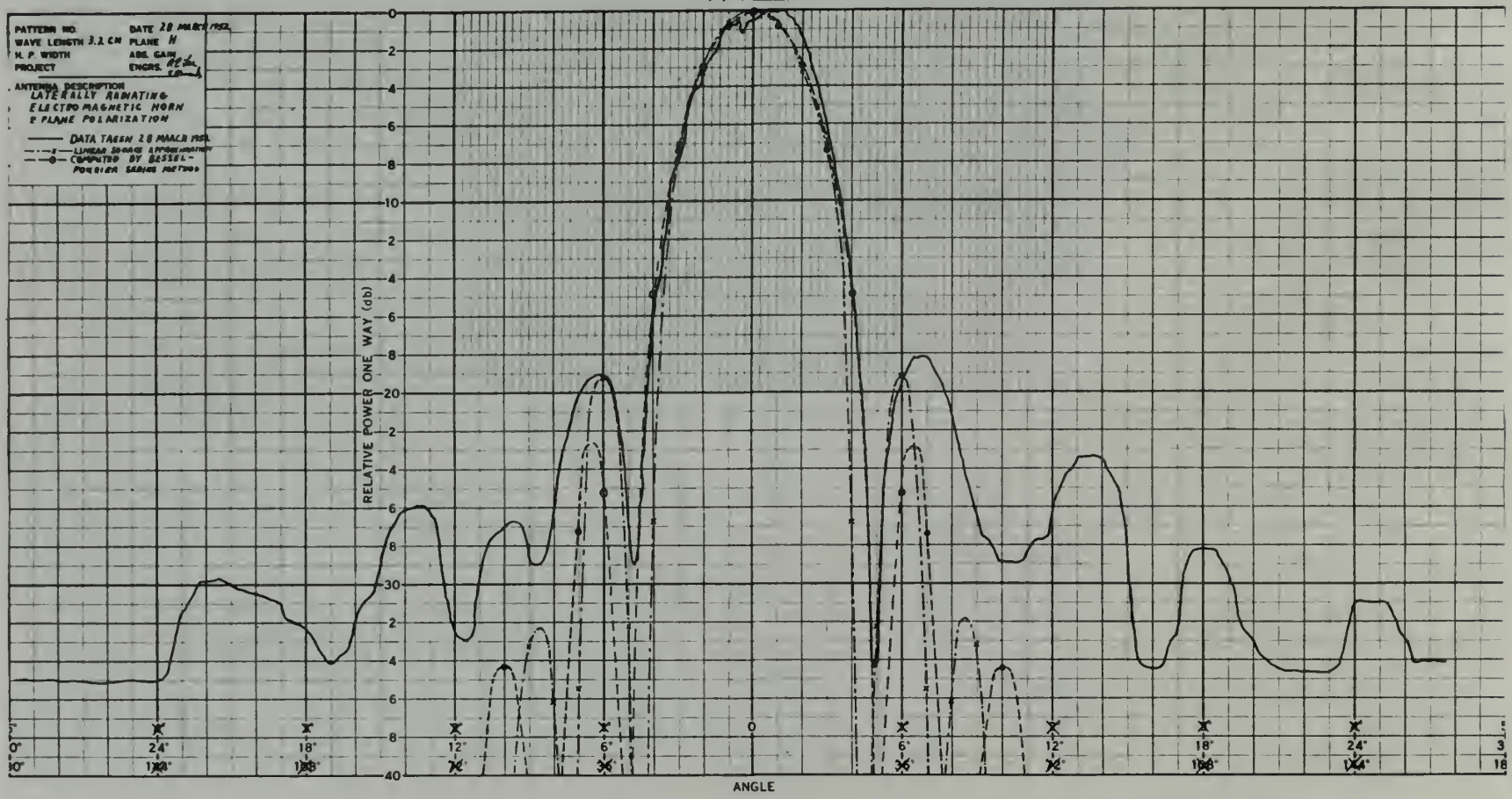
PATTERN NO.
WAVE LENGTH 3.2 CM
H. P. WIDTH
PROJECT
DATE 28 MARCH 1952
PLANE H
ABS. GAIN
ENGRS.
ANTENNA DESCRIPTION
LATERALLY RADIATING
ELECTRO MAGNETIC HORN
E PLANE POLARIZATION
DATA TAKEN 28 MARCH 1952
COMPUTED BY BESSEL-FOURIER SERIES METHOD
RELATIVE POWER ONE WAY (db)
0
2
4
6
8
10
20
30
40
24°
18°
12°
6°
0
ANGLE

FIG. XVIII

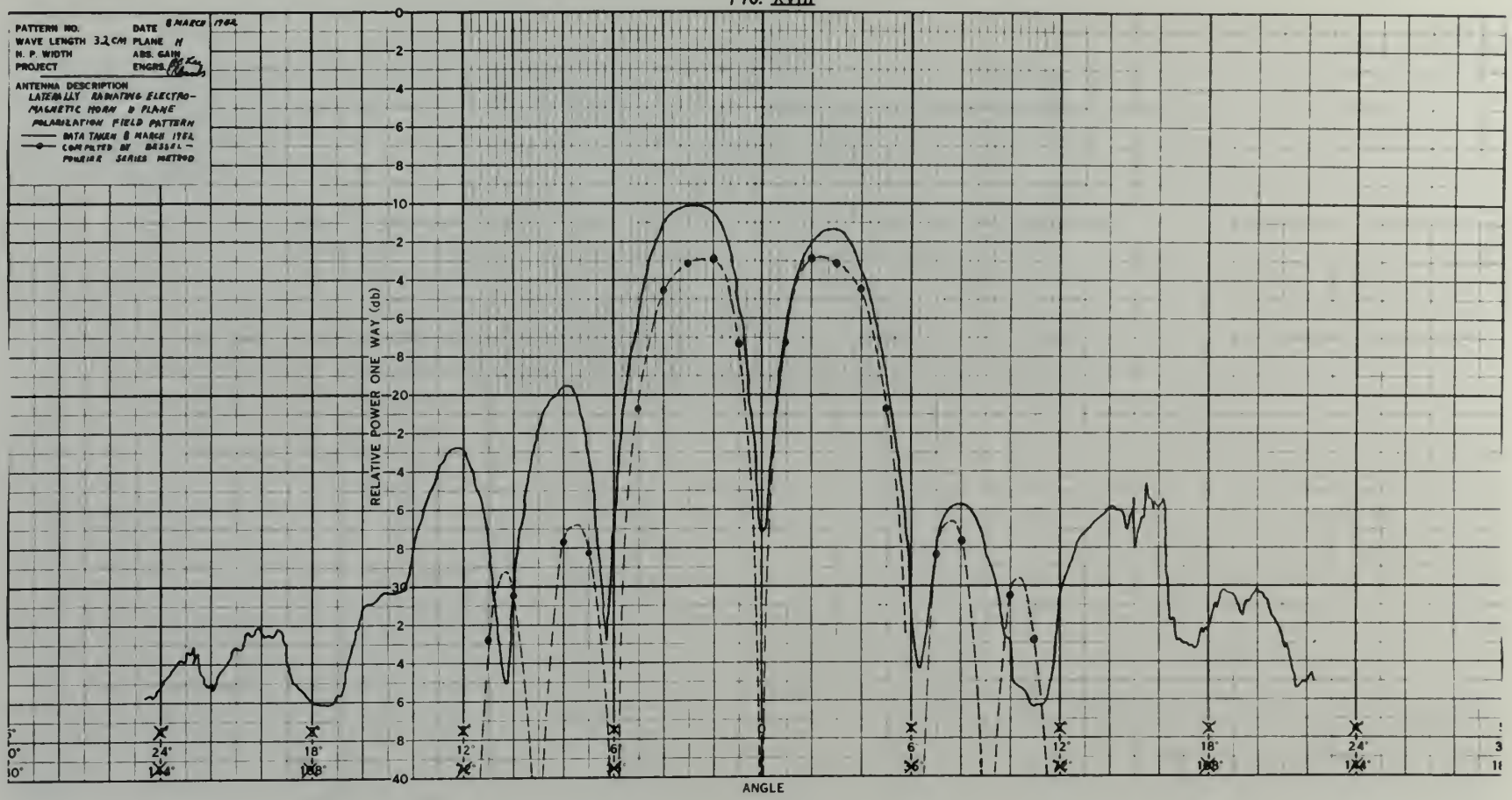
PATTERN NO.
DATE 8 MARCH 1952
WAVE LENGTH 3.2 CM
PLANE H
N. P. WIDTH
ABS. GAIN
PROJECT
ENGRS.
ANTENNA DESCRIPTION
LATERALLY RADIATING ELECTRO-MAGNETIC HORN H PLANE
POLARIZATION FIELD PATTERN
DATA TAKEN 8 MARCH 1952
COMPUTED BY BESSEL-FOURIER SERIES METHOD
RELATIVE POWER ONE WAY (db)
0
2
4
6
8
10
20
30
40
24°
18°
12°
6°
0
6°
12°
18°
24°
ANGLE

FIG. XIX

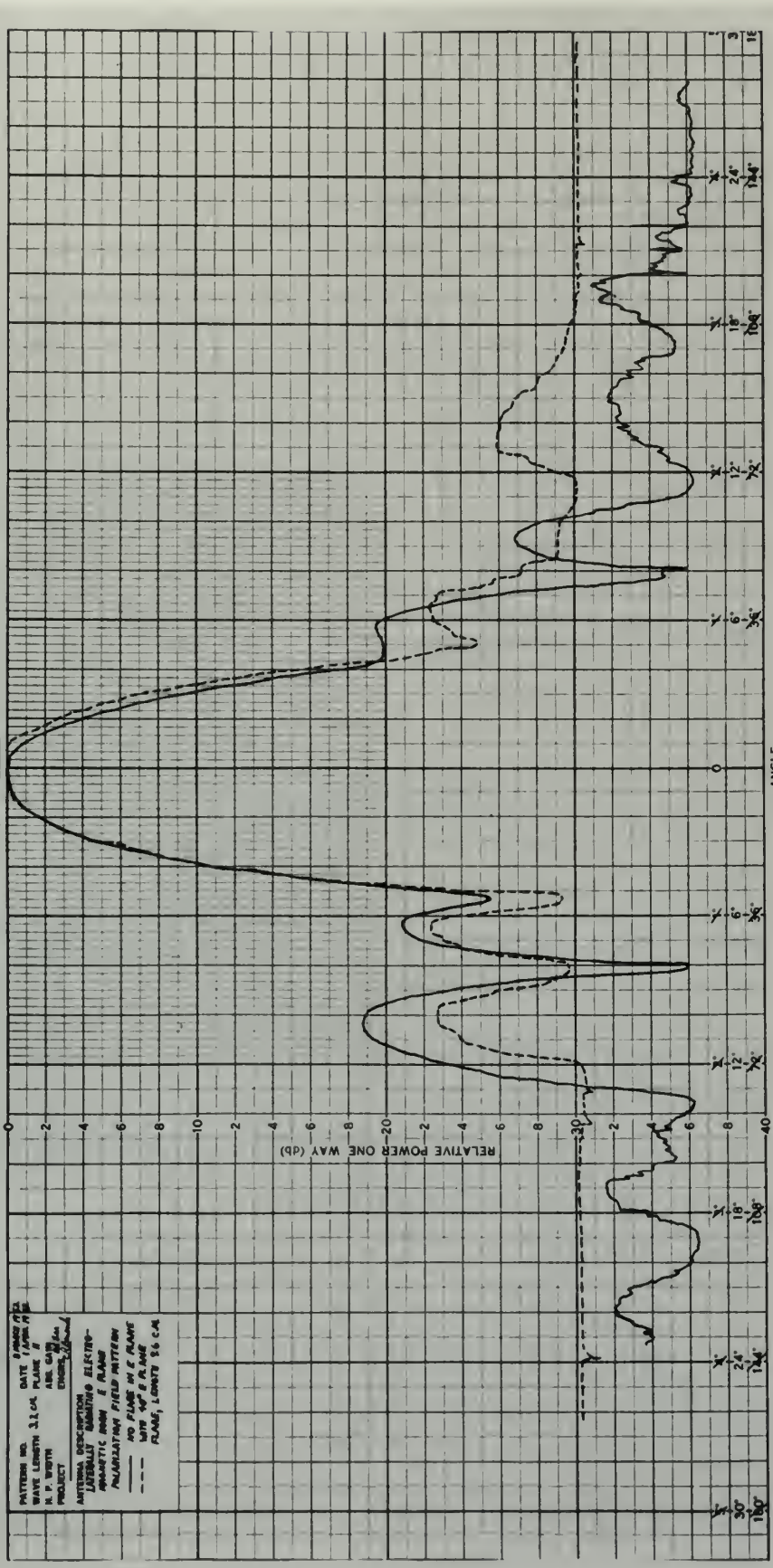
RELATIVE POWER ONE WAY (db)
ANGLE
0
2
4
6
8
10
20
30
40
180°
120°
60°
0
60°
120°
180°
PATTERN NO.
WAVE LENGTH 3.1 CM
H. P. WIDTH
PROJECT
DATE
PLANE H
ANTENNA DESCRIPTION
LATERALLY RADIATING ELECTRO-MAGNETIC HORN E PLANE POLARIZATION FIELD PATTERN
NO FLARE IN E PLANE
WITH 90° E PLANE FLARE, LENGTH 5.6 C.M.

FIG. XX

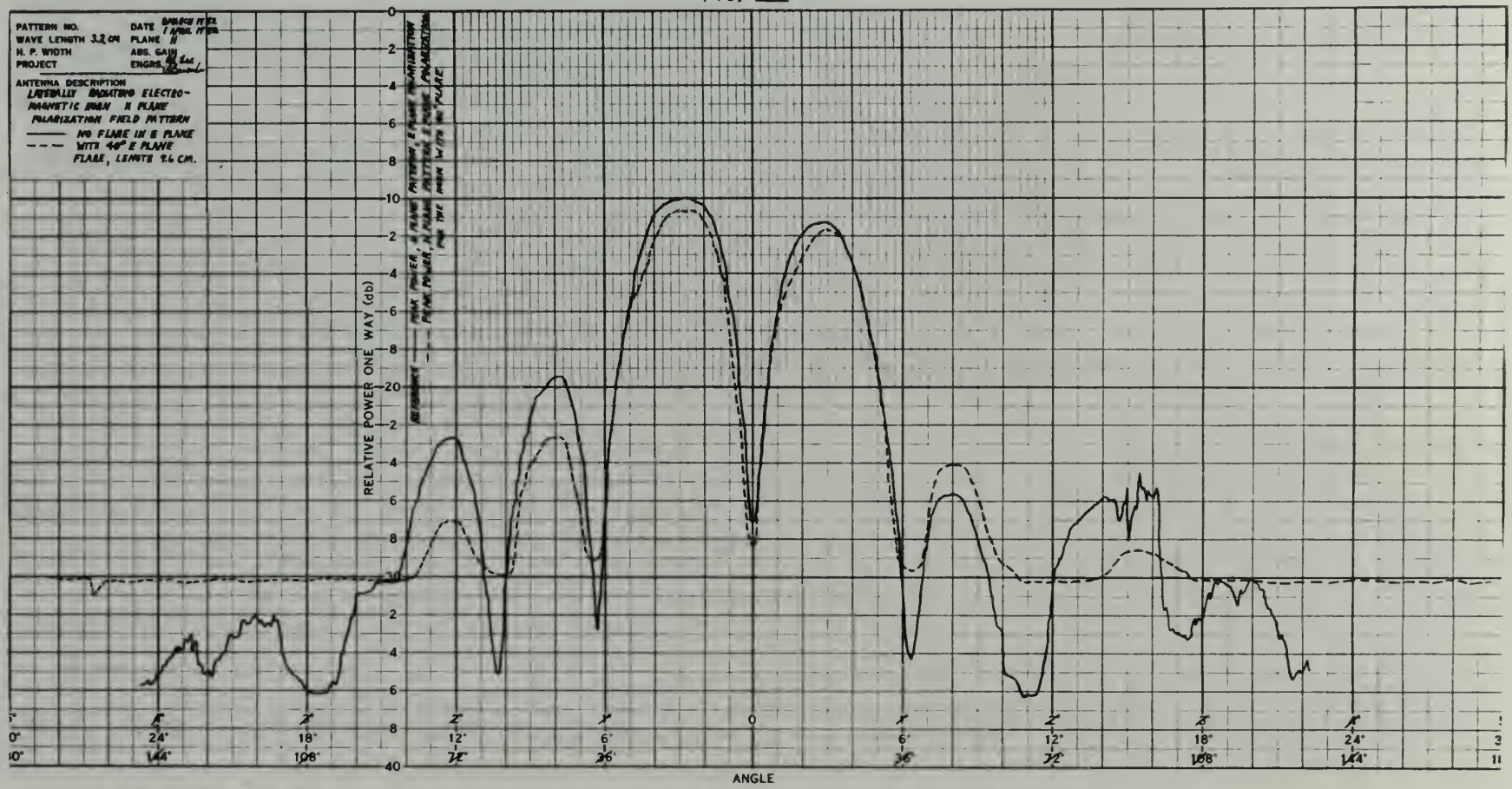
PATTERN NO.
DATE
WAVE LENGTH 3.2 CM
PLANE H
H. P. WIDTH
ABS. GAIN
PROJECT
ENGRS.
ANTENNA DESCRIPTION
LATERALLY ROTATING ELECTRO-MAGNETIC HORN H PLANE POLARIZATION FIELD PATTERN
——— NO FLARE IN E PLANE
– – – WITH 40° E PLANE FLARE, LENGTH 9.6 CM.
RELATIVE POWER ONE WAY (db)
0
2
4
6
8
10
20
40
24°
144°
18°
108°
12°
72°
6°
36°
0
ANGLE

FIG XXI

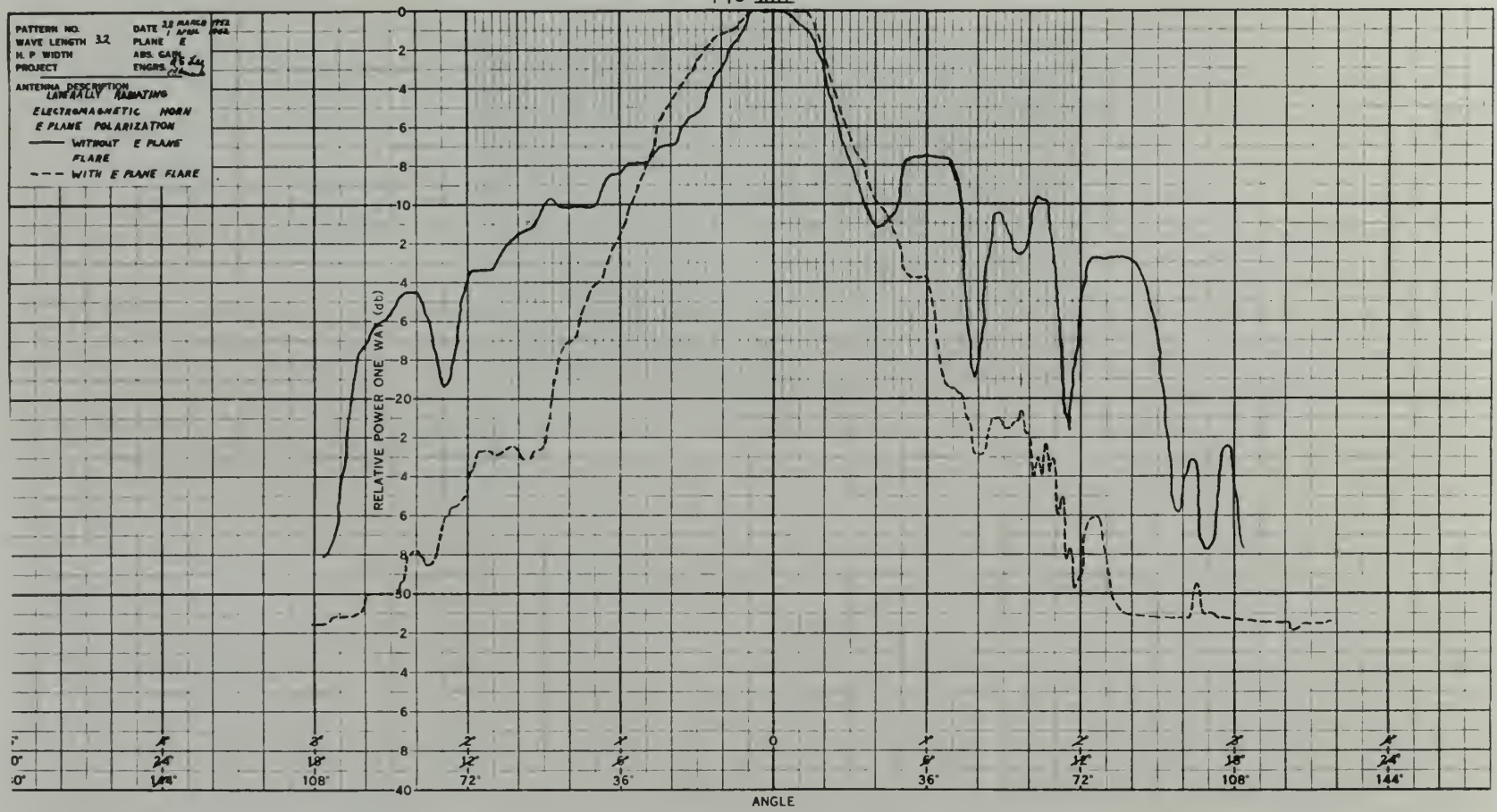
PATTERN NO.
WAVE LENGTH 3.2
H. P WIDTH
PROJECT
DATE 28 MARCH 1952
PLANE E
ABS. GAIN
ENGRS.
ANTENNA DESCRIPTION
LONGITUDINALLY RADIATING
ELECTROMAGNETIC HORN
E PLANE POLARIZATION
WITHOUT E PLANE FLARE
WITH E PLANE FLARE
RELATIVE POWER ONE WAY (db)
0
2
4
6
8
10
20
30
40
144°
108°
72°
36°
0
36°
72°
108°
144°
ANGLE

FIG. XXII

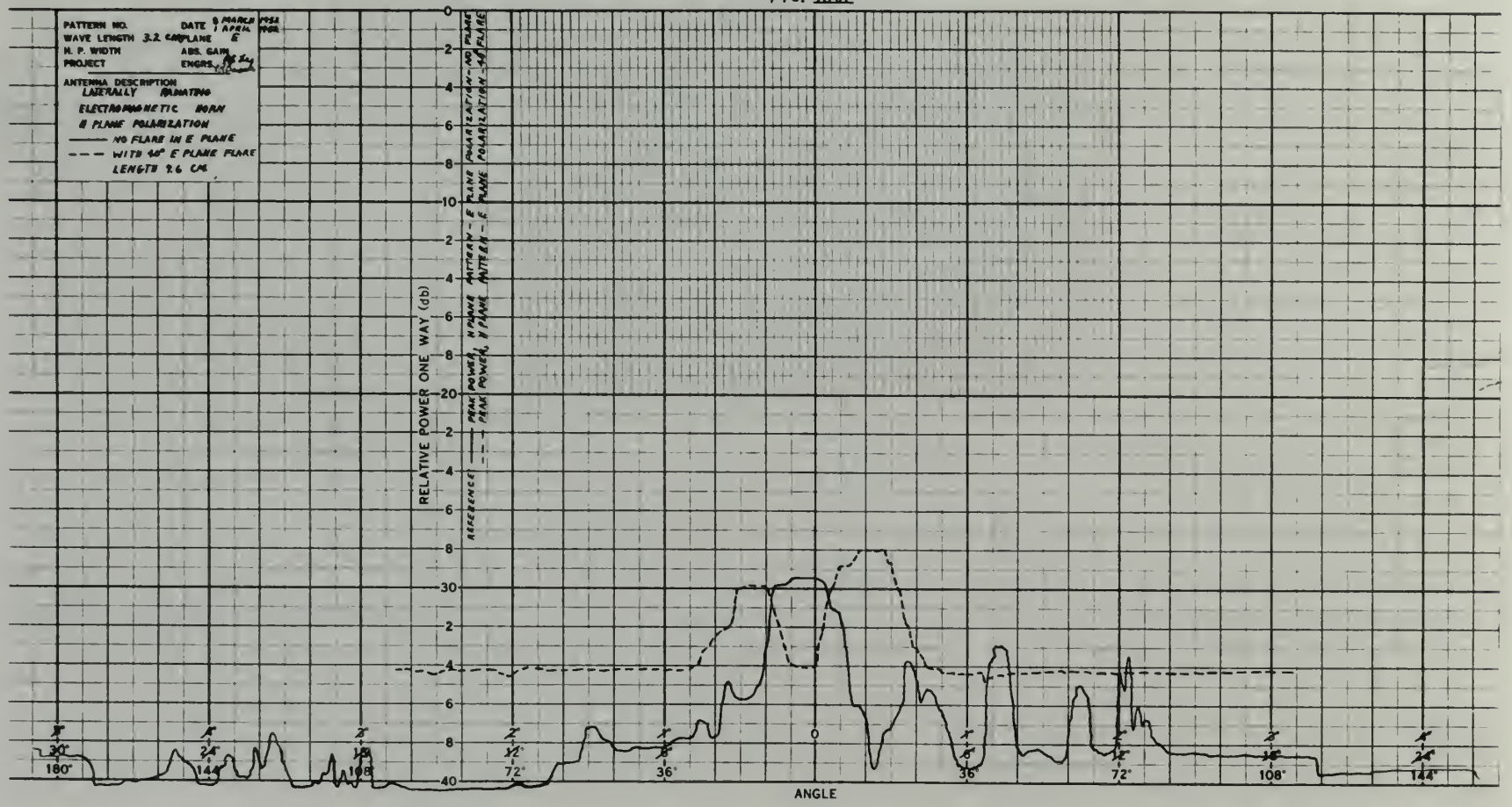
PATTERN NO.
DATE 9 MARCH 1951
WAVE LENGTH 3.2 CM PLANE E
H. P. WIDTH
ABS. GAIN
PROJECT
ENGRS.
ANTENNA DESCRIPTION
LATERALLY RADIATING
ELECTROMAGNETIC HORN
E PLANE POLARIZATION
——— NO FLARE IN E PLANE
– – – WITH 40° E PLANE FLARE
LENGTH 7.6 CMS.
REFERENCE
PEAK POWER, H PLANE ANTENNA - E PLANE POLARIZATION - NO FLARE
PEAK POWER, H PLANE ANTENNA - E PLANE POLARIZATION - 40° FLARE
RELATIVE POWER ONE WAY (db)
0
2
4
6
8
10
20
30
40
180°
144°
108°
72°
36°
0
36°
72°
108°
144°
ANGLE

FIG. XXIII

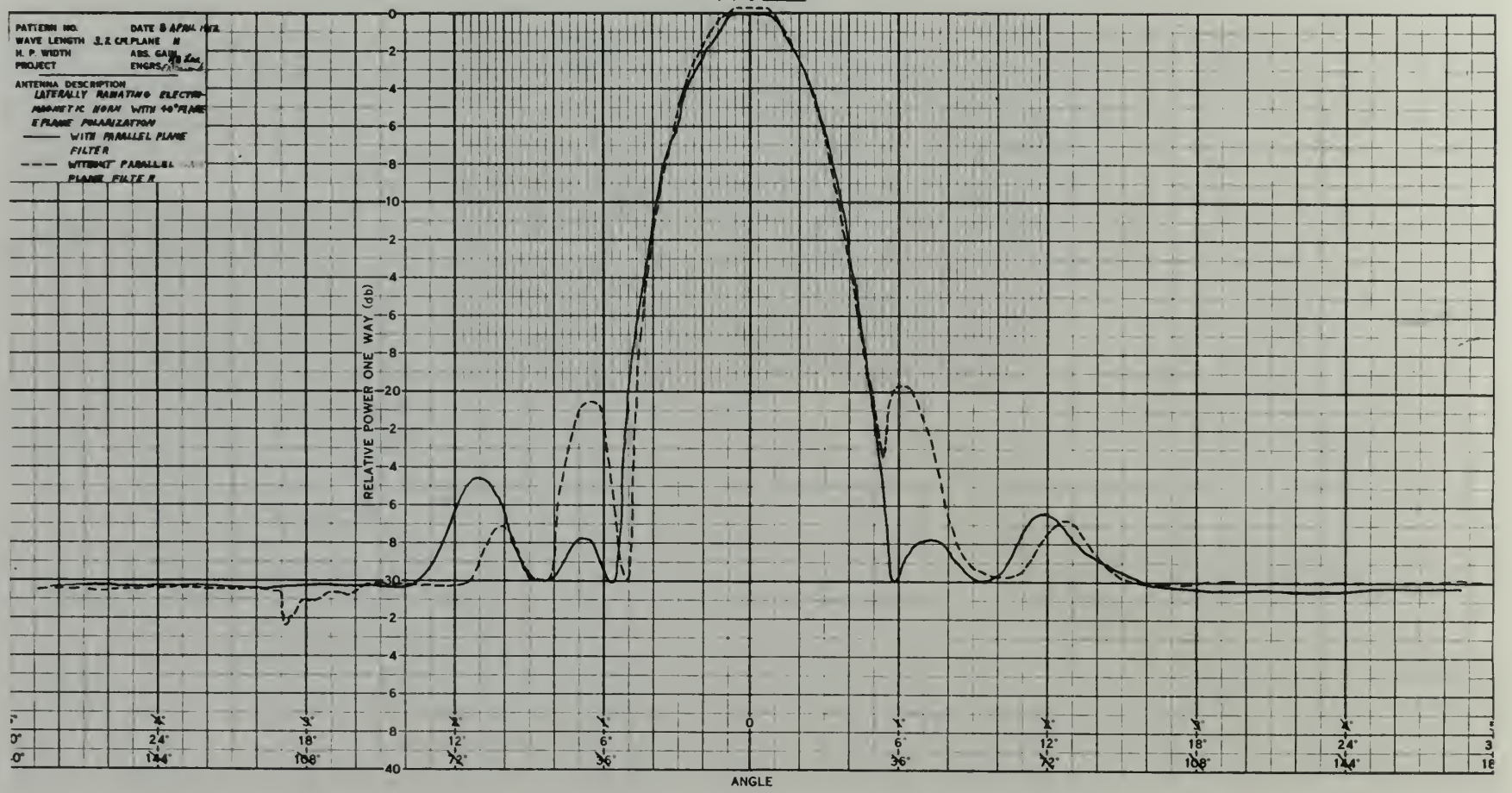
PATTERN NO.
DATE 8 APRIL 1942
WAVE LENGTH 3.2 CM. PLANE H
H. P. WIDTH
ABS. GAIN
PROJECT
ENGRS.
ANTENNA DESCRIPTION
LATERALLY RADIATING ELECTRO-MAGNETIC HORN WITH 40° FLARE
E PLANE POLARIZATION
WITH PARALLEL PLANE FILTER
WITHOUT PARALLEL PLANE FILTER
RELATIVE POWER ONE WAY (db)
0
2
4
6
8
10
20
30
40
24°
144°
18°
108°
12°
72°
6°
36°
0
ANGLE

FIG. XXIV

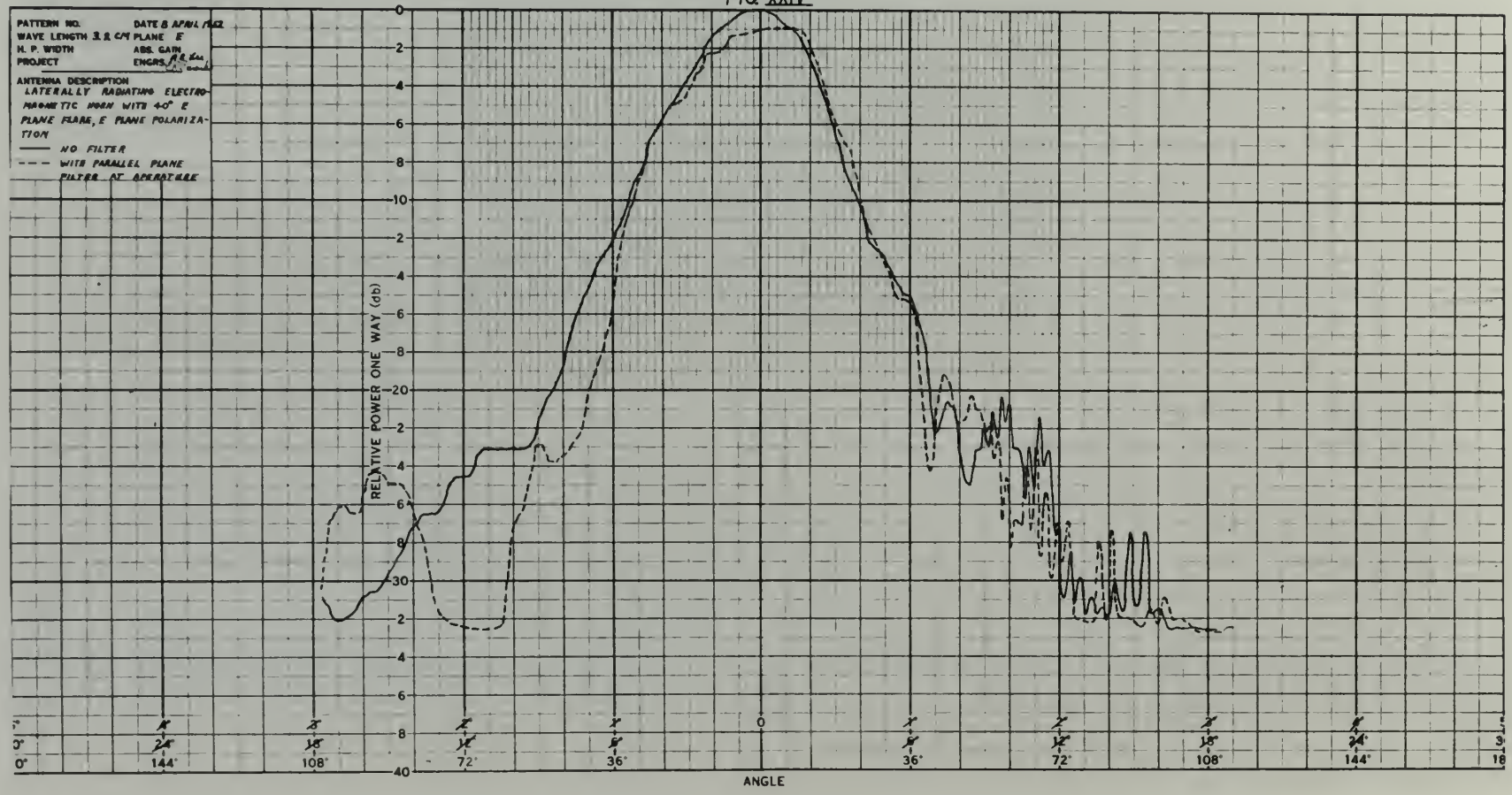
PATTERN NO.
DATE 8 APRIL 1942
WAVE LENGTH 3.2 CM
PLANE E
H. P. WIDTH
ABS. GAIN
PROJECT
ENGRS.
ANTENNA DESCRIPTION
LATERALLY RADIATING ELECTRO-MAGNETIC HORN WITH 40° E PLANE FLARE, E PLANE POLARIZATION
NO FILTER
WITH PARALLEL PLANE FILTER AT APERATURE
RELATIVE POWER ONE WAY (db)
0
2
4
6
8
10
20
30
40
144°
108°
72°
36°
0
36°
72°
108°
144°
ANGLE

FIG. XXV

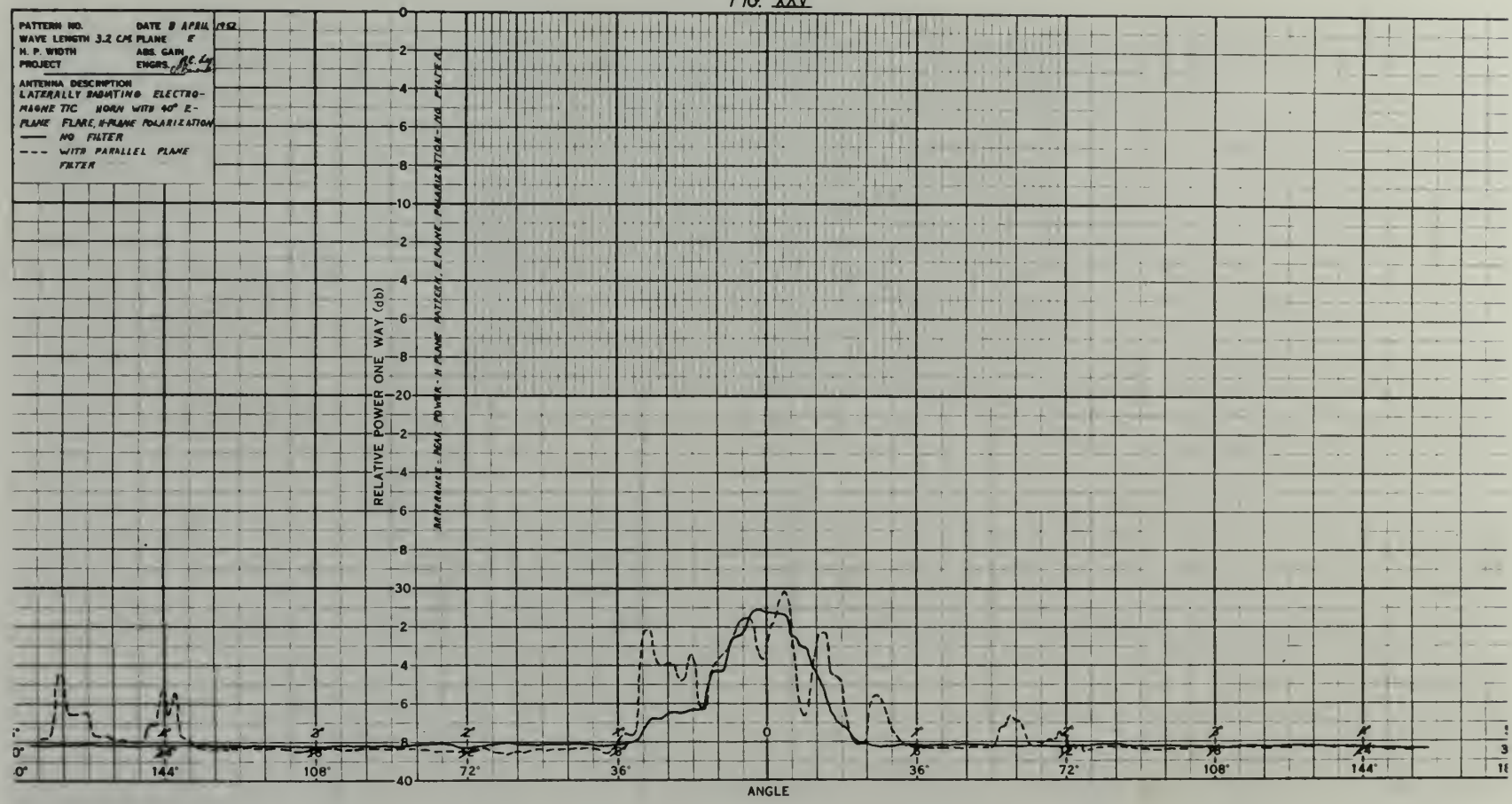
PATTERN NO.
DATE 8 APRIL 1952
WAVE LENGTH 3.2 CMS PLANE E
H. P. WIDTH
ABS. GAIN
PROJECT
ENGRS.
ANTENNA DESCRIPTION
LATERALLY RADIATING ELECTRO-MAGNETIC HORN WITH 40° E-PLANE FLARE, H-PLANE POLARIZATION
—— NO FILTER
--- WITH PARALLEL PLANE FILTER
REFERENCE = HOM POWER - H PLANE PATTERN, E PLANE POLARIZATION - NO FILTER
RELATIVE POWER ONE WAY (db)
0
2
4
6
8
10
20
30
40
144°
108°
72°
36°
0
36°
72°
108°
144°
ANGLE

FIG. XXVI

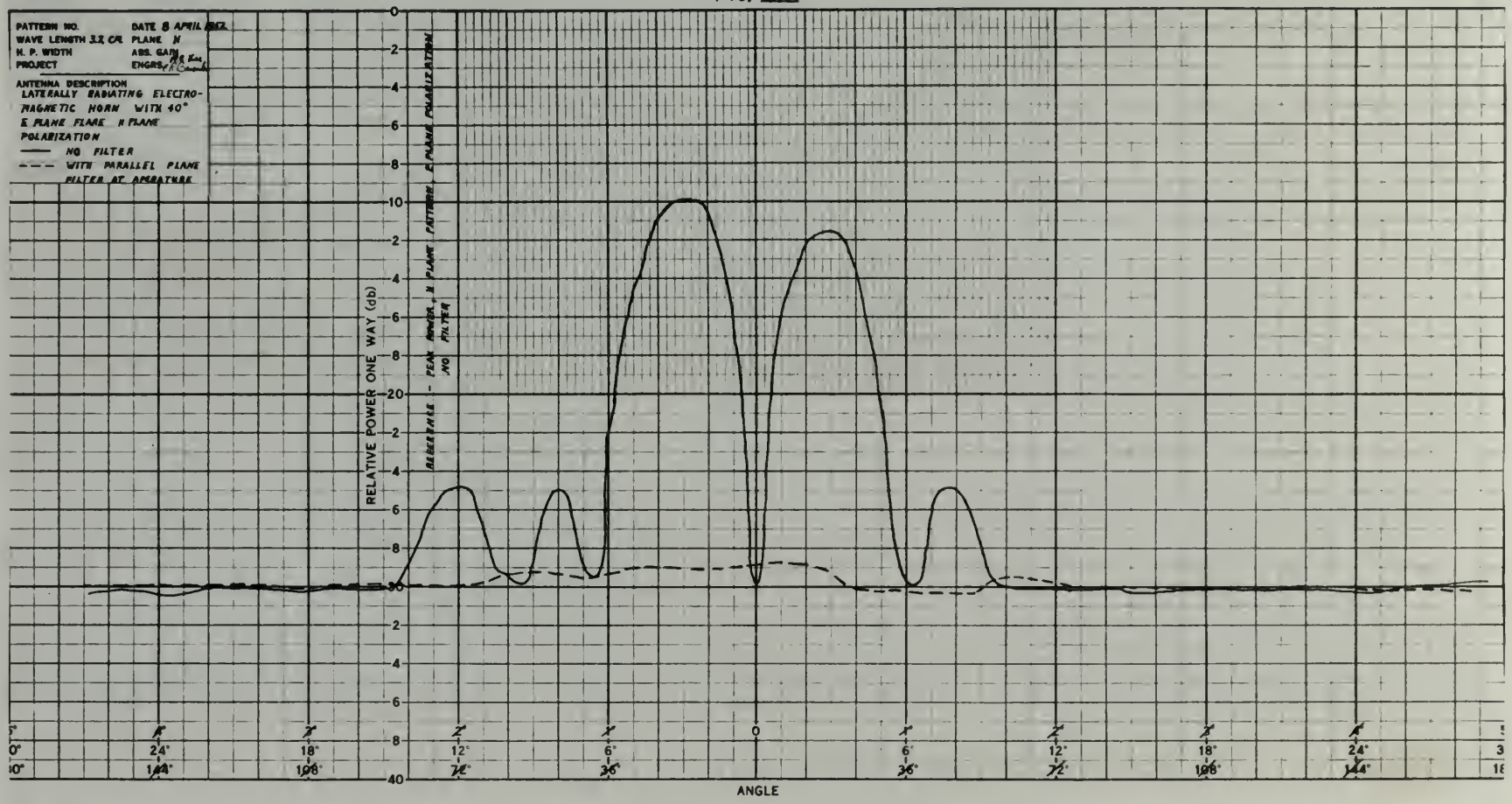
PATTERN NO.
DATE 8 APRIL 1942
WAVE LENGTH 3.2 CM
PLANE H
H. P. WIDTH
ABS. GAIN
PROJECT
ENGRS.
ANTENNA DESCRIPTION
LATERALLY RADIATING ELECTRO-MAGNETIC HORN WITH 40° E PLANE FLARE H PLANE POLARIZATION
NO FILTER
WITH PARALLEL PLANE FILTER AT APERATURE
REFERENCE - PEAK POWER, H PLANE PATTERN, E PLANE POLARIZATION, NO FILTER
RELATIVE POWER ONE WAY (db)
0
2
4
6
8
10
20
30
40
24°
18°
12°
6°
0
6°
12°
18°
24°
144°
108°
72°
36°
36°
72°
108°
144°
ANGLE

FIG. XXVII

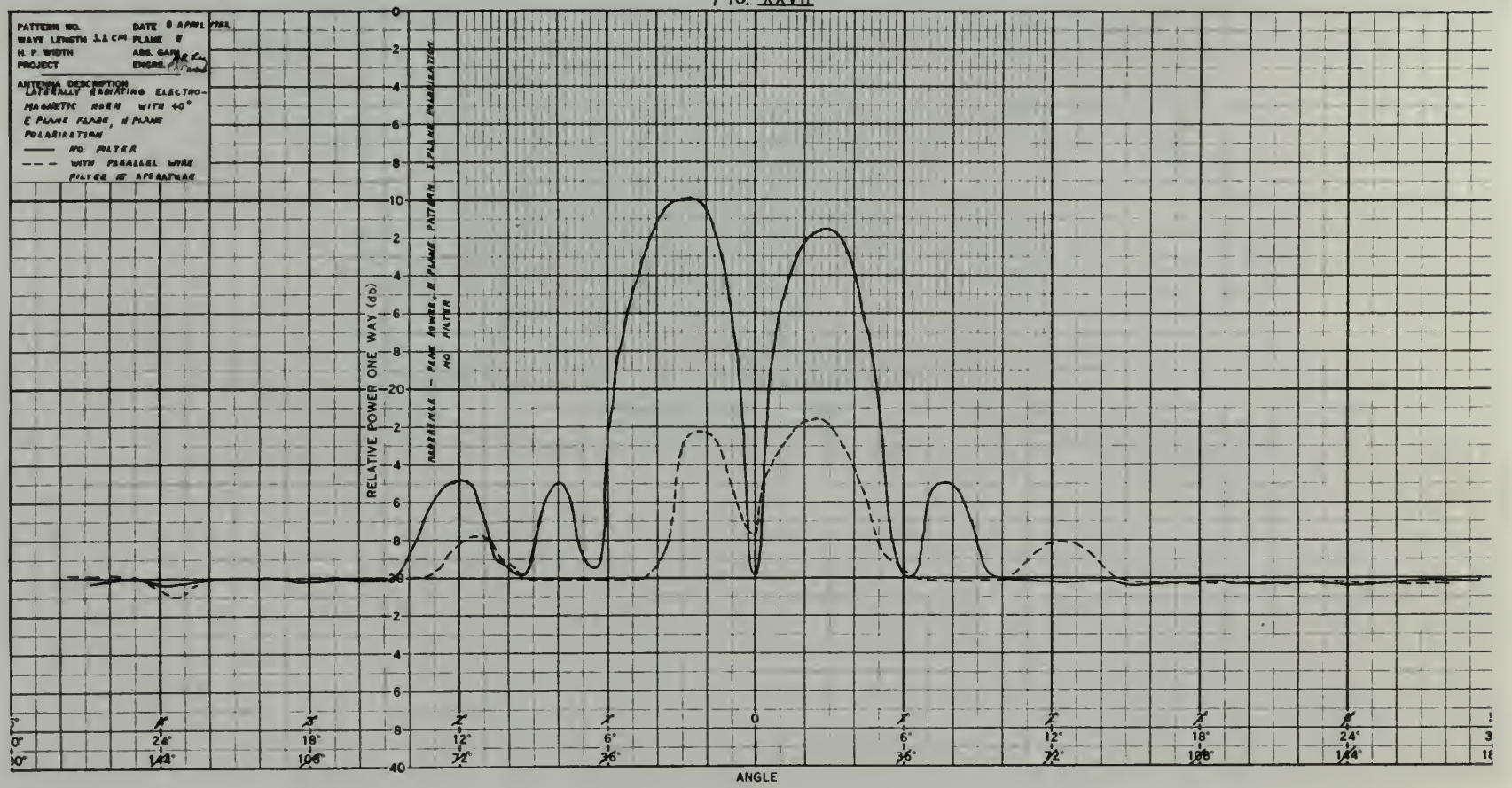
PATTERN NO.
DATE 8 APRIL 1952
WAVE LENGTH 3.2 CM
PLANE H
H. P. WIDTH
ABS. GAIN
PROJECT
ENGRS.
ANTENNA DESCRIPTION
LATERALLY RADIATING ELECTRO-MAGNETIC HORN WITH 40° E PLANE FLARE, H PLANE POLARIZATION
—— NO FILTER
– – – WITH PARALLEL WIRE FILTER IN APERATURE
REFERENCE - PEAK POWER, H PLANE PATTERN, E PLANE POLARIZATION NO FILTER
RELATIVE POWER ONE WAY (db)
0
2
4
6
8
10
2
4
6
8
20
2
4
6
8
30
2
4
6
8
40
24°
144°
18°
108°
12°
72°
6°
36°
0
6°
36°
12°
72°
18°
108°
24°
144°
ANGLE

FIG. XXVIII

PLOT OF ELLIPTICITY OF THE LATERALLY RADIATING ELECTRO-MAGNETIC HORN FOR POSITIVE e AND RIGHT ELLIPTICAL POLARIZATION

P.deR.Bourdeau R.E.Lee

16 April 1952

Relative Power is in Brackets

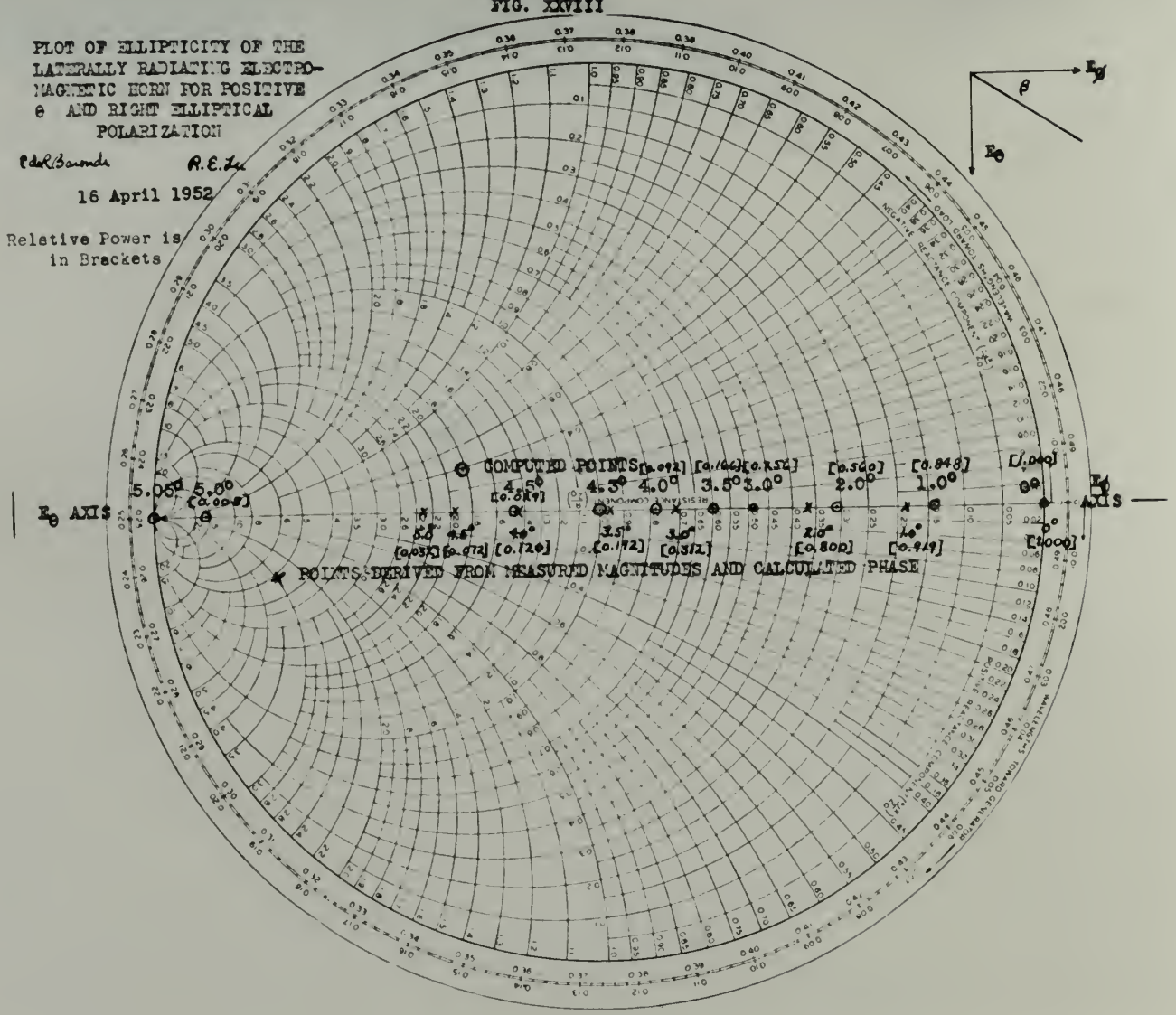

FIG. XXIX

PLOT OF ELLIPTICITY OF THE LATERALLY RADIATING ELECTRO-MAGNETIC HORN FOR NEGATIVE θ AND LEFT ELLIPTICAL POLARIZATION

E.A.R. Barnes R.E. Lee
16 April 1952

Relative Power is in Brackets.

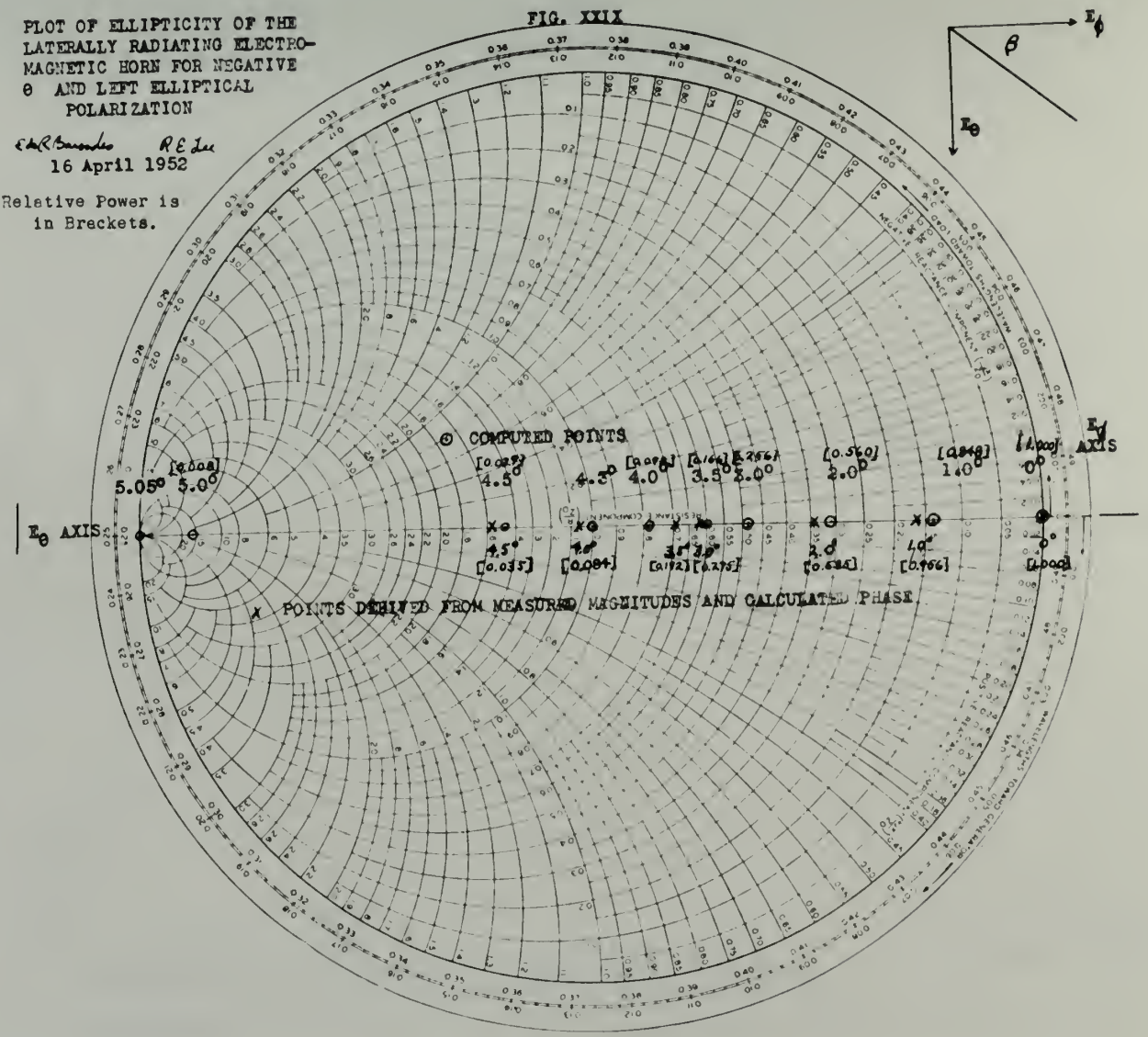

FIG. XXX

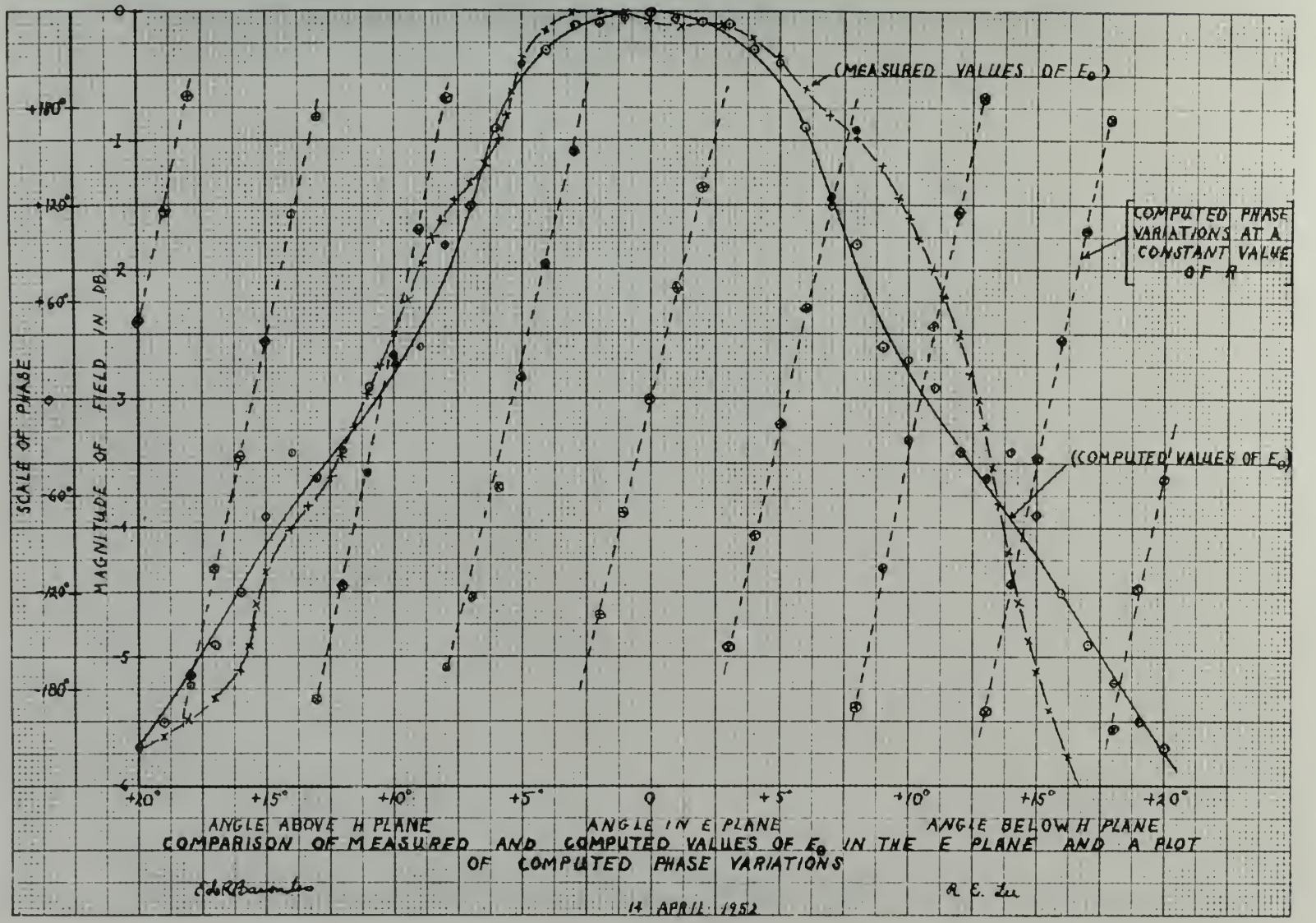

COMPARISON OF MEASURED AND COMPUTED VALUES OF E_θ IN THE E PLANE AND A PLOT OF COMPUTED PHASE VARIATIONS

E. R. Ramsay

14 APRIL 1952

R. E. Lee

FIG. XXXI

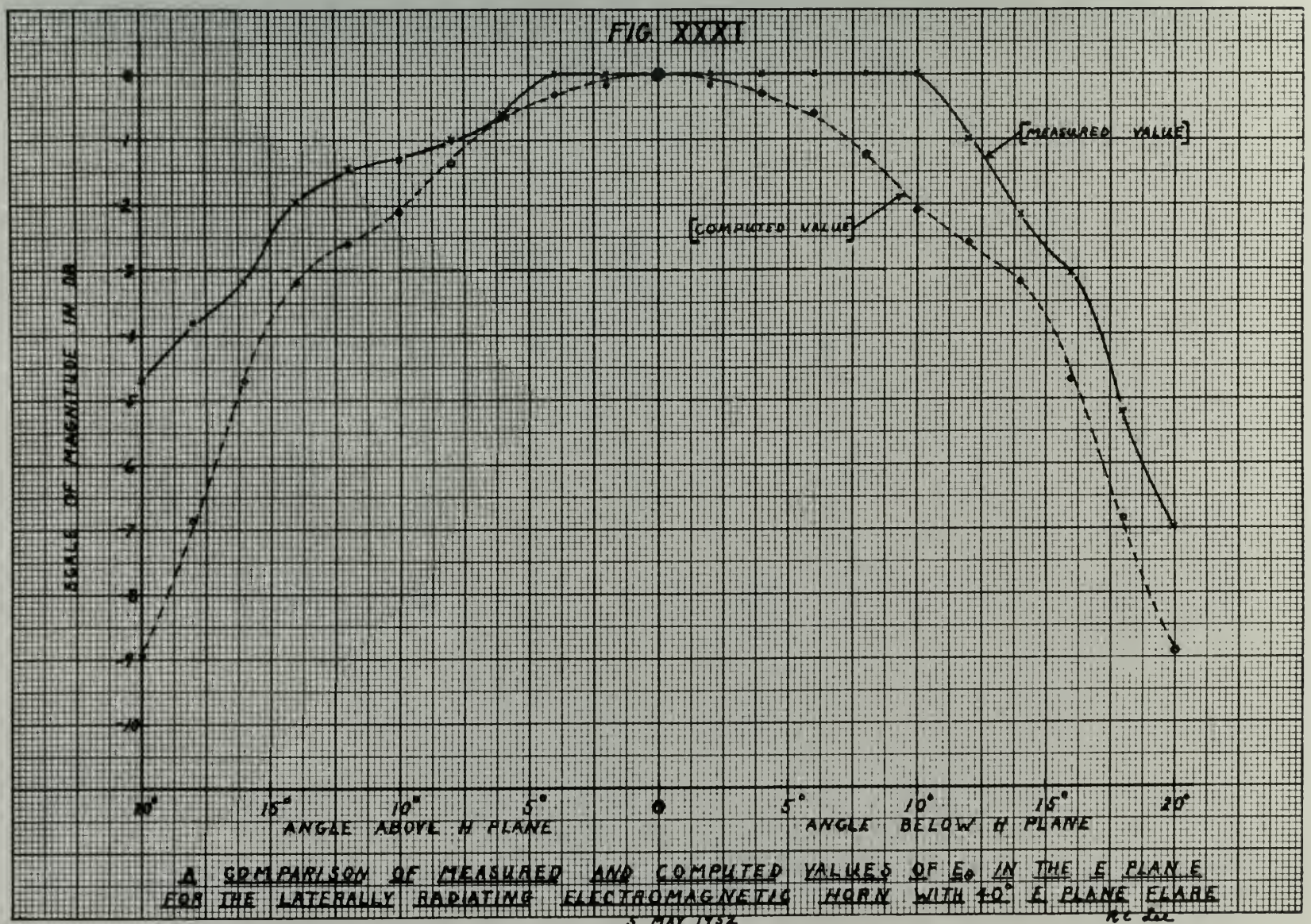

A COMPARISON OF MEASURED AND COMPUTED VALUES OF E_ϕ IN THE E PLANE FOR THE LATERALLY RADIATING ELECTROMAGNETIC HORN WITH 40° E PLANE FLARE

3 MAY 1932

R C Lee

XXXII

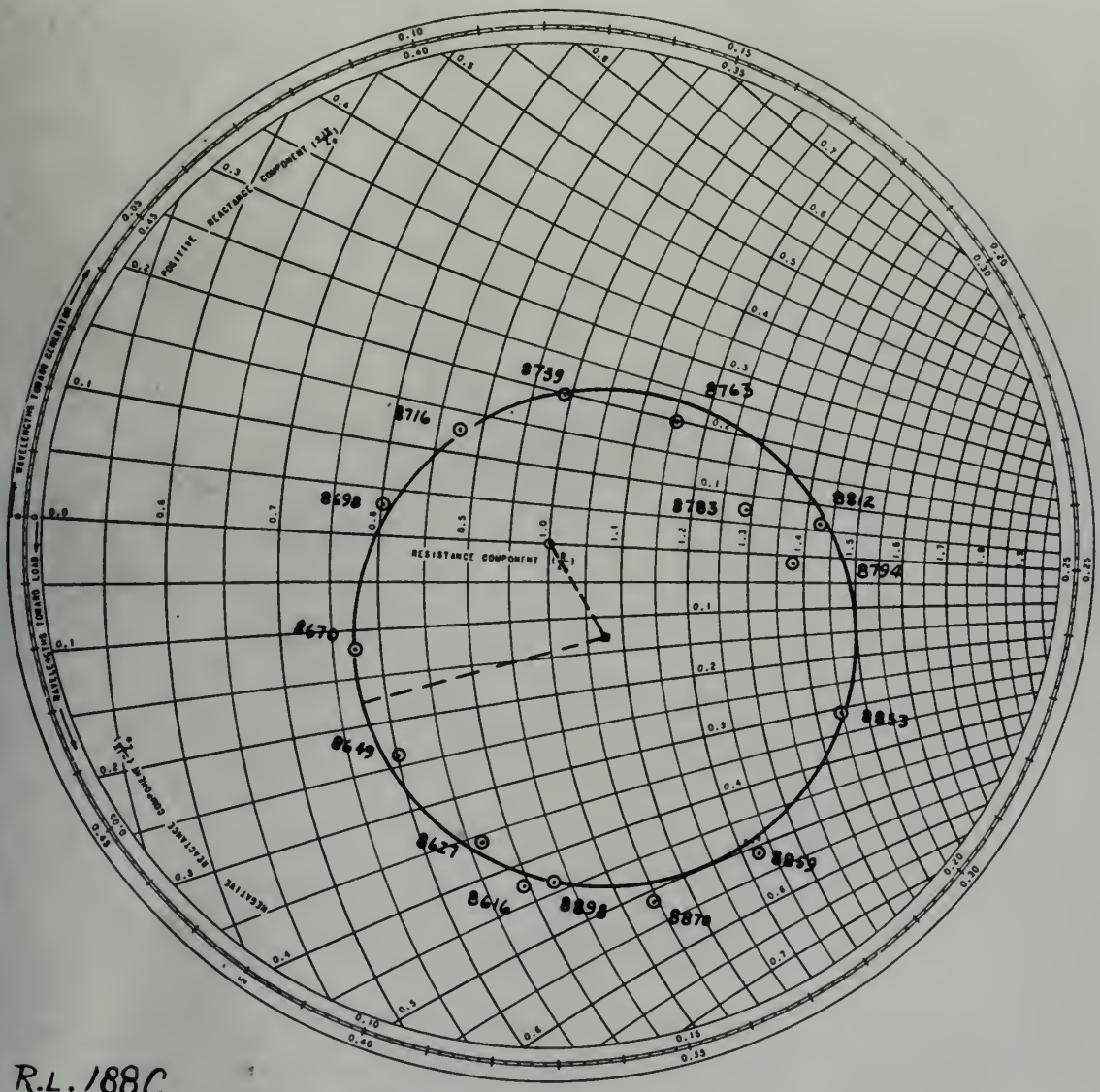

R.L. 188C

ADMITTANCES OF THE UNCOMPENSATED HORN,
(CONDITION 1), FOR DIFFERENT FREQUENCY,
TRANSFERRED TO THE THROAT.

R.E. Lee
E.R. Barandes
1 May 1952

XXXIII

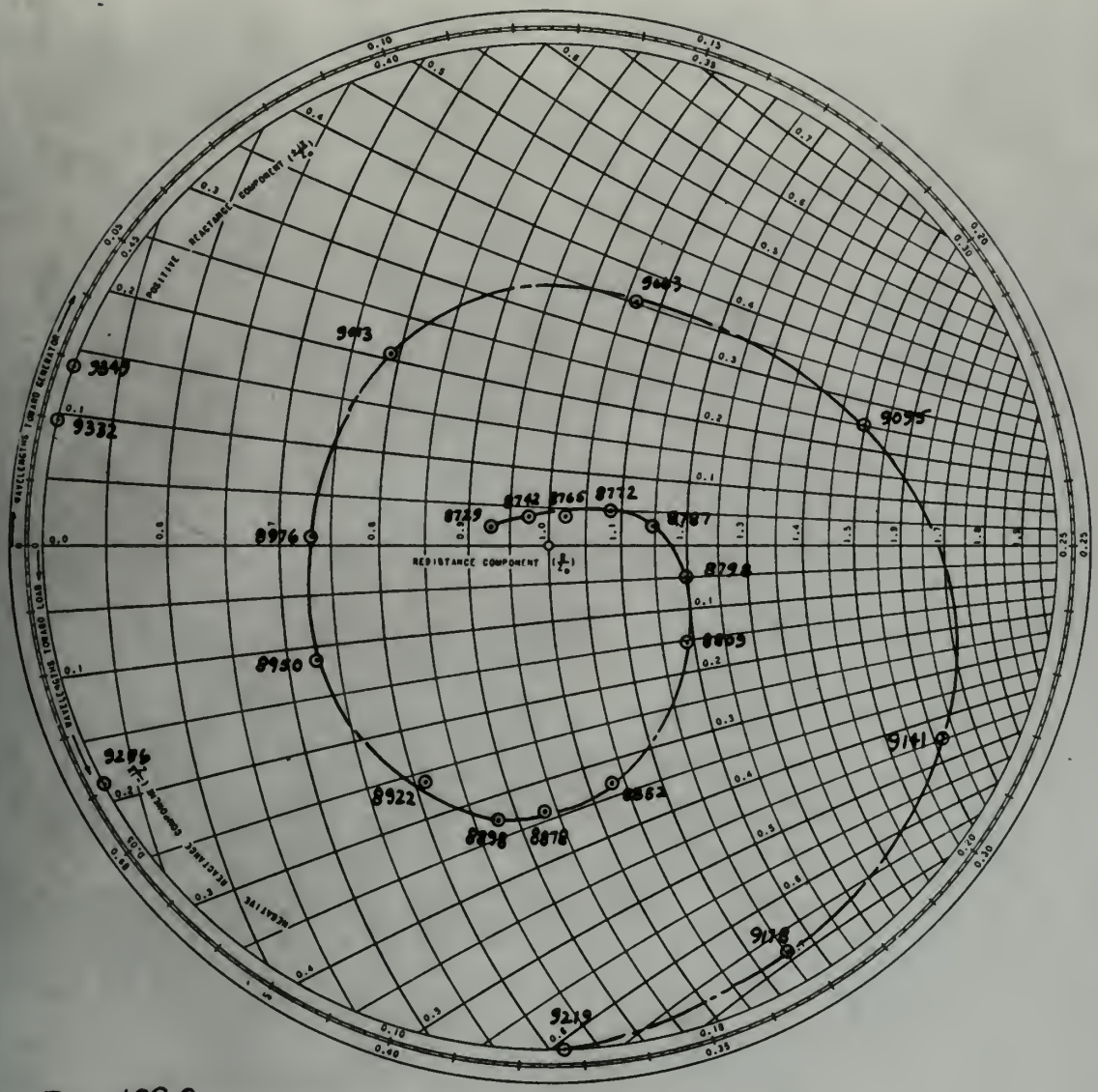

R.L. 188C

ADMITTANCES OF THE HORN WITH PLANE PARALLEL PLATE FILTER, NO E PLANE FLARE, (CONDITION 2), FOR DIFFERENT FREQUENCY, TRANSFERRED TO THE THROAT.

R E Lee
E R Barnes
1 May 1952

XXXIV

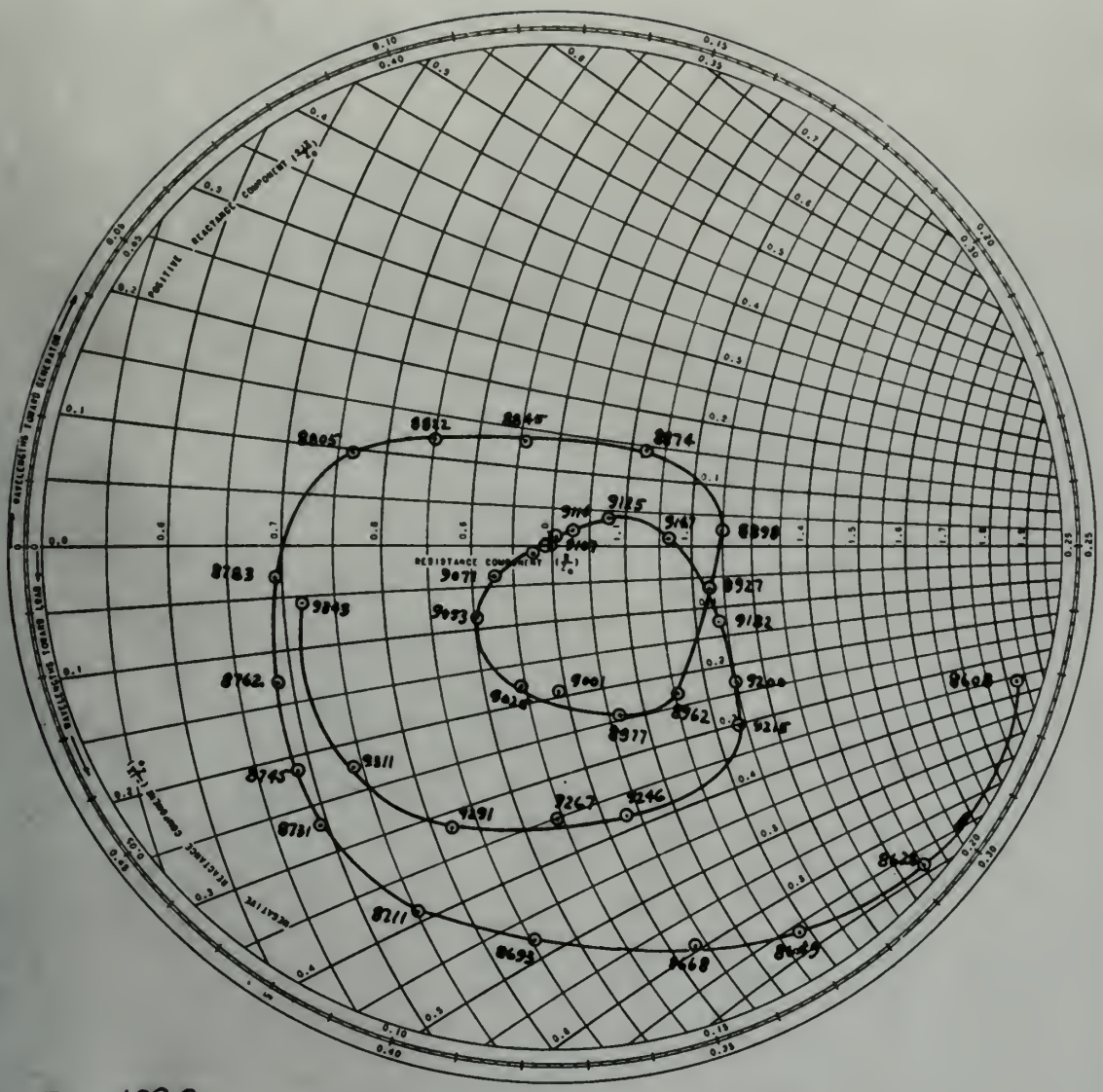

R.L. 188C

ADMITTANCES OF THE HORN WITH E PLANE FLARE, NO FILTER, (CONDITION 4), FOR DIFFERENT FREQUENCY, TRANSFERRED TO THE THROAT.

R E Lee
E R Barnards
1 May 1952

XXXV

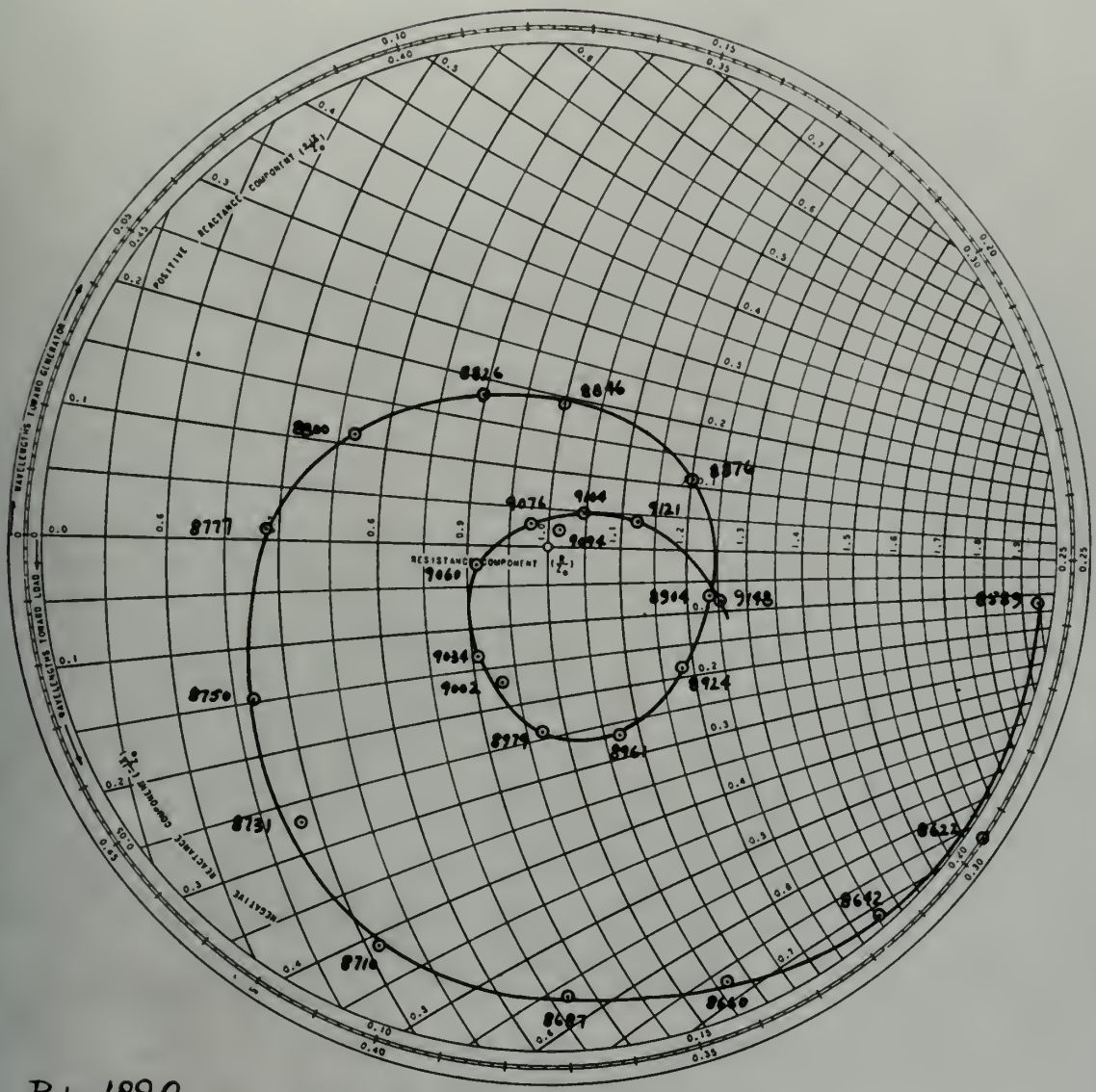

R.L. 188C

ADMITTANCES OF THE HORN WITH E PLANE FLARE, PLANE PARALLEL FILTER, (CONDITION 4), FOR DIFFERENT FREQUENCY, TRANSFERRED TO THE THROAT.

R E Lee
E R Barandes
1 May 1952

XXXVI

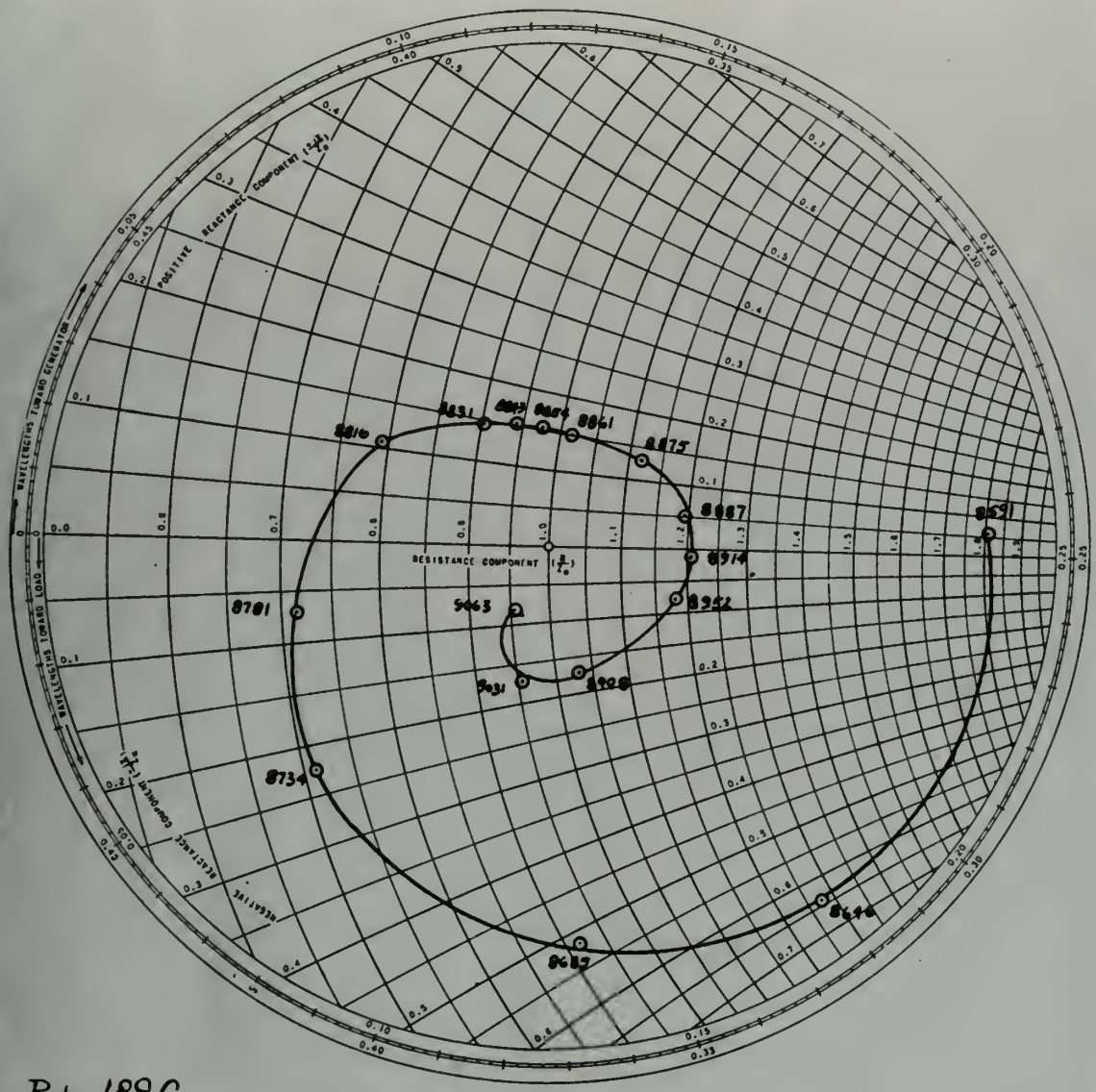

R.L. 188C

ADMITTANCES OF THE HORN WITH E PLANE FLARE, PARALLEL WIRE FILTER, (CONDITION 5), FOR DIFFERENT FREQUENCY, TRANSFERRED TO THE THROAT.

R C Lee
E R Barnes
1 May 1952

XXXVII

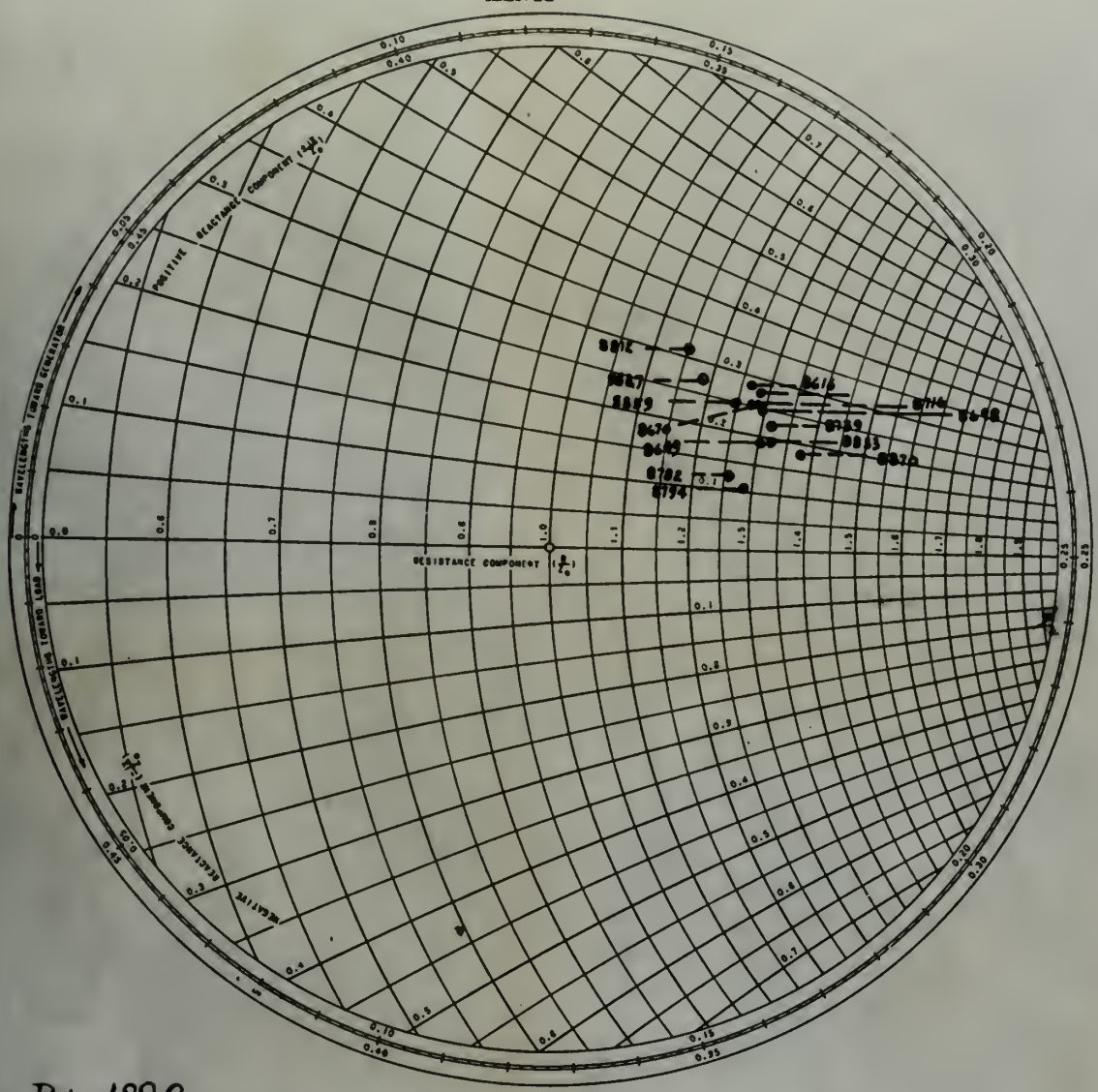

R.L. 188C

ADMITTANCE COMPONENTS AT THE HORN APERATURE FOR THE UNCOMPENSATED HORN, (CONDITION 1), FOR DIFFERENT FREQUENCY, TRANSFERRED TO THE APERATURE FROM THE THROAT.

R E Lee
E R Barandes
1 May 1952

Fig. XXXVIII
The Laterally Radiating
Horn on the Turntable.

Fig. XXXIX
The Laterally Radiating
Horn with 40° Plane Flare)
on the Turntable.

APPENDIX, SECTION B

DETAILS OF PROCEDURE

The Fraunhofer Diffraction Theory Applied to the Laterally Radiating Electromagnetic Horn

In order to determine analytically the performance of the horn, the first step is to develop the integral field equations applicable to the Fraunhofer region of space. These equations have been developed[30] and will be integrated to obtain the radiation pattern of the horn. The coordinate system is given in Figure II.

$$E_{p\theta} = \frac{jk\,\varepsilon^{-jkR}}{4\pi R}\left(1+\alpha\sqrt{\frac{\mu}{\varepsilon_o}}\,\mathrm{Cos}\,\theta\right)\left[N_x\,\mathrm{Cos}\,\phi + N_y\,\mathrm{Sin}\,\phi\right] \qquad (A\text{-}1)$$

$$E_{p\phi} = \frac{-jk\,\varepsilon^{-jkR}}{4\pi R}\left(\mathrm{Cos}\,\theta+\alpha\sqrt{\frac{\mu}{\varepsilon_o}}\right)\left[N_x\,\mathrm{Sin}\,\phi - N_y\,\mathrm{Cos}\,\phi\right] \qquad (A\text{-}2)$$

Where α is defined by the relationship,

$$H = \alpha(S \times E) \qquad (A\text{-}3)$$

and

$$N_x = \int_s E_{sx}\,\varepsilon^{jk(x\,\mathrm{Sin}\,\theta\,\mathrm{Cos}\,\phi + y\,\mathrm{Sin}\,\theta\,\mathrm{Sin}\,\phi)}\delta s \qquad (A\text{-}4)$$

$$N_y = \int_s E_{sy}\,\varepsilon^{jk(x\,\mathrm{Sin}\,\theta\,\mathrm{Cos}\,\phi + y\,\mathrm{Sin}\,\theta\,\mathrm{Sin}\,\phi)}\delta s \qquad (A\text{-}5)$$

In order to integrate the field expressions it is necessary to make a valid assumption of the fields existing at the aperture of the horn. Consider the laterally radiating electromagnetic horn as an H plane flared sectoral horn with a gradual E plane bend of low curvature as illustrated in Figure I. The fields in the sectoral horn[31] for the geometry in Figure III are given by:

Appendix (Section 3

Theory of Operation

The Theodolite Positioning System Applied to the Interactive Qualitative Electromagnetic Model

It seems to be necessary analytically the performance of the Bistro, the first step is to derive the four-part field equations explicitly to the Fraunhofer region of space. Three equations have been developed[10] and will be implemented to obtain the radiating patterns of the horn. The coordinate system is given in Figure 12.

$$E_{\theta} = \frac{-jke^{-jkr}}{4\pi r}\left(1+\cos\theta\right)\left[N_x \cos\phi + N_y \sin\phi\right] \tag{3-3}$$

$$E_{\phi} = \frac{jke^{-jkr}}{4\pi r}\left(\cos\theta+1\right)\left[N_y \sin\phi - N_x \cos\phi\right] \tag{3-4}$$

where e is defined by the relationship,

$$N = e(r \times E) \tag{3-5}$$

and

$$E_x = \int_0^a E_{ax}\, e^{jk(x \sin\theta \cos\phi + y \sin\theta \sin\phi)}\, dx \tag{3-6}$$

$$N_y = \int_0^a E_{ay}\, e^{jk(x \sin\theta \cos\phi + y \sin\theta \sin\phi)}\, dy \tag{3-7}$$

It would be interesting to extend the finite computations to the resulting to make a valid examination of the field existing at the aperture of the horn. Consider the internally reflecting electromagnetic wave in an H plane flared waveguide horn with a finite wall of skew band of four waveforms as illustrated in Figure 1. The finite in the previous horn[12] for the geometry in Figure III are given by:

$$E_y = A_1 \left[\operatorname{Cos} \frac{\pi\theta}{2\theta_o} \right] \left[H^{(2)}_{\left(\frac{\pi}{2\theta}\right)_o}(kr) + C_1 H^{(1)}_{\left(\frac{\pi}{2\theta}\right)_o}(kr) \right] \tag{A-6}$$

$$H_r = \frac{\pi A_1}{2r\theta_o\, j\omega\mu} \left[\operatorname{Sin} \frac{\pi\theta}{2\theta_o} \right] \left[H^{(2)}_{\left(\frac{\pi}{2\theta}\right)_o}(kr) + C_1 H^{(1)}_{\left(\frac{\pi}{2\theta}\right)_o}(kr) \right] \tag{A-7}$$

$$H_\theta = \frac{kA_1}{j\omega\mu} \left[\operatorname{Cos} \frac{\pi\theta}{2\theta_o} \right] \left[H^{(2)'}_{\frac{\pi}{2\theta_o}}(kr) + C_1 H^{(1)'}_{\frac{\pi}{2\theta_o}}(kr) \right] \tag{A-8}$$

$H^{(1)}(kr)$ and $H^{(2)}(kr)$ are Hankel functions of the first and second kinds respectively. Because only large flare angles and large radii will be employed in this investigation the asymptotic expressions for the Hankel functions may be employed.

$$H^{(1)}_n(kr) \cong \left[\frac{2}{\pi kr}\right]^{\frac{1}{2}} \varepsilon^{\,j\left(kr - \frac{(2n+1)\pi}{4}\right)} \tag{A-9}$$

$$H^{(2)}_n(kr) \cong \left[\frac{2}{\pi kr}\right]^{\frac{1}{2}} \varepsilon^{-j\left(kr - \frac{(2n+1)\pi}{4}\right)} \tag{A-10}$$

Equations (A-9) and (A-10) indicate that the equiphase surfaces are separated by free space wavelength near the aperture. Considering only the solution of the wave traveling in the positive r direction, the fields at a fixed radius, r_o, from the origin in Figure III become:

$$E_y = A_1 \operatorname{Cos}\left(\frac{\pi\theta}{2\theta_o}\right) H^{(2)}_{\left(\frac{\pi}{2\theta}\right)_o}(kr_o) \tag{A-11}$$

$$H_r = \frac{\pi A_1}{2r_o\theta_o\, j\omega\mu} \operatorname{Sin}\left(\frac{\pi\theta}{2\theta_o}\right) H^{(2)}_{\left(\frac{\pi}{2\theta}\right)_o}(kr_o) \tag{A-12}$$

$$\begin{bmatrix} \cos\frac{\pi\theta}{2} & \frac{\sin\frac{\pi\theta}{2}}{\left(\frac{\pi\theta}{2}\right)} \\ -\left(\frac{\pi\theta}{2}\right)\sin\frac{\pi\theta}{2} & \cos\frac{\pi\theta}{2} \end{bmatrix} \begin{bmatrix} J_{\theta}(kr) \\ \left(\frac{kr}{2}\right)^{\theta} J_{\theta+1}(kr) \end{bmatrix} \tag{1-8}$$

$$\begin{bmatrix} \sin\frac{\pi\theta}{2} & -\frac{\cos\frac{\pi\theta}{2}}{\left(\frac{\pi\theta}{2}\right)} \\ \left(\frac{\pi\theta}{2}\right)\cos\frac{\pi\theta}{2} & \sin\frac{\pi\theta}{2} \end{bmatrix} \begin{bmatrix} Y_{\theta}(kr) \\ \left(\frac{kr}{2}\right)^{\theta} Y_{\theta+1}(kr) \end{bmatrix} \tag{1-9}$$

$$\begin{bmatrix} \cos\frac{\pi\theta}{2} & \frac{\sin\frac{\pi\theta}{2}}{\left(\frac{\pi\theta}{2}\right)} \\ -\left(\frac{\pi\theta}{2}\right)\sin\frac{\pi\theta}{2} & \cos\frac{\pi\theta}{2} \end{bmatrix} \begin{bmatrix} H^{(1)}_{\theta}(kr) \\ \left(\frac{kr}{2}\right)^{\theta} H^{(1)}_{\theta+1}(kr) \end{bmatrix} \tag{1-10}$$

$H^{(1)}_{\theta}(kr)$ and $H^{(2)}_{\theta}(kr)$ are Hankel functions of the first and second kinds respectively. Because only Taylor Claire solutions and large radii will be employed in this investigation the asymptotic approximations for the Hankel functions may be employed.

$$H^{(1)}_{\theta}(kr) \simeq \left[\frac{2}{\pi kr}\right]^{\frac{1}{2}} e^{j\left(kr - \frac{\theta\pi}{2} - \frac{\pi}{4}\right)} \tag{1-11}$$

$$H^{(2)}_{(3)}(kr) \simeq \left[\frac{2}{\pi kr}\right]^{\frac{1}{2}} e^{-j\left(kr - \frac{(\theta+1)\pi}{2}\right)} \tag{1-12}$$

Equations (1-9) and (1-10) indicate that the cylindrical surfaces are separated by free space wavelength and the electric, Consequently only the solution of the wave traveling in the positive r direction, the fields at a fixed radius, r_0, from the origin in figure III become

$$E^{\theta}_{\theta} = E^{\theta}_{\theta} \cos\left(\frac{\pi\theta}{2}\right) H^{(1)}_{(1)}(kr_0) \tag{1-13}$$

$$H^{\theta}_{\theta} = \frac{\pi r_0 \theta_0 \, j\pi}{\mu\lambda^2} \cos\left(\frac{\pi\theta}{2}\right) H^{(1)}_{(1)}(kr_0) \tag{1-14}$$

$$H_\theta = \frac{KA_1}{j\omega\mu} \cos\left[\frac{\pi\theta}{2\theta_o}\right] \frac{H^{(2)'}(kr_o)}{\left(\frac{\pi}{2\theta}\right)_o} \tag{A-13}$$

Because the laterally radiating electromagnetic horn design in Figure I has a constant mean path length between the origin and any point on the aperture, the aperture can be considered to be a surface of constant phase with a distance between constant phase surfaces in the traveling wave of free space wavelength. These constant phase surfaces lie in a plane, but the surface is fixed by geometry as an arc of a circle. Consider the aperture arc in the coordinate system in Figure II. E_y in Figure III becomes E_r in Figure II; H_r in Figure III becomes H_z in Figure II; and H_θ in Figure III becomes H_ϕ in Figure II. The field expressions near the aperture become:

$$E_r = A_1 \cos\left(\frac{\pi\phi}{\phi_o}\right) \frac{H^{(2)}(kr_o)}{\left(\frac{\pi}{\phi}\right)_o} \tag{A-14}$$

$$H_z = \frac{A_1 \pi}{\phi_o j\omega\mu r_o} \sin\left(\frac{\pi\phi}{\phi_o}\right) \frac{H^{(2)}(kr_o)}{\left(\frac{\pi}{\phi}\right)_o} \tag{A-15}$$

$$H_\phi = -j\, A_1 \sqrt{\frac{\varepsilon_o}{\mu}} \cos\left(\frac{\pi\phi}{\phi_o}\right) \frac{H^{(2)}(kr_o)}{\left(\frac{\pi}{\phi}\right)_o} \tag{A-16}$$

At moderately large values of r_o

$$-j\, H_n^{(2)'} = H_n^{(2)} \tag{A-17}$$

and approximately free space wave impedance exists at the aperture. The field components which lie in the aperture plane can now be written as:

$$E_r = B_1 \cos\frac{\pi\phi}{\phi_o} \tag{A-18}$$

$$H_\phi = B_1 \sqrt{\frac{\varepsilon_o}{\mu}} \cos\frac{\pi\phi}{\phi_o} \tag{A-19}$$

$$A^0 = \frac{\mu_0 J^0}{4\pi} \cos\left[\frac{\omega_0}{c}\right] \frac{H_{(2)}^{(1)}(kr^0)}{\left(\frac{\omega_0}{c}\right)^2} \tag{4-15}$$

Because the internally radiating electromagnetic wave design in Figure I has a constant wave path length between the origin and any point on the aperture, the aperture can be considered to be a portion of constant phase with a distance between constant phase surfaces in the traveling wave of free space wavelength. These constant phase surfaces lie in a plane, but the surface is fixed by geometry as an arc of a circle. Consider the aperture are in the coordinate system in Figure IX. E_ϕ^2 in Figure IIX becomes F_r^2 in Figure II; H_r^2 in Figure III becomes H_ϕ^2 in Figure II; and H_ϕ^2 in Figure III becomes E_ϕ^2 in Figure II. The field expressions near the aperture become:

$$E_\phi^2 = A^1 \cos\left(\frac{\omega_0}{c}\right) \frac{H_{(2)}^{(1)}}{\left(\frac{\omega_0}{c}\right)} (kr^0) \tag{4-14}$$

$$H_r^2 = \frac{\omega_0 \mu_0 r^0}{r^1 c} \sin\left(\frac{\omega_0}{c}\right) \frac{H_{(2)}^{(1)}}{\left(\frac{\omega_0}{c}\right)} (kr^0) \tag{4-15}$$

$$H_\phi^2 = -1 \sqrt{\frac{\mu}{\varepsilon}} \cos\left(\frac{\omega_0}{c}\right) \frac{H_{(2)}^{(1)}}{\left(\frac{\omega_0}{c}\right)} (kr^0) \tag{4-16}$$

at moderately large values of r^0

$$-j\, H_{(r)}^{(2)} = H_{(2)}^{(1)} \tag{4-17}$$

and approximately free space wave impedance outside of the aperture. The field components within the aperture plane may now be written as:

$$E_\phi^2 = E^1 \cos\frac{\omega_0}{c} \tag{4-18}$$

$$H_\phi^2 = E^1 \sqrt{\frac{\mu}{\varepsilon}} \cos\frac{\omega_0}{c} \tag{4-19}$$

Where:

$$B_1 = A_1 \left(\frac{\pi}{\phi}\right)_o H^{(2)}(kr_o) \tag{A-20}$$

From Equation (A-18) the values of the x and y components of the electric field intensities can be written.

$$E_{sx} = B_1 \operatorname{Cos}\left(\frac{\pi\phi}{\phi_o}\right) \operatorname{Cos}\phi \tag{A-21}$$

$$E_{sy} = B_1 \operatorname{Cos}\left(\frac{\pi\phi}{\phi_o}\right) \operatorname{Sin}\phi \tag{A-22}$$

Higher order H modes may exist at the aperture, but these will be considered later.

The Linear Equivalent Source Method of Determining the E Plane Polarized, H Plane Field Pattern

Because this pattern is of primary interest and because this method of approach yields simple expressions for the field patterns, the linear equivalent source method will be presented first. The geometry of this linear equivalent source is given in Figure IV. The assumed fields in this linear equivalent source are the fields projected from the arc to the line.

$$y_o = r_{av} \operatorname{Sin}\left(\frac{\phi_o}{2}\right) \tag{A-23}$$

$$E_{sx} = B_1 \operatorname{Cos}\left(\frac{\pi y}{2y_o}\right) \operatorname{Cos}\left(\frac{\phi_o y}{2y_o}\right) \tag{A-24}$$

$$E_{sy} = B_1 \operatorname{Cos}\left(\frac{\pi y}{2y_o}\right) \operatorname{Sin}\left(\frac{\phi y}{2y_o}\right) \tag{A-25}$$

N_x may now be computed by first substituting Equation (A-24) into Equation (A-4)

$$N_x = B_1 \int_{-y_o}^{+y_o} \int_{-\Delta x_o}^{+\Delta x_o} \operatorname{Cos}\frac{\pi y}{2y_o} \operatorname{Cos}\frac{\phi_o y}{2y_o} \varepsilon^{jkx \operatorname{Sin}\theta \operatorname{Cos}\phi} \varepsilon^{jk\, y \operatorname{Sin}\theta \operatorname{Sin}\phi} \delta x\, \delta y \tag{A-26}$$

$$S^{\beta} = \gamma^{\tau} \, \delta_{(n)}^{(\frac{\beta}{c})^{\circ}} \, (\beta r_{n}) \tag{A-20}$$

From Equation (A-19) the values of $\frac{\omega}{c}$ and β corresponding to the acoustic fluid impedance can be written.

$$Z^{ac} = \beta^{\tau} \cos\left(\frac{\omega}{c}\right)^{\circ} \cos \beta \tag{A-21}$$

$$S^{ac} = \beta^{\tau} \cos\left(\frac{\omega}{c}\right)^{\circ} \sin \beta \tag{A-22}$$

Either order 0 modes may exist in the aperture, but these will be considered later.

The Linear Equivalent Source Method of Determining the 2 Plane Impedance, 2 Plane Fluid Pattern

Because this material is of primary interest and because this method of approach yields simple expressions for the field pattern, the linear equivalent source method will be presented first. The geometry of this linear equivalent source is given in Figure IV. The assumed fluids in this linear equivalent source are the fluids projected from the ends of the line.

$$Z^{o} = \tau^{ac} \sin\left(\frac{\tau}{\beta^{o}}\right) \tag{A-23}$$

$$S^{ac} = \beta^{\tau} \cos\left(\frac{\omega}{c}\right) \tan\left(\frac{\beta^{o}}{\beta^{o}}\right) \tag{A-24}$$

$$S^{ac} = \beta^{\tau} \cos\left(\frac{\omega}{c}\right) \sin\left(\frac{\beta^{o}}{\beta^{o}}\right) \tag{A-25}$$

S^{ac} may be computed by first substituting Equation (A-23) into Equation (A-1)

$$S^{ac} = \beta^{\tau} \int_{-\frac{\beta^{o}}{2}}^{\frac{\beta^{o}}{2}} \cos \frac{\omega}{c} \cos \frac{\beta^{o}}{\beta^{o}} \, e^{-\beta x} \, dx \tag{A-26}$$

After integrating Equation (A-26) becomes:

$$N_x = \frac{B_1\ 2j\ \Delta x_o}{\Delta x_o\ jk\ \text{Sin}\ \theta\ \text{Cos}\ \phi}\left[\frac{\varepsilon^{+jk\Delta x_o\ \text{Sin}\ \theta\ \text{Cos}\ \phi}{}^{2} - \varepsilon^{-jk\Delta x_o\ \text{Sin}\ \theta\ \text{Cos}\ \phi}{}^{2}}{2j}\right]$$

$$\frac{y_o}{2}\left[\frac{\text{Sin}\left\{\frac{(\pi+\phi_o)}{2y_o} - k\ \text{Sin}\ \phi\ \text{Sin}\ \theta\right\}y_o}{\left\{\frac{(\pi+\phi_o)}{2y_o} - k\ \text{Sin}\ \phi\ \text{Sin}\ \theta\right\}y_o} + \frac{\text{Sin}\left\{\frac{(\pi+\phi_o)}{2y_o} + k\ \text{Sin}\ \phi\ \text{Sin}\ \theta\right\}y_o}{\left\{\frac{(\pi+\phi_o)}{2y_o} + k\ \text{Sin}\ \phi\ \text{Sin}\ \theta\right\}y_o}\right.$$

$$\left. + \frac{\text{Sin}\left\{\frac{(\pi-\phi_o)}{2y_o} - k\ \text{Sin}\ \phi\ \text{Sin}\ \theta\right\}y_o}{\left\{\frac{(\pi-\phi_o)}{2y_o} - k\ \text{Sin}\ \phi\ \text{Sin}\ \theta\right\}y_o} + \frac{\text{Sin}\left\{\frac{(\pi-\phi_o)}{2y_o} + k\ \text{Sin}\ \phi\ \text{Sin}\ \theta\right\}y_o}{\left\{\frac{(\pi-\phi_o)}{2y_o} + k\ \text{Sin}\ \phi\ \text{Sin}\ \theta\right\}y_o}\right] \qquad \text{(A-27)}$$

In the H plane $\phi = \frac{\pi}{2}$

$$N_x = \frac{B_1\ \Delta x_o\ y_o}{2}\left[\frac{\text{Sin}\left\{\frac{(\pi+\phi_o)}{2y_o} - k\ \text{Sin}\ \theta\right\}y_o}{\left\{\frac{(\pi+\phi_o)}{2y_o} - k\ \text{Sin}\ \theta\right\}y_o} + \frac{\text{Sin}\left\{\frac{(\pi+\phi_o)}{2y_o} + k\ \text{Sin}\ \theta\right\}y_o}{\left\{\frac{(\pi+\phi_o)}{2y_o} + k\ \text{Sin}\ \theta\right\}y_o}\right.$$

$$\left. + \frac{\text{Sin}\left\{\frac{(\pi-\phi_o)}{2y_o} - k\ \text{Sin}\ \theta\right\}y_o}{\left\{\frac{(\pi-\phi_o)}{2y_o} - k\ \text{Sin}\ \theta\right\}y_o} + \frac{\text{Sin}\left\{\frac{(\pi-\phi_o)}{2y_o} + k\ \text{Sin}\ \theta\right\}y_o}{\left\{\frac{(\pi-\phi_o)}{2y_o} + k\ \text{Sin}\ \theta\right\}y_o}\right] \qquad \text{(A-28)}$$

Equation (A-28) will give highly accurate values for the half power beam widths, and moderately accurate results for the peak power densities of the first side lobes and the angles at which the side lobes occur.

Other intermediate figuration (4-29) becomes

$$\left[\frac{\frac{\pi}{2}}{\frac{\pi}{2}} \right] \frac{\text{[illegible]}}{\text{[illegible]}} \left[\frac{\text{[illegible]}}{\text{[illegible]}} \right]$$

$$\left[\frac{\left\{ \frac{\pi^2}{(\pi+\beta)^2} + x \sin\beta \sin\theta \right\}^2}{\left\{ \frac{\pi^2}{(\pi+\beta)^2} - x \sin\beta \sin\theta \right\}^2} + \frac{\left\{ \frac{\pi^2}{(\pi+\beta)^2} + x \sin\beta \cos\theta \right\}^2}{\left\{ \frac{\pi^2}{(\pi+\beta)^2} - x \sin\beta \cos\theta \right\}^2} \right]^{\frac{\pi}{2}}$$

$$+ \sin\left\{ \frac{\pi^2}{(\pi-\beta)^2} - x \sin\beta \sin\theta \right\}^2 + \frac{\left\{ \frac{\pi^2}{(\pi-\beta)^2} + x \sin\beta \cos\theta \right\}^2}{\left\{ \frac{\pi^2}{(\pi-\beta)^2} + x \sin\beta \cos\theta \right\}^2}$$

(4-27)

In the β plane $\beta = \frac{\pi}{2}$

$$\left[\frac{\left\{ \frac{\pi^2}{(\pi+\beta)^2} - x \cos\theta \right\}^2}{\left\{ \frac{\pi^2}{(\pi+\beta)^2} - x \sin\theta \right\}^2} \right]^{\frac{\pi}{2}} \frac{\left\{ \frac{\pi^2}{(\pi+\beta)^2} + x \sin\theta \right\}^2}{\left\{ \frac{\pi^2}{(\pi+\beta)^2} + x \sin\theta \right\}^2}$$

$$+ \sin\left\{ \frac{\pi^2}{(\pi-\beta)^2} - x \sin\theta \right\}^2 + \frac{\left\{ \frac{\pi^2}{(\pi-\beta)^2} + x \sin\theta \right\}^2}{\left\{ \frac{\pi^2}{(\pi-\beta)^2} + x \sin\theta \right\}^2}$$

(4-28)

Equation (4-28) will give slightly different values for the half power beam width, and noticeably accurate results for the main lobe

lamelike of the first side lobes and the angles at which the side lobes occur.

Linear equivalent source methods used in computing the other three principal patterns in the H and E planes are highly inaccurate. If the fields are assumed to be projected directly without any factors which take into account the curvature of the physical source and the effect of equivalent area variations with curvature, then the integrals will result in functions which have the same symmetry, but erroneous relative magnitudes.

The Array Factor Applied to the Antenna, Type B

$$F = \int_{-\phi_o}^{+\phi_o} \text{Cos}\, \frac{\pi\phi'}{\phi_o}\, \text{Cos}\, \phi'\, \varepsilon^{+jkr_{av}\, \text{Sin}\, \theta\, \text{Sin}\, \phi'}\, \delta\phi' \qquad \text{(A-29)}$$

When $\phi_o = \frac{\pi}{2}$, $r_{av}\, \text{Sin}\, \phi' = y$ (A-30)

is substituted in Equation (A-29), it becomes:

$$F = \int_{-y_o}^{+y_o} 1 - 2\frac{y^2}{r_{av}^2}\, \varepsilon^{ay}\, \delta y \qquad \text{(A-31)}$$

Where

$$a = jk\, \text{Sin}\, \theta \qquad \text{(A-32)}$$

This changes the variable of integration to an integration with respect to y. (Straight line equivalent).

$$F = \frac{\varepsilon^{ay_o} - \varepsilon^{-ay_o}}{a} - \frac{2}{r^2 a^3}\left[(\varepsilon^{ay_o} - \varepsilon^{-ay_o})(a^2 y_o^2 + 2) - 2ay_o(\varepsilon^{ay_o} + \varepsilon^{-ay_o})\right] \qquad \text{(A-33)}$$

Which reduces to:

$$F = 2\left\{\frac{\text{Sin}\, ay_o}{j}\left(\frac{1}{k\, \text{Sin}\, \theta} - \frac{2y_o^2}{r_{av}^2\, k\, \text{Sin}\, \theta} + \frac{4}{r_{av}^2\, k^3\, \text{Sin}^3\theta}\right) + \right.$$

$$\left. + \frac{\text{Cos}\, ay_o}{j}\left[\frac{4y_o}{-r_{av}^2\, k^2\, \text{Sin}^2\theta}\right]\right\} \qquad \text{(A-34)}$$

Linear equivalent source methods used in computing the other three principal patterns in the H and E planes are highly inaccurate. If the fields are assumed to be projected directly without any factors which take into account the curvature of the physical source and the effect of equivalent area variations with curvature, then the integrals will result in functions which have the same character, but erroneous relative magnitudes.

The Linear Factor Applied to the Aperture, Type 3

$$I = \int_{-\psi_0}^{\psi_0} (\cos \tfrac{\pi x'}{a})^{\alpha} \cos \psi_1' \, e^{+jkx' \sin\theta \cos\psi_1'} \, d\psi_1' \qquad (4\text{-}29)$$

When $\psi_0' = \frac{\pi}{2}$, $\frac{\pi x'}{a} \sin\psi_1' = \chi$ (4-30)

is substituted in Equation (4-29), it becomes:

$$I = \int_{-\psi_0}^{\psi_0} \left(1 - \frac{2}{\pi}\chi\right)^{\alpha} e^{jv\chi} \, d\chi \qquad (4\text{-}31)$$

Where

$$v = \tfrac{1}{2} ka \sin\theta \qquad (4\text{-}32)$$

This changes the variable of integration to an integration with respect to χ. (Straight line equivalent).

$$I = \frac{e^{jv\psi_0} - e^{-jv\psi_0}}{jv} - \frac{2^{\alpha}}{jv}\left[(e^{jv\psi_0} - e^{-jv\psi_0})(a_1 c^{\alpha} + 2) - 2jv(a_{\alpha} e^{jv\psi_0} + a_{\alpha-2} e^{jv\psi_0})\right] \qquad (4\text{-}33)$$

Which reduces to:

$$E = \sum \left\{ \sin n\psi_0 \left(\frac{1}{\gamma} \left(K \sin\theta - \frac{\pi^{2\alpha}}{\gamma^2} \epsilon \sin\theta + \sum_{\gamma}^{2\alpha} K_{\gamma} \frac{\pi^{\gamma} \sin\theta}{\gamma^{\gamma}} \right) + \right. \right.$$

$$\left. \left. + \cos n\psi_0 \frac{1}{n\psi_0} \left[\sum_{\gamma}^{2\alpha} \frac{\pi^{\gamma} \sin\theta}{\psi_0^{\gamma}} \right] \right) \right\} \qquad (4\text{-}34)$$

For the dimensions of the horn this reduces to:

$$F = +0.000728 \frac{\text{Sin}\,(ky_o \text{ Sin } \theta)}{\text{Sin}^3\theta} - 0.038 \frac{\text{Cos}\,(ky_o \text{ Sin } \theta)}{\text{Sin}^2\theta} \qquad \text{(A-35)}$$

The Fourier-Bessel Series Method of Field Pattern Evaluation

Converting Equations (A-4) and A-5) into an integration in the xy plane in plane polar coordinates by means of the relationships:

$$x = r' \text{ Cos } \phi' \qquad \text{(A-36)}$$

$$y = r' \text{ Sin } \phi' \qquad \text{(A-37)}$$

the diffraction integrals become

$$N_{\substack{x \\ y}} = \int_s E_{\substack{x \\ y}} \varepsilon^{jk \text{ Sin } \theta \, r' \text{ Cos } (\phi - \phi')} \, r' \, \delta r' \, \delta\phi' \qquad \text{(A-38)}$$

Solving first for N_x we must substitute Equation (A-21) into Equation (A-38).

$$N_x = B_1 \int_{\frac{-\phi_o}{2}}^{\frac{+\phi_o}{2}} \int_{r_1}^{r_2} \text{Cos } \frac{\pi\phi'}{\phi_o} \text{ Cos } \phi' \, \varepsilon^{jkr' \text{ Sin } \theta \text{ Cos } (\phi - \phi')} \, r' \, \delta r' \, \delta\phi' \qquad \text{(A-39)}$$

Integrating first with respect to ϕ' can be accomplished employing the expansion:

$$\varepsilon^{jur \text{ Cos } (\phi - \phi')} = \sum_{n=-\infty}^{+\infty} j^n J_n(ur) \, \varepsilon^{jn(\phi - \phi')} \qquad \text{(A-40)}$$

or by the approximation

$$\text{Cos } (\phi - \phi') = 1 - \frac{(\phi - \phi')^2}{2!} \qquad \text{(A-41)}$$

Either method yields extremely complicated formulas that cannot be integrated with respect to r' readily.

However, Equation (A-39) may be integrated first with respect to r'.

to x_i.

However, Equation (7-39) may be integrated first with respect

to be integrated with respect to ϕ_i from 0 to 2π.

Either method yields entirely equivalent formulas that cannot

or $\Delta\phi$ the substitution

$$\cos(\phi - \phi_i) = \tau - \frac{(\phi - \phi_i)^2}{2} \qquad (7-41)$$

$$\sin_1(\pi\cos(\phi - \phi_i)) = \sum_{n=-\infty}^{+\infty} J_n^2(n\pi)\, e^{in(\phi - \phi_i)} \qquad (7-42)$$

ing the summation

Interchanging first with respect to ϕ_i may be accomplish-

$$\beta^2 = \tau^2 \int_{-\frac{\pi}{2}}^{\frac{\pi}{2}} \int_{-\pi}^{\pi} \cos\frac{\pi}{2}\cos\phi\, e^{ik\rho\cos\phi}\sin\phi\cos(\phi - \phi_i)\, d\phi\, d\phi_i \qquad (7-43)$$

Applying first for β^2 the above substitute equation (7-41) into

Equation (7-38),

$$\beta^2 = \int_{-\frac{\pi}{2}}^{\frac{\pi}{2}} \int_{-\pi}^{\pi} \cos\frac{\pi}{2}\cos\phi\, e^{ik\rho\cos\phi}\sin\phi\cos(\phi - \phi_i)\, d\phi\, d\phi_i \qquad (7-44)$$

Integrating first with respect to ϕ_i may be accomplishing the summation

$$\sin_1(\pi\cos(\phi - \phi_i)) = \sum_{n=-\infty}^{+\infty} J_n^2(n\pi)\, e^{in(\phi - \phi_i)} \qquad (7-45)$$

or $\Delta\phi$ the substitution

$$\cos(\phi - \phi_i) = \tau - \frac{(\phi - \phi_i)^2}{2} \qquad (7-46)$$

Either method yields entirely equivalent formulas that cannot

be integrated with respect to ϕ_i from 0 to 2π.

However, Equation (7-39) may be integrated first with respect

to x_i.

For the discussion of the laser light produced by

$$\beta = \sigma/\cos\theta \qquad (7-47)$$

The Fraction-Beam Device Method of Field Pattern Evaluation

Conventional Equations (7-1) and (7-2) have to interpreted in the

$\Delta\phi$ plane in polar coordinates β means of the relationships

$$x = \rho\cos\phi \qquad (7-48)$$

$$y = \rho\sin\phi \qquad (7-49)$$

the differentials integrals become

$$\beta^2 = \int_{-\frac{\pi}{2}}^{\frac{\pi}{2}} \int_{-\pi}^{\pi} \cos\frac{\pi}{2}\cos\phi\, e^{ik\rho\cos\phi}\sin\phi\cos(\phi - \phi_i)\, \rho\, d\rho\, d\phi \qquad (7-50)$$

Applying first for β^2 the above substitute equation (7-41) into

Equation (7-38),

Let

$$M = k \cos(\phi - \phi') \sin\theta \tag{A-42}$$

Integrate and evaluate limits.

$$N_x = B_1 \int_{-\frac{\phi_o}{2}}^{+\frac{\phi_o}{2}} \frac{\cos\frac{\pi\phi'}{\phi_o}\cos\phi'}{-M^2}\left[\varepsilon^{jMr_2}(jMr_2 - 1) - \varepsilon^{jMr_1}(jMr_1 - 1)\right]\delta\phi' \tag{A-43}$$

Let

$$r_2 = r_1 + \delta r \tag{A-44}$$

$$N_x = B_1 \int_{-\frac{\phi_o}{2}}^{+\frac{\phi_o}{2}} \frac{\cos\frac{\pi\phi'}{\phi_o}\cos\phi'}{-M^2}\left[\varepsilon^{jMr_1 + jM\delta r}(jMr_1 + jM\delta r - 1) - \varepsilon^{jMr_1}(jMr_1 - 1)\right]\delta\phi \tag{A-45}$$

As a second order approximation, let

$$\varepsilon^{jM\delta r} = 1 + jM\delta r + \frac{(jM\delta r)^2}{2} \tag{A-46}$$

Substitute Equation (A-46) into Equation (A-45). After an elimination of terms of higher order than the third power of δr, the equation becomes:

$$N_x = B_1 \int_{-\frac{\phi_o}{2}}^{+\frac{\phi_o}{2}} \cos\frac{\pi\phi'}{\phi_o}\ \varepsilon^{jMr_1}\left(r_1\delta r + \frac{(\delta r)^2}{2} + \frac{jM(\delta r)^2 r_1}{2}\right)\cos\phi'\ \delta\phi' \tag{A-47}$$

Because M appears in the terms which are also a function of r, it is necessary to resort to only a first order approximation to the field pattern. Substituting Equation (A-42) into (A-47)

$$\psi = \gamma \cos(\theta - \theta_1) \sin\theta \qquad (4-43)$$

Integrate for circulate limits.

$$\beta^2 = \gamma^2 \int_{-\frac{\pi}{2}}^{+\frac{\pi}{2}} \frac{\cos\frac{\theta_1}{2}\cos\theta_1 d\theta_1}{\cos\frac{\theta}{2}} \left[\pi e^{\frac{i\pi}{2}(\beta\pi^2 - 1)} - \pi e^{-\frac{i\pi}{2}(\beta\pi^2 - 1)} \right] \sin\theta$$

(4-44)

Let

$$\delta^2 = \chi^2 d\alpha \qquad (4-45)$$

$$\beta^2 = \beta^2 \int_{-\frac{\pi}{2}}^{+\frac{\pi}{2}} \frac{\cos\frac{\theta_1}{2}\cos\theta_1 d\theta_1}{\cos\frac{\theta}{2}} \left[\pi e^{\frac{i\pi}{2}(\beta\pi^2 + 2\beta\pi - 1)} - \pi e^{-\frac{i\pi}{2}(\beta\pi^2 - 1)} \right] \sin\theta$$

(4-46)

as a second order approximation, let

$$\beta_{1\beta\pi} = 1 + i\beta\pi + \frac{\pi}{(i\beta\pi)_2} \qquad (4-47)$$

Substitute Equation (4-47) into Equation (4-46). After an elimination of terms of higher order than the third power of $\beta\pi$, the equation becomes

$$\beta^2 = \beta^2 \int_{-\frac{\pi}{2}}^{+\frac{\pi}{2}} \frac{\cos\frac{\theta_1}{2}}{\cos\frac{\theta}{2}} e^{i\beta\pi(\cos\theta + (\frac{\theta}{\theta_1})^2 - \frac{\pi}{16}\beta\pi(2\pi)^2\cos^2\theta)} \cos\theta_1 d\theta_1$$

(4-48)

Because β appears in the terms which are also a function of γ, it is necessary to resort to only a first order approximation to the above equation. Substituted Equation (4-48) into

$$N_x = B_1 r_1 \delta r \int_{-\frac{\phi_o}{2}}^{+\frac{\phi_o}{2}} \text{Cos}\,\frac{\pi\phi'}{\phi_o}\,\text{Cos}\,\phi'\,\varepsilon^{jkr_1\,\text{Sin}\,\theta\,\text{Cos}\,(\phi-\phi')}\,\delta\phi' \qquad \text{(A-48)}$$

Employing the identity[28]

$$\varepsilon^{jkr_1\,\text{Sin}\,\theta\,\text{Cos}\,(\phi-\phi')} = \sum_{n=-\infty}^{+\infty} j^n\,J_n(kr_1\,\text{Sin}\,\theta)\,\varepsilon^{jn(\phi-\phi')} \qquad \text{(A-49)}$$

and the obvious trigonometric identity, we obtain

$$N_x = \frac{B_1 r_1 \delta r}{2} \sum_{n=-\infty}^{+\infty} j^n\,J_n(kr_1\,\text{Sin}\,\theta)\,\varepsilon^{jn\theta} \int_{-\frac{\phi_o}{2}}^{+\frac{\phi_o}{2}} \left[\text{Cos}\left(\frac{\pi}{\phi_o}+1\right)\phi' + \text{Cos}\left(\frac{\pi}{\phi_o}-1\right)\phi'\right]$$

$$\left[\text{Cos}\,n\phi' - j\,\text{Sin}\,n\phi'\right]\delta\phi' \qquad \text{(A-50)}$$

Because the limits on the integrals are symmetrical, the integrals having odd functions integrands will be zero. After integrating and evaluating limits, Equation (A-50) becomes:

$$N_x = \frac{B_1 r_1 \delta r}{2} \sum_{n=-\infty}^{+\infty} j^n\,J_n(kr_1\,\text{Sin}\,\theta)\,\varepsilon^{jn\theta}\left(\frac{\phi_o}{2}\right)A(n,\phi_o) \qquad \text{(A-51)}$$

Where

$$A(n,\phi_o) = \frac{\text{Sin}\left(\frac{\pi}{\phi_o}+1+n\right)\frac{\phi_o}{2}}{\left(\frac{\pi}{\phi_o}+1+n\right)\frac{\phi_o}{2}} + \frac{\text{Sin}\left(\frac{\pi}{\phi_o}+1-n\right)\frac{\phi_o}{2}}{\left(\frac{\pi}{\phi_o}+1-n\right)\frac{\phi_o}{2}} +$$

$$+ \frac{\text{Sin}\left(\frac{\pi}{\phi_o}-1+n\right)\frac{\phi_o}{2}}{\left(\frac{\pi}{\phi_o}-1+n\right)\frac{\phi_o}{2}} + \frac{\text{Sin}\left(\frac{\pi}{\phi_o}-1-n\right)\frac{\phi_o}{2}}{\left(\frac{\pi}{\phi_o}-1-n\right)\frac{\phi_o}{2}} \qquad \text{(A-52)}$$

$$\left. + \int_{-\frac{\pi}{k_0}}^{\frac{\pi}{k_0}} \right\} \quad (1-22)$$

$$B_n^{\pm} = \alpha^{\mp} h^{\mp} \rho_n \cdot \frac{k^0}{\pi} \int_0^{\frac{\pi}{k_0}} \cos k_0 x \; J_{1n}^{\mp}(\rho_n x^{\mp}) \sin n(\phi - \phi_i) \, dx \quad (1-23)$$

Employing the identity (2-6)

$$e^{\mp j\rho_n x^{\mp}} \sin n(\phi - \phi_i) = \sum_{m=-\infty}^{+\infty} J_m^{\mp}(\rho_n x^{\mp}) \sin \phi) \; e^{jm(\phi - \phi_i)} \quad (1-24)$$

and the obvious multiplication identity, we obtain

$$B_n^{\pm} = \frac{\varepsilon}{j^n \alpha^{\mp} \rho_n} \sum_{m=-\infty}^{+\infty} J_m^{\mp}(\rho_n x^{\mp} \sin \phi) \; e^{jm\phi} \int_{-\frac{\pi}{k_0}}^{+\frac{\pi}{k_0}} \left[\cos\left(\frac{k^0}{k_0} + 1\right) k_0 + \cos\left(\frac{k^0}{k_0} - 1\right) k_0 \right] dx$$

$$\left[\cos n\phi_i - j \sin n\phi_i \right] \delta_{mn} \quad (1-25)$$

Because the limits on the integrals are symmetrical, the integrals involving odd functions integrate will be zero. After integrating and multiplying

Since Equation (1-20) becomes

$$E_n^{\pm} = \frac{\varepsilon}{j^n \alpha^{\mp} \rho_n} \sum_{m=-\infty}^{+\infty} J_m^{\mp}(\rho_n x^{\mp} \sin \phi) \; e^{jm\phi} \left(\frac{\varepsilon}{k_0}\right) \psi(x, k_0^0) \quad (1-27)$$

where

$$\psi(x, k_0^0) = \frac{\left(\frac{k^0}{k_0} + 1 + n\right) \frac{\varepsilon}{k_0^0}}{\left(\frac{k^0}{k_0} + 1 + n\right) \frac{\varepsilon}{k_0^0}} \cdot \frac{\left(\frac{k^0}{k_0} + 1 - n\right) \frac{\varepsilon}{k_0^0}}{\left(\frac{k^0}{k_0} + 1 - n\right) \frac{\varepsilon}{k_0^0}} +$$

$$+ \frac{\left(\frac{k^0}{k_0} - 1 + n\right) \frac{\varepsilon}{k_0^0}}{\left(\frac{k^0}{k_0} - 1 + n\right) \frac{\varepsilon}{k_0^0}} \cdot \frac{\left(\frac{k^0}{k_0} - 1 - n\right) \frac{\varepsilon}{k_0^0}}{\left(\frac{k^0}{k_0} - 1 - n\right) \frac{\varepsilon}{k_0^0}} \quad (1-28)$$

Employing the identity

$$J_{-n}(kr_1 \text{ Sin } \theta) = (-)^n J_n(kr_1 \text{ Sin } \theta) \tag{A-53}$$

Equation (A-51) becomes

$$N_x = \frac{B_1 r_1 \delta r \, \phi_o}{4}\left[A(0,\phi_o)\, J_o(kr_1 \text{ Sin } \theta) + \right.$$

$$\left. + \sum_{n=1}^{\infty} J_n(kr_1 \text{ Sin } \theta)\, A(n,\phi_o)\, B(n,\phi)\right] \tag{A-54}$$

where

$$B(n,\phi) = j^n \varepsilon^{jn\phi} + (-)^n j(-n)\, \varepsilon^{-jn\phi} \tag{A-55}$$

The computation of N_y by direct integration may also be accomplished by substituting Equation (A-22) into Equation (A-38) and repeating the steps from Equation (A-39) to Equation (A-50).

$$N_y = \frac{B_1 r_1 \delta r}{2} \sum_{n=-\infty}^{+\infty} j^n J_n(kr_1 \text{ Sin } \theta)\, \varepsilon^{jn\phi} \int_{-\frac{\phi_o}{2}}^{+\frac{\phi_o}{2}}$$

$$\left[\text{Sin}(1-\frac{\pi}{\phi_o})\phi' + \text{Sin } (1+\frac{\pi}{\phi_o})\phi'\right]\left[\text{Cos } n\phi' - j \text{ Sin } n\phi'\right]\delta\phi' \tag{A-56}$$

Because the limits on the integrals are symmetrical, the integrals having odd function integrands will be zero. After integrating and evaluating limits and employing the identity given in Equation (A-53), Equation (A-56) becomes

$$N_y = \frac{B_1 r_1 \, \delta r \, \phi_o}{4}\left[C(0,\phi_o)\, J_o(kr_1 \text{ Sin } \theta) + \right.$$

$$\left. + \sum_{n=1}^{\infty} J_n(kr_1 \text{Sin } \theta)\, C(n,\phi_o)\, D(n,\phi)\right] \tag{A-57}$$

Employing the identity

$$J_{-n}(kr^1 \sin\theta) = (-)_n J_n(kr^1 \sin\theta) \tag{A-33}$$

Equation (A-32) becomes

$$B^x = \frac{4}{\beta^1 r^1 \rho z \, k^0} \left[\epsilon(0^1 k^0) \, J^0(kr^1 \sin\theta) + \right.$$

$$\left. + \sum_{m=1}^{\infty} J^n(kr^1 \sin\theta) \, \epsilon(n^1 k^0) \, B(n^1 k) \right] \tag{A-34}$$

where

$$B(n^1 k) = J_{-n} \epsilon^{-jn\phi} + (-)^n J_n(-n) \, \epsilon^{-jn\phi} \tag{A-35}$$

The computation of H^x by direct integration may also be accomplished by substituting Equation (A-32) into Equation (A-38) and repeating the steps from Equation (A-35) to Equation (A-30).

$$H^x = \frac{2}{\beta^1 r^1 \rho z} \sum_{n=-\infty}^{+\infty} J_n \, J^n(kr^1 \sin\theta) \, \epsilon^{jn\phi} \left\{ \begin{matrix} \frac{\pi}{2} \\ - \phi_k \end{matrix} \right. \begin{matrix} \\ \\ \frac{\pi}{2} \\ + \phi_k \end{matrix}$$

$$\left[\sin\left(\frac{\pi}{2} - \phi_k\right) \phi_k + \sin\left(\frac{\pi}{2} + \phi_k\right) \phi_k \right] \left[\cos n\phi_k - j \sin n\phi_k \right] d\phi_k \tag{A-36}$$

Because the limits on the integrals are symmetrical, the integrals having odd function integrands will be zero. After integrating and evaluating limits and employing the identity given in Equation (A-33), Equation (A-35) becomes

$$H^x = \frac{4}{\beta^1 r^1 \rho z \, k^0} \left[\alpha(0^1 k^0) \, J^0(kr^1 \sin\theta) + \right.$$

$$\left. + \sum_{m=1}^{\infty} J^n(kr^1 \sin\theta) \, \epsilon(n^1 k^0) \, D(n^1 k) \right] \tag{A-37}$$

where

$$C(n,\phi_o) = \frac{\text{Sin}\,(1-\frac{\pi}{\phi_o}-n)\,\frac{\phi_o}{2}}{(1-\frac{\pi}{\phi_o}-n)\,\frac{\phi_o}{2}} + \frac{\text{Sin}\,(1+\frac{\pi}{\phi_o}-n)\,\frac{\phi_o}{2}}{(1+\frac{\pi}{\phi_o}-n)\,\frac{\phi_o}{2}} - \frac{\text{Sin}\,(1-\frac{\pi}{\phi_o}+n)\,\frac{\phi_o}{2}}{(1-\frac{\pi}{\phi_o}+n)\,\frac{\phi_o}{2}} - \frac{\text{Sin}\,(1-\frac{\pi}{\phi_o}-n)\,\frac{\phi_o}{2}}{(1+\frac{\pi}{\phi_o}+n)\,\frac{\phi_o}{2}} \qquad \text{(A-58)}$$

and

$$D(n,\phi) = j^n\,\varepsilon^{jn\phi} - (-)^n j(-n)\,\varepsilon^{-jn\phi} \qquad \text{(A-59)}$$

N_x and N_y substituted in Equations (A-1) and (A-2) adequately express the fields for any point in Fraunhofer space. As a result of the approximation employed, these formulas are limited to the case when the aperture distance in the radial direction is small in comparison to the average radius of the aperture. However, we may apply the continuous array factor concept to the aperture to obtain a better approximation to the E plane fields that will result when the E plane flare is added to the laterally radiating horn.

Employing the Array Factor to Obtain the E Plane Fields of a Large Aperture Horn

By symmetry and the Fourier-Bessel series field equations E_ϕ is zero in the E plane. Consider the field from the differential radiating element in the aperture in Figure IX to be given by the Fourier-Bessel field pattern equations. Let δr become $\delta x'$ and integrate in the x' direction.

$$E_{\theta,1} = \int_{\frac{-\Delta x'_o}{2}}^{\frac{+\Delta x'_o}{2}} \frac{E_\theta}{\delta r}\,\varepsilon^{jk\,\text{Sin}\,\theta\,\text{Cos}\,\phi\,x'}\,\delta r' \qquad \text{(A-60)}$$

After integrating, evaluating, and letting

$$C(n,k_0) = \frac{\sin\left(\frac{\pi}{2} - n\right)\frac{k_0}{2}}{\left(1 - \frac{k_0}{\pi} - n\right)\frac{k_0}{2}} \frac{\sin\left(1 + \frac{k_0}{\pi} - n\right)\frac{k_0}{2}}{\left(1 + \frac{k_0}{\pi} - n\right)\frac{k_0}{2}} -$$

$$- \frac{\sin\left(1 - \frac{k_0}{\pi} + n\right)\frac{k_0}{2}}{\left(1 - \frac{k_0}{\pi} + n\right)\frac{k_0}{2}} \frac{\sin\left(1 - \frac{k_0}{\pi} - n\right)\frac{k_0}{2}}{\left(1 + \frac{k_0}{\pi} + n\right)\frac{k_0}{2}} \qquad (4\text{-}39)$$

and

$$D(n,\xi) = \frac{1}{\pi} \xi_{tan} - (-)^n \Big]^{(-n)} \xi^{-ik\xi} \qquad (4\text{-}39)$$

H_ϕ^3 and E_ϕ^3 substituted in Equations (4-1) and (4-2) respectively express the fields for any point in Fraunhofer space. As a result of the approximations employed, these formulae are limited to the case when the aperture dimensions is the result direction it would in comparison to the average radius of the aperture. However, we may apply the continuous multiplying factor concept to the aperture to obtain a better approximation to the E plane field; this will result when the K plane field is added to the laboriously radiating horn.

Procedure Use Fourier Series to Obtain the K Plane Field of a Large Aperture Horn

By symmetry and the Fourier-Bessel series field equations E_ϕ^3 is zero in the E plane. Consider the field from the differential radiating element in the aperture in Figure IX to be given by the Fourier-Bessel field pattern equations. Let θr become $\theta r'$ and interprete in the r' direction.

$$E^3_{\theta'} = \int_{\frac{-\pi}{2}\theta}^{\frac{\pi}{2}\theta} \frac{\beta r}{2} \xi_{jk} \sin\theta \cos\frac{\chi}{2} \, r_{dr'} \qquad (4\text{-}60)$$

after integrating, evaluating, and letting

$$\delta x' = \delta r \tag{A-61}$$

the field expression becomes for $\phi = 0^{\circ}$

$$E_{\theta,1} = E_{\theta} \frac{\operatorname{Sin}\left(\frac{\pi \Delta x'_{o}}{\lambda} \operatorname{Sin} \theta\right)}{\left(\frac{\pi \Delta x'_{o}}{\lambda} \operatorname{Sin} \theta\right)} \tag{A-62}$$

In this integration the area M was excluded and the area N was included although it was not physically in the aperture. However, in the majority of antennas of this type errors due to this approximation are negligible because the fields in the ends of the aperture are very small in magnitude.

The Fraunhofer Field Expressions for $H_{i,0}$ Modes at the Aperture

The radiation fields for modes of higher order than H_{10} may be developed by employing an identical procedure as that employed in the development of the Fourier-Bessel series method. Because of the narrow aperture dimensions, the E modes are attenuated before they reach the aperture from the bend. By symmetry the even ordered $H_{i,0}$ modes cannot exist at the aperture. The odd order $H_{i,0}$ modes may exist by symmetry. Through a similar analysis to that preceeding this discussion, for the fields given by

$$E_{xi} = B_i \operatorname{Cos} \frac{i\pi\phi'}{\phi_o} \operatorname{Cos} \phi' \tag{A-63}$$

$$E_{yi} = B_i \operatorname{Cos} \frac{i\pi\phi'}{\phi_o} \operatorname{Sin} \phi' \tag{A-64}$$

the diffraction integrals are given by

$$N_x = \sum_{i=1}^{\infty} \frac{B_i r_1 \delta r \phi_o}{4} \left[A_i(0,\phi_o)\, J_o(kr_1 \operatorname{Sin} \theta) + \right.$$

$$\left. + \sum_{n=1}^{\infty} J_n(kr_1 \operatorname{Sin} \theta)\, A_i(n,\phi_o)\, B(n\phi) \right] \tag{A-65}$$

$$\rho x_1 = \rho r \tag{4-91}$$

the field expression becomes for $\phi = 0$,

$$E^{\theta}{}_{y} = E^{\theta}_{1} \frac{\left(\frac{\nu}{\rho x_1} \sin\theta\right)}{\sin(\pi \nu x_1 \sin\theta)} \tag{4-92}$$

In this interpretation the area A was considered and the area B was ignored although it was not physically in the aperture. However, in the majority of problems of this type errors due to this approximation are negligible because the fields in the ends of the aperture are very small in magnitude.

The Transverse Field Components for $E^{1,0}$ Modes at the Aperture

The radiation fields for modes of higher order than E^{10} may be developed by employing an identical procedure as that employed in the development of the Fourier-Bessel series method. Because of the narrow aperture dimension, the E modes are attenuated before they reach the aperture from the load. By symmetry the even ordered $H^{1,0}$ modes cannot exist at the aperture. The odd order $H^{1,0}$ modes may exist by symmetry. Through a similar analysis to that preceding this discussion, for the fields given by

$$E^{ex} = A' \cos\frac{\pi\rho_1}{\rho_1^0} \cos\phi, \tag{4-93}$$

$$E^{ey} = B' \cos\frac{\pi\rho_1}{\rho_1^0} \sin\phi \tag{4-94}$$

the diffraction integrals are given by

$$E^{x} = \sum_{i=j}^{\infty} \frac{j^{i} J^{i}}{\rho_1^0} \left[J^{i}(0,k^0) \, I^{0}(kr^{1} \sin\theta) + \right.$$

$$\left. + \sum_{n=j}^{\infty} I^{n}(x^{1} \sin\theta) \, Y^{i}(a,k^0) \, B(x) \right] \tag{4-95}$$

$$N_y = \sum_{i=1}^{\infty} \frac{B_i r_1 \delta r \phi_o}{4} \left[C_i(0,\phi_o)\, J_o(kr_1 \operatorname{Sin}\theta) + \right.$$

$$\left. + \sum_{n=1}^{\infty} J_n(kr_1 \operatorname{Sin}\theta)\, C_i(n,\phi_o)\, D(n,\phi) \right] \qquad \text{(A-66)}$$

where

$$A_i(n,\phi_o) = \frac{\operatorname{Sin}\left(\frac{i\pi}{\phi_o}+1+n\right)\frac{\phi_o}{2}}{\left(\frac{i\pi}{\phi_o}+1+n\right)\frac{\phi_o}{2}} + \frac{\operatorname{Sin}\left(\frac{i\pi}{\phi_o}+1-n\right)\frac{\phi_o}{2}}{\left(\frac{i\pi}{\phi_o}+1-n\right)\frac{\phi_o}{2}} +$$

$$+ \frac{\operatorname{Sin}\left(\frac{i\pi}{\phi_o}-1+n\right)\frac{\phi_o}{2}}{\left(\frac{i\pi}{\phi_o}-1+n\right)\frac{\phi_o}{2}} + \frac{\operatorname{Sin}\left(\frac{i\pi}{\phi_o}-1-n\right)\frac{\phi_o}{2}}{\left(\frac{i\pi}{\phi_o}-1-n\right)\frac{\phi_o}{2}} \qquad \text{(A-67)}$$

$$C_i(n,\phi_o) = \frac{\operatorname{Sin}\left(1-n-\frac{i\pi}{\phi_o}\right)\frac{\phi_o}{2}}{\left(1-n-\frac{i\pi}{\phi_o}\right)\frac{\phi_o}{2}} + \frac{\operatorname{Sin}\left(1+\frac{i\pi}{\phi_o}-n\right)\frac{\phi_o}{2}}{\left(1+\frac{i\pi}{\phi_o}-n\right)\frac{\phi_o}{2}} -$$

$$- \frac{\operatorname{Sin}\left(1-\frac{i\pi}{\phi_o}+n\right)\frac{\phi_o}{2}}{\left(1-\frac{i\pi}{\phi_o}+n\right)\frac{\phi_o}{2}} - \frac{\operatorname{Sin}\left(1+\frac{i\pi}{\phi_o}+n\right)\frac{\phi_o}{2}}{\left(1+\frac{i\pi}{\phi_o}+n\right)\frac{\phi_o}{2}} \qquad \text{(A-68)}$$

Employment of the Smith Chart to Plot Ellipticity in the H Plane

In order to make use of the ellipticity of the uncompensated laterally radiating electromagnetic horn the H plane field pattern ellipticity from $\theta = -5^\circ$ to $\theta = +5^\circ$ is plotted on the Smith chart in Figures XXVIII and XXIX. The computed values were obtained from Equations (6) and (7) and the measured values were obtained from the values on Figures XIX and XX and by assuming the phase relationships given by Equations (6) and (7) hold. The following conventions are employed:

$$\frac{\partial^2}{\partial r^2} = \sum_{n=1}^{\infty} \frac{\pi^2 n^2}{r^2} \left[\frac{\partial^2}{\partial r^2}(Q^n_{2k}) \cdot \frac{\partial^2}{\partial r^2}(\sin \theta) \right] +$$

$$+ \sum_{n=1}^{\infty} \frac{\pi^2}{r^2}(\sin \theta) \cdot \frac{\partial^2}{\partial r^2}(Q^n_{2k}) \cdot D(r,k) \Big] \qquad (C-20)$$

where

$$\frac{\partial^2}{\partial r^2}(Q^n_{2k}) = \frac{\sin\left(\frac{n}{2k}+2+n\right)\frac{\pi}{2}}{\left(\frac{n}{2k}+2+n\right)\frac{\pi}{2}} + \frac{\sin\left(\frac{n}{2k}+2-n\right)\frac{\pi}{2}}{\left(\frac{n}{2k}+2-n\right)\frac{\pi}{2}} +$$

$$+ \frac{\sin\left(\frac{n}{2k}-1+n\right)\frac{\pi}{2}}{\left(\frac{n}{2k}-1+n\right)\frac{\pi}{2}} + \frac{\sin\left(\frac{n}{2k}-1-n\right)\frac{\pi}{2}}{\left(\frac{n}{2k}-1-n\right)\frac{\pi}{2}} \qquad (C-21)$$

$$\frac{\partial^2}{\partial r^2}(Q^n_{2k}) = \frac{\sin\left(2-n-\frac{n}{2k}\right)\frac{\pi}{2}}{\left(2-n-\frac{n}{2k}\right)\frac{\pi}{2}} + \frac{\sin\left(2+\frac{n}{2k}-n\right)\frac{\pi}{2}}{\left(2+\frac{n}{2k}-n\right)\frac{\pi}{2}}$$

$$- \frac{\sin\left(1-\frac{n}{2k}+n\right)\frac{\pi}{2}}{\left(1-\frac{n}{2k}+n\right)\frac{\pi}{2}} - \frac{\sin\left(1+\frac{n}{2k}+n\right)\frac{\pi}{2}}{\left(1+\frac{n}{2k}+n\right)\frac{\pi}{2}} \qquad (C-22)$$

Development of the Double Sweep for Plane Diffraction in Zone II Cases

In order to make use of the ellipticity of the reconstructed laterally radiating electromagnetic beam the E plane field pattern displaced from $\theta = -\frac{\pi}{2}$ to $\theta = +\frac{\pi}{2}$ is plotted on the double sweep in Figures IXVIII and IXIX. The computed values were obtained from Equations (6) and (7) and the measured values were obtained from the values on Figures XII and IX and by assuming the plane reflecting plane by Equations (6) and (7) held. The following computations were employed:

1. All points having the same direction of rotation are plotted on one Smith Chart.
2. Circles of constant standing wave ratio are circles of constant $\frac{E_\theta}{E_\phi}$ ratio.
3. The angle at which the major axis of the ellipse is oriented with respect to the E_ϕ axis is half the physical angle on the Smith chart.

The Method of Computing E_θ in the E Plane for the Horn with 40° E Plane Flare

Equation (8) was employed. $G(\theta)$ was obtained from Figure 10.11 of Reference (36) which gave the values for a 40° E plane sectoral horn with a length of 3λ. $E_{p\theta}(G,0)$ was taken from the values of the computed E plane field pattern given in Figure XXXI.

1. All points having the same direction of rotation are plotted on one delta diagram.
2. Circles of constant standing wave ratio are plotted on constant $\frac{R}{Z_0}$ ratio.
3. The angle at which the major axis of the ellipse is oriented with respect to the $\frac{E}{I}$ axis is half the projected angle on the Smith chart.

The method of Computing β_1 is the I Plane for the Beam with $d\phi_0$ I Plane Plane

Equations (3) were applied. $\alpha(\omega)$ was obtained from Figure 10.11 of reference (3e) which gave the values for a $\Delta\phi_0$ S plane contour beam with a length of λ. $E_{\beta_0}(\alpha,\omega)$ was taken from the values of the computed H plane field pattern given in Figure XXII.

APPENDIX, SECTION C

ADMITTANCE DATA

ADMITTANCE DATA

Condition 1 - Uncompensated Horn

freq.	VSWR	λ	λg	minima	to space	short circ.	minima	rotation
9266	2.30	3.2376	4.56	10.55	12.86	10.22	12.50	0.065
9190	2.20	3.2649	4.66	9.82	12.18	9.99	12.32	0.166
9153	2.00	3.2776	4.69	9.49	11.87	9.90	12.21	0.213
8898	1.57	3.3715	5.00	8.99	11.42	9.02	11.52	0.130
8870	1.65	3.3822	5.00	8.89	11.39	9.12	11.58	0.151
8859	1.65	3.3864	5.02	8.70	11.24	9.06	11.56	0.176
8833	1.57	3.3963	5.06	8.48	10.97	9.00	11.53	0.212
8812	1.43	3.4045	5.10	8.12	10.62	8.90	11.45	0.260
8794	1.375	3.4114	5.12	7.86	10.45	8.64	11.17	0.248
8783	1.30	3.4157	5.15	7.70	10.30	8.60	11.15	0.268
8763	1.26	3.4235	5.16	7.36	9.98	8.49	11.09	0.315
8739	1.225	3.4329	5.18	7.03	9.58	8.43	11.02	0.371
8716	1.21	3.4419	5.20	9.15	11.35	10.90	13.50	0.432
8698	1.25	3.4491	5.22	8.84	11.45	10.90	13.47	0.486
8670	1.335	3.4602	5.25	8.39	11.03	8.15	10.71	0.044
8649	1.41	3.4686	5.27	8.07	10.76	8.03	10.68	0.080
8627	1.50	3.4775	5.28	7.83	10.48	7.95	10.59	0.112
8616	1.58	3.4818	5.34	7.70	10.40	7.90	10.58	0.123

"a" = 3.3 cm.

Condition 2 - Horn with Plane Parallel Filter, No Flare

9349	2.00	3.2089	4.98	9.04	11.36	10.47	0.471
9332	2.00	3.2148	4.52	8.94	11.16	10.40	0.480
9286	2.00	3.2306	4.56	8.49	10.73	10.25	0.039
9219	2.00	3.2542	4.64	7.77	10.09	10.04	0.127
9178	1.90	3.2687	4.70	7.37	9.75	9.91	0.167
9141	1.80	3.2819	4.74	9.40	11.73	9.80	0.214
9095	1.57	3.2985	4.80	8.91	11.25	9.65	0.279
9063	1.41	3.3102	4.82	8.47	10.87	9.54	0.347
9013	1.38	3.3285	4.86	7.89	10.30	9.37	0.429
8976	1.37	3.3422	4.94	9.82	12.23	9.24	0.497
8950	1.40	3.3520	4.94	9.54	12.00	9.15	0.036
8922	1.42	3.3625	4.96	9.18	11.65	9.05	0.086
8898	1.45	3.3715	5.00	8.95	11.40	8.95	0.110
8878	1.42	3.3791	5.01	8.72	11.22	8.89	0.123
8852	1.38	3.3891	5.04	8.59	10.91	8.78	0.145
8809	1.25	3.4056	5.12	8.10	10.58	8.61	0.201
8787	1.15	3.4142	5.14	10.28	12.82	11.09	0.264
8772	1.10	3.4199	5.18	7.52	10.05	8.46	0.291
8765	1.05	3.4227	5.18	9.97	12.40	11.02	0.331
8742	1.05	3.4317	5.22	9.41	11.85	10.94	0.421
8729	1.08	3.4376	5.22	8.98	11.53	10.90	0.474

"a" = 3.3 cm.

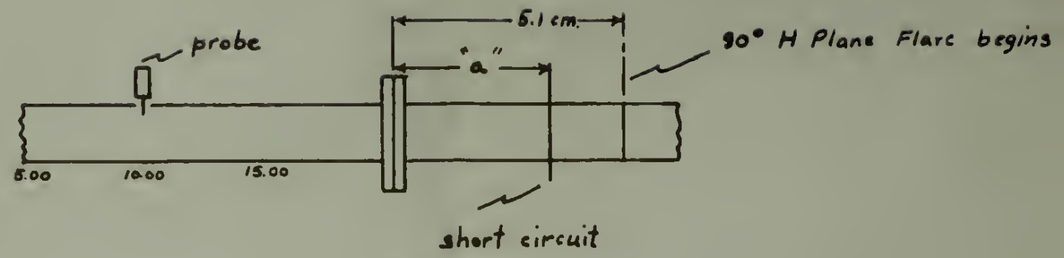

Schematic of Measuring Equipment

Note:

1. All frequencies are megacycles, all distances centimeters.
2. "a" is the distance from the short circuit to the flange.
3. "Rotation" signifies the Smith Chart rotation toward the load to be used for plotting admittances.

Condition 3 - Horn with E Plane Flare, No Filter

freq.	VSWR	λ	λg	minima to space		short circ. minima		rotation
9343	1.40	3.2109	4.98	10.97	13.28	10.74	12.98	0.018
9311	1.48	3.2221	4.54	10.70	12.96	10.63	12.90	0.067
9291	1.49	3.2291	4.60	10.97	12.74	10.57	12.84	0.098
9267	1.44	3.2373	4.60	10.25	12.56	10.49	12.79	0.126
9246	1.95	3.2447	4.62	10.14	12.40	10.42	12.73	0.146
9215	1.405	3.2555	4.65	9.82	12.11	10.32	12.65	0.189
9200	1.35	3.2608	4.66	9.65	12.02	10.28	12.61	0.194
9182	1.27	3.2672	4.70	9.54	11.88	10.22	12.57	0.216
9147	1.165	3.2798	4.72	9.30	11.59	10.11	12.48	0.256
9125	1.08	3.2877	4.74	8.98	11.37	10.04	12.42	0.288
9114	1.03	3.2916	4.76	8.86	11.25	10.00	12.39	0.305
9107	1.01	3.2942	4.76	8.67	11.02	9.98	12.37	0.397
9102.5	1.005	3.2958	4.78	8.32	10.35	9.97	12.36	0.484
9102	1.01	3.2959	4.78	10.26	12.67	9.97	12.36	0.499
9093	1.025	3.2992	4.78	10.19	12.46	9.94	12.33	0.036
9071	1.08	3.3072	4.82	10.00	12.37	9.87	12.27	0.041
9053	1.15	3.3138	4.83	9.80	12.21	9.80	12.22	0.062
9025	1.21	3.3241	4.84	9.50	1190	9.71	12.13	0.108
9001	1.21	3.3329	4.88	9.32	11.72	9.62	12.07	0.129
8977	1.27	3.3418	4.90	9.10	11.54	9.54	12.00	0.155
8962	1.29	3.3475	4.94	8.96	11.32	9.48	11.95	0.181
8927	1.24	3.3605	4.96	8.50	10.96	9.36	11.84	0.229
8898	1.245	3.3678	5.00	8.25	10.72	9.26	11.76	0.258
8874	1.19	3.3806	5.01	10.32	12.86	9.17	11.68	0.314
8845	1.15	3.3917	5.04	8.86	12.35	9.06	11.58	0.395
8822	1.23	3.4005	5.08	9.97	12.04	8.96	11.51	0.441
8805.5	1.33	3.4072	5.12	9.27	11.85	8.90	11.45	0.465
8783	1.44	3.4157	5.17	8.96	11.55	8.80	11.39	0.009
8762	1.50	3.4239	5.18	8.72	11.32	8.72	11.31	0.037
8745.5	1.57	3.4305	5.26	8.60	11.16	8.65	11.26	0.058
8731	1.62	3.4361	5.22	8.40	11.06	8.59	11.21	0.070
8711	1.69	3.4439	5.25	8.17	10.82	8.50	11.14	0.097
8693	1.70	3.4511	5.28	8.00	10.62	8.43	11.08	0.121
8668	1.77	3.4610	5.32	10.39	13.02	8.32	10.98	0.162
8649	1.86	3.4685	5.34	10.16	12.80	8.23	10.90	0.170
8628	1.94	3.4771	5.35	9.95	12.59	8.15	10.82	0.193
8608	1.92	3.4852	5.39	9.68	12.38	8.06	10.75	0.227

"a" = 3.6 cm.

Condition 4 - Horn with E Plane Flare, Plane Parallel Plate Filter

freq.	VSWR	λ	λg	minima to space		short circ. minima		rotation
9148	1.25		4.74	11.73	14.06	12.18		0.229
9121	1.135		4.76	11.40	13.78	12.10		0.275
9104	1.07		4.78	11.15	13.60	9.68		0.313
9094	1.025		4.80	10.98	13.50	9.64		0.333
9076	1.03		4.80	10.62	12.94	9.62		0.425
9060	1.10		4.82		12.45	9.55		0.022
9034	1.18		4.86	12.06	14.52	9.46		0.083
9002	1.205		4.90	11.86	14.30	9.33		0.102
8979	1.275		4.92	11.67	14.10	9.24		0.125
8961	1.305		4.96	11.44	13.91	9.17		0.156
8924	1.27		5.00	11.13	13.59	9.03		0.194
8904	1.27		5.02	10.82	13.41	8.95		0.228
8876	1.23		5.08	10.45	12.99	8.84		0.287
8846	1.21		5.10	9.96	12.47	8.72		0.368
8826	1.24		5.10	9.64	12.19	8.65		0.409
8800	1.34		5.14	9.26	11.85	8.55		0.460
8777	1.45		5.18	8.98	11.58	8.46		0.497
8750	1.55		5.22	8.64	11.24	8.35		0.090
8731	1.64		5.24	8.40	11.04	8.28		0.069
8710	1.79		5.26	8.18	10.82	8.20		0.095
8687	1.84		5.28	7.90	10.53	8.10		0.130
8660	1.89		5.30	7.62	10.30	8.00		0.158
8642	1.96		5.34	7.42	10.08	7.94		0.185
8622	2.05		5.36	7.20	9.84	7.82		0.205
8589	1.96		5.41	6.80	9.51	7.67		0.243

"a" = 3.3 cm.

Condition 5 - Horn with E Plane Flare, Parallel Wire Filter

9063	1.10	4.82	9.80	12.11	11.98	0.097
9031	1.20	4.88	9.55	11.91	11.87	0.111
8998	1.18	4.92	9.14	11.63	11.77	0.124
8952	1.20	4.98	8.65	11.08	11.62	0.220
8914	1.205	5.02	8.26	10.73	11.49	0.246
8887	1.20	5.05	8.10	10.64	11.40	0.259
8875	1.175	5.08	7.79	10.32	11.37	0.311
8861	1.16	5.08	7.52	10.02	11.32	0.361
8860	1.11	5.08	7.51	10.17	11.32	0.
8854	1.17	5.08	7.39	9.89	11.30	0.381
8843	1.18	5.10	7.23	9.67	11.27	0.393
8831	1.20	5.12	7.01	9.63	11.22	0.415
8810	1.30	5.14	6.70	9.32	11.15	0.457
8781	1.41	5.18	8.95	11.45	11.06	0.022
8734	1.53	5.24	8.40	11.04	10.90	0.063
8685	1.71	5.30	7.86	10.52	10.15	0.133
8646	1.83	5.32	7.49	10.15	10.63	0.179
8591	1.81	5.40	6.86	9.53	10.45	0.254

"a" = 3.3 cm.

APPENDIX, SECTION D

SAMPLE CALCULATIONS

Sample Calculations of the Linear Equivalent Source Method of Computing the E Plane Polarized, H Plane Field Pattern

Formula (2) is applicable.

$$E_x = \frac{jk\, e^{-jkR}(1+\cos\theta)\, B\, x_o y_o}{4\pi R}\left[\frac{\sin\left[\frac{(\pi+\phi_o)}{2} - ky_o \sin\theta\right]}{\left[\frac{(\pi+\phi_o)}{2} - ky_o \sin\theta\right]}\right.$$

$$+\frac{\sin\left[\frac{(\pi+\phi_o)}{2} + ky_o \sin\theta\right]}{\left[\frac{(\pi+\phi_o)}{2} + ky_o \sin\theta\right]} + \frac{\sin\left[\frac{(\pi-\phi_o)}{2} - ky_o \sin\theta\right]}{\left[\frac{(\pi-\phi_o)}{2} - ky_o \sin\theta\right]}$$

$$\left.+\frac{\sin\left[\frac{(\pi-\phi_o)}{2} + ky_o \sin\theta\right]}{\left[\frac{(\pi-\phi_o)}{2} + ky_o \sin\theta\right]}\right]$$

Let $\phi_o = \frac{\pi}{2}$; $r_{av} = 37.7$ cm.; $\lambda = 3.2$ cm.; $ky_o = \frac{2\pi}{\lambda}\, r_{av} \sin\frac{\phi}{2}$o

Table I

Linear Equivalent Source Sample Calculation

θ	A	B	C	D	E	F
Degrees	$ky_o \sin\theta$	$\frac{(\pi+\phi_o)}{2} - A$	$\frac{(\pi+\phi_o)}{2} + A$	$\frac{\sin B}{B}$	$\frac{\sin C}{C}$	$\frac{(\pi-\phi_o)}{2} - A$
0	0	2.3562	2.3562	0.3000	0.3000	0.7854
1	1.087	1.2692	3.4432	0.7520	-0.0854	-0.3016
2	2.175	0.1812	4.5312	0.9946	-0.2171	-1.3896
3	3.260	-0.9038	5.6162	0.8695	-0.1111	-2.4746
4	4.340	-1.984	6.6960	0.4610	0.0604	-3.5550
5	5.420	-3.064	7.7760	0.0245	0.1281	-4.5350

SAMPLE CALCULATIONS

Sample Calculation of the Linear Equivalent Source Method of Computing the E Plane Polarized, H Plane Field Pattern

Formula (2) is applicable.

$$E^x = \frac{-ie^{-ikr}}{2\pi r}(1+\cos\theta)\, h\, q_y^0 \left[\frac{\sin\left[\frac{\pi}{2}(a+b_0^0) - kb^0 \sin\theta\right]}{\left[\frac{\pi}{2}(a+b_0^0) - kb^0 \sin\theta\right]}\right.$$

$$+ \frac{\cos\left[\frac{\pi}{2}(a+b_0^0) + kb^0 \sin\theta\right]}{\left[\frac{\pi}{2}(a+b_0^0) + kb^0 \sin\theta\right]} + \frac{\sin\left[\frac{\pi}{2}(a-b_0^0) - kb^0 \sin\theta\right]}{\left[\frac{\pi}{2}(a-b_0^0) - kb^0 \sin\theta\right]}$$

$$\left. + \frac{\sin\left[\frac{\pi}{2}(a-b_0^0) + kb^0 \sin\theta\right]}{\left[\frac{\pi}{2}(a-b_0^0) + kb^0 \sin\theta\right]} \right]$$

Let $b_0^0 = \frac{\pi}{E}$; $\varepsilon_{RA} = 31.7$ cm.; $\gamma = 3.\varepsilon$ cm.; $kb^0 = \frac{\gamma}{2\varepsilon}\ \varepsilon_{RA} \sin\frac{\pi}{E}\theta$

Table I

Linear Equivalent Source Sample Calculation

Degree	$kb^0 \sin\theta$	$\frac{\pi}{2}(a+b_0^0) - A$	$\frac{\pi}{2}(a+b_0^0)+A$	$\frac{\sin B}{B}$	$\frac{\sin C}{C}$	$\frac{\pi}{2}(a-b_0^0) - A$
θ	A	B	C	D	E	F
0	0	-3.1563	3.1563	0.3000	0.3000	0.7854
1	1.009	1.1893	5.1433	0.1750	-0.0834	-0.3014
2	2.175	0.1814	4.5312	0.0946	-0.1171	-1.3864
3	3.200	-0.9038	5.6182	0.0695	-0.1111	-2.4749
4	4.380	-1.764	6.6960	0.1430	0.0004	-3.5550
5	5.420	-3.064	7.7760	0.0249	0.1283	-4.5350

θ Degrees	G $\frac{(\pi - \phi_o)}{2} + A$	H $\frac{\text{Sin } F}{F}$	I $\frac{\text{Sin } G}{G}$	J D+E+H+G	K E_x in db.
0	0.7854	0.9000	0.9000	2.400	0.00
1	1.8724	0.9850	0.5110	2.163	- 0.90
2	2.9604	0.7077	0.0610	1.646	- 3.26
3	4.0454	0.4900	-0.1936	1.0548	- 7.12
4	5.1250	-0.1125	-0.1785	0.1096	-26.84
5	6.2050	-0.2170	-0.0125	0.057	-32.48

Variations in the term $(1 + \text{Cos } \theta)$ are considered to be negligible in this range. A plot of E_x is given on Figure XVII.*

The Fourier-Bessel Series Method of Computing the E Plane Polarized, H Plane Field Pattern

In order to determine the H plane field pattern, let $\phi = \frac{\pi}{2}$ in Formula (6), and the resultant equation becomes:

$$E_x = -E_\phi = \frac{ik\, \varepsilon^{-jkR}_B\, r\, \delta r}{32\, R} (1 + \text{Cos } \theta) \left[A(0, \tfrac{\pi}{2})\, J_o(kr_1 \text{ Sin } \theta) + \right.$$

$$\left. + \sum_{n=1}^{\infty} J_n(kr_1 \text{ Sin } \theta)\, A(n, \tfrac{\pi}{2})\, B(n, \tfrac{\pi}{2}) \right]$$

The argument of the Bessel function can be computed. For this antenna

$$kr_1 = \frac{2\pi}{\lambda} r_1 = \frac{2\pi\ 37.7}{3.2} = 73.$$

The first step is to make a table of $A(n, \phi_o)$ and $B(n, \phi)$.

---

* In order to simplify the calculations of $\frac{\text{Sin } x}{x}$ terms Reference (10) may be employed.

Degrees	$\frac{(\pi - \psi_0')}{2} + A$	$\frac{\sin \Gamma}{\Gamma}$	$\frac{\sin \Omega}{\Omega}$	$D + E + A + C$	E^x in db
0	0.7854	0.9000	0.9000	2.490	0.00
1	1.0754	0.9830	0.9110	3.169	- 0.90
2	2.0004	0.7077	0.0610	1.649	- 7.46
3	1.0134	0.4900	-0.1936	1.0648	- 7.11
4	1.1390	-0.1145	-0.1783	0.1850	-26.84
5	0.2030	-0.2170	-0.0145	0.021	-32.48

Variations in the term $(1 + \cos \theta)$ are considered to be negligible in this range. A plot of E^x is given on Figure XVII.*

The Fourier-Bessel Series Method of Computing the H Plane Polarized H Plane Field Pattern

In order to determine the H plane field pattern, let $\psi = \frac{\pi}{2}$ in formula (6), and the resultant equation becomes:

$$E^x = -E^\theta = \frac{ik\, e^{-ikr}}{2\pi R} \int_0^{2\pi} (1 + \cos\theta) \left[A(\Omega, \tfrac{\pi}{2})\, J_0(kr' \sin\theta) + \right.$$

$$\left. + \sum_{n=1}^{\infty} 2 J_n(kr' \sin\theta)\, A(n, \tfrac{\pi}{2})\, B(n, \tfrac{\pi}{2}) \right]$$

The argument of the Bessel function can be computed. For this example

$$kr' = \frac{\gamma}{\lambda} \pi' = \frac{3\pi}{3.2} \pi = 7\pi.$$

The first step is to make a table of $A(n, \frac{\pi}{2})$ and $B(n, \frac{\pi}{2})$.

---

* In order to simplify the calculations of $\frac{E^x}{E}$ these references (12) may be employed.

Table II

Values of $A(n,\phi_o)$ for $\phi_o = \frac{\pi}{2}$ and n = 0, $\pm$ 1, $\pm$ 2, ...

N	$\frac{\sin[\frac{\pi}{\phi_o}+N+1]\frac{\phi_o}{2}}{[\frac{\pi}{\phi_o}+N+1]\frac{\phi_o}{2}}$	$\frac{\sin[\frac{\pi}{\phi_o}-N+1]\frac{\phi_o}{2}}{[\frac{\pi}{\phi_o}-N+1]\frac{\phi_o}{2}}$	$\frac{\sin[\frac{\pi}{\phi_o}+N+1]\frac{\phi_o}{2}}{[\frac{\pi}{\phi_o}+N-1]\frac{\phi_o}{2}}$	$\frac{\sin[\frac{\pi}{\phi_o}-N-1]\frac{\phi_o}{2}}{[\frac{\pi}{\phi_o}-N-1]\frac{\phi_o}{2}}$	$A(N,\frac{\pi}{2})$
0	0.2984	0.2984	0.9000	0.9000	2.3968
$\pm$1	0	0.6360	0.6360	1.0000	2.2720
$\pm$2	-0.1800	0.9000	0.2984	0.9000	1.9184
$\pm$3	-0.2118	1.0000	0	0.6360	1.4242
$\pm$4	-0.1283	0.9000	-0.1800	0.2984	0.8900
$\pm$5	0.1000	0.6360	-0.2118	0	0.4240
$\pm$6		0.2984	-0.1283	-0.1800	0.0900

The table of $B(n,\phi)$ may also be constructed. This table will apply to any antenna design.

Table III

Values of $B(n,\phi)$ for $\phi = 0$, $\phi = \pi/2$, and n = $\pm$1, $\pm$2, $\pm$3, ...

n	$B(n,\phi)$	$\phi = 0$	$\phi = \frac{\pi}{2}$	n	$B(n,\phi)$	$\phi = 0$	$\phi = \frac{\pi}{2}$
$\pm$1	2j Cos ϕ	2j	0	$\pm$4	+2j Cos 4ϕ	2	2
$\pm$2	-2 Cos 2ϕ	-2	2	$\pm$5	+2j Cos 5ϕ	2j	0
$\pm$3	-2j Cos 3ϕ	-2j	0	$\pm$6	-2j Cos 6ϕ	-2	2

Table IV

Computation of E_x for the H Plane Field Pattern (Use Equation (7))

θ	$J_o(K\eta_1 \sin\theta)$ $A(0,\pi/2)$	$J_2(K\eta_1 \sin\theta)$ $A(2,\pi/2)$ $B(2,\frac{\pi}{2})$	$J_4(K\eta_1 \sin\theta)$ $A(4,\pi/2)$ $B(4,\frac{\pi}{2})$	$J_6(K\eta_1 \sin\theta)$ $A(6,\pi/2)$ $B(6,\pi/2)$	E_x	db.
0	+4.7936	0	0	0	+4.7936	0.00
1	+2.9900	+1.3480	+0.0221	0	+4.3601	-0.79
2	-0.3260	+3.4650	+0.2760	+0.0017	+3.4174	-2.93

The E_x H plane pattern field is plotted on Figure XVII.

The Fourier-Bessel Series Method of Computing the H Plane Polarized H Plane Field Pattern

Table II

Values of $J_n(n\beta_0)$ for $\beta_0 = \frac{\pi}{2}$ and $n = 0, \pm 1, \pm 2, \pm 3, \ldots$.

n	$\frac{\sin[\frac{\pi}{2}(n+1)]}{\frac{\pi}{2}}$	$\frac{\sin[\frac{\pi}{2}(-n+1)]}{\frac{\pi}{2}}$	$\frac{\sin[\frac{\pi}{2}(n+1)]}{[\frac{\pi}{2}(n+1)]\frac{\pi}{2}}$	$\frac{\sin[\frac{\pi}{2}(-n+1)]}{[\frac{\pi}{2}(-n+1)]\frac{\pi}{2}}$	$H(n,\frac{\pi}{2})$
0	0.63662	0.63662	0.90000	0.90000	1.80000
± 1	0	0.42440	0.60000	1.80000	2.40000
± 2	-0.12732	0.25464	0.36000	1.08000	1.44000
± 3	-0.09095	0.18189	0.25714	0.77143	1.02857
± 4	-0.07074	0.14147	0.20000	0.60000	0.80000
± 5	-0.05789	0.11578	0.16364	0.49091	0.65455
± 6	-0.04897	0.09794	0.13846	0.41538	0.55385
± 7	-0.04244	0.08488	0.12000	0.36000	0.48000

The table of $B(n,\beta)$ may also be constructed. This table will apply to any antenna design.

Table III

Values of $B(n,\beta)$ for $\beta = 0, \beta = \frac{\pi}{2}$, and $n = \pm 1, \pm 2, \pm 3, \ldots$.

n	$B(n,\beta)$	$\beta = 0$	$\beta = \frac{\pi}{2}$	n	$B(n,\beta)$	$\beta = 0$	$\beta = \frac{\pi}{2}$
± 1	$-j$	$-j$	0	$+1$	$+j$	$+j$	0
± 2	-2	-2	2	± 3	$+3j$	$+3j$	$3j$
± 3	$-3j$	$-3j$	0	± 5	$+5j$	$+5j$	0

Table IV

Computation of E_x^x for the H Plane Fields Pattern (Use Symbols (?))

θ	$H(\rho,\frac{\pi}{2})$	$J_0(n\beta_0)B(n,\frac{\pi}{2})$	$J_1(n\beta_0\sin\theta)B(n,\frac{\pi}{2})$	$J_2(n\beta_0\sin\theta)B(n,\frac{\pi}{2})H(n,\frac{\pi}{2})$	E_x^x	dB
0	+4.7139	0	0	0	+4.7139	0.00
1	+4.7940	+1.1480	+0.0212	0	+4.3260	-0.79
2	-0.3368	+1.1480	+0.2750	+0.0217	+3.4.174	-3.81

The E_x^x H plane pattern field is plotted on Figure XVII.

The Fourier-Bessel Series Method of Computation for H Plane Polarized H Plane Field Pattern

Let $\phi = \frac{\pi}{2}$ in Equation (6), $\phi_o = \frac{\pi}{2}$ in the equation for $C(n,\phi_o)$ and construct a table for values of $C(n,\frac{\pi}{2})$

Table V

Values of $C(n,\frac{\pi}{2})$ for n = 0, ±1, ±2, ±3, ...

n	$C(n,\frac{\pi}{2})$	n	$C(n,\frac{\pi}{2})$
0	0	±4	+0.550
±1	+0.272	±5	+0.424
±2	+0.478	±6	+0.090
±3	+0.575		

Next a table of $D(n,\phi)$ is constructed. This table is applicable to all antennas.

Table VI

Table of $D(n,\phi)$ for $\phi = 0$, $\phi = \frac{\pi}{2}$, and n = 1, 2, 3, ...

n	$D(n,\phi)$	$\phi = 0$	$\phi = \frac{\pi}{2}$	n	$D(n,\phi)$	$\phi = 0$	$\phi = \frac{\pi}{2}$
1	$-2 \sin \phi$	0	-2	4	$+2j \sin 4\phi$	0	0
2	$-2j \sin 2\phi$	0	0	5	$-2 \sin 5\phi$	0	-2
3	$+2 \sin 3\phi$	0	-2	6	$-2j \sin 6\phi$	0	0

Evaluating Equation (6) the following table results.

Table VII

Computation of E_θ in the H Plane Field Pattern ($\phi = \frac{\pi}{2}$ in Equation (6))

θ^o	$J_1(K\lambda, \sin\theta)$ $C(1,\frac{\pi}{2})\,D(1,\frac{\pi}{2})$	$J_3(K\lambda, \sin\theta)$ $C(3,\frac{\pi}{2})\,D(3,\frac{\pi}{2})$	$J_5(K\lambda, \sin\theta)$ $C(5,\frac{\pi}{2})\,D(5,\frac{\pi}{2})$	E_θ	db.
0	+0.0000	+0.0000	+0.00000	+0.00000	$-\infty$
1	+0.5610	+0.0868	+0.0014	+0.6512	-17.32
2	+0.5300	+0.5170	+0.0354	+1.0824	-12.93
3	+0.0051	+0.9650	+0.1890	+1.0053	-13.78

Let $\beta = \frac{\pi}{2}$ in equation (6), $\beta^0 = \frac{\pi}{4}$ in the equation for $\Theta(\alpha, \beta_0^0)$ and construct a table for values of $\Theta(\alpha, \frac{\pi}{4})$

Table I

Values of $\Theta(\alpha, \frac{\pi}{4})$ for $\alpha = 0^\circ, \frac{+1}{-1}^\circ, \frac{+2}{-2}^\circ, \frac{+3}{-3}^\circ$ ...

α	$\Theta(\alpha, \frac{\pi}{4})$	α	$\Theta(\alpha, \frac{\pi}{4})$
0	0	$\frac{+}{-}2^\circ$	+0.1320
$\frac{+}{-}1$	+0.2274	$\frac{+}{-}3$	+0.1824
$\frac{+}{-}2$	+0.4726	$\frac{+}{-}4$	+0.2080
$\frac{+}{-}3$	+0.7275		

Next a table of $D(\alpha, \beta)$ is constructed. This table is applicable to all antennae.

Table VI

Table of $D(\alpha, \beta)$ for $\beta = 0^\circ, \beta = \frac{\pi}{2}, \frac{+1}{-1}\beta, \frac{+2}{-2}\beta, \frac{+3}{-3}\beta$ ....

α	$D(\alpha, \beta)$ $\beta = 0$	$\beta = \frac{\pi}{2}$	α	$D(\alpha, \beta)$	$\beta = 0$	$\beta = \frac{\pi}{2}$
1	$-2 \sin \beta$	0	-1	$+2 \sin \frac{\beta}{2}$	0	0
2	$-2 \sin 2\beta$	0	0	$-2 \sin \beta$	0	-2
3	$+2 \sin 3\beta$	0	-3	$-2 \sin \frac{3\beta}{2}$	0	0

Evaluating Equation (6) the following table results.

Table VII

Computation of E^θ in the H Plane Field Pattern ($\beta = \frac{\pi}{2}$ in Equation (6))

θ_0	$C(\alpha, \frac{\pi}{4}) D(\alpha, \frac{\pi}{2})$	$C(\alpha, \frac{\pi}{4}) D(\alpha, \frac{\pi}{2})$	E^θ	dB.
	$J_1(k r, \sin \theta)$	$J_2(k r, \sin \theta)$		
0	+0.0023	+1.0000	+0.00000	- ∞
1	+0.5820	+1.0694	+0.00224	-47.36
2	+0.5820	+0.9170	+0.01924	-17.16
3	+0.0231	+0.4930	+0.00231	-32.36

The Fourier-Bessel Series Method of Computing the E Plane Polarized E Plane Field Pattern

Substitute $\phi = 0^\circ$ and $\phi_o = \frac{\pi}{2}$ in Equation (6). The $A(n,\phi_o)$ and the $B(n,0)$ tables have already been computed.

Table VIII

Computation of the Real Part of E_θ in the E plane

θ°	$J_0(KA, \sin\theta)$ $A(0, \pi/2)$	$J_2(KA, \sin\theta)$ $A(2, \pi/2)$ $B(2,0)$	$J_4(KA, \sin\theta)$ $A(4, \pi/2)$ $B(4,0)$	$J_6(KA, \sin\theta)$ $A(6, \pi/2)$ $B(6,0)$	$Re[E_\theta]$
0	+4.7936	0.0000	0.0000	0.0000	+4.7936
1	+2.9900	-1.3491	+0.0220	0.0000	+1.6613
2	+0.3260	-3.4634	+0.2760	-0.0017	-2.8630
3	-1.9280	-3.1071	+0.9030	-0.0141	-4.1762

Table IX

Computation of the Imaginary Part of E_θ in the E Plane

θ°	$J_1(KA, \sin\theta)$ $A(1, \pi/2)$ $B(1,0)$	$J_3(KA, \sin\theta)$ $A(3, \pi/2)$ $B(3,0)$	$J_5(KA, \sin\theta)$ $A(5, \pi/2)$ $B(5,0)$	$Im[E_\theta]$
0	0.0000	0.0000	0.0000	0.0000
1	+4.6830	-0.2195	+0.00136	+4.4649
2	+4.4254	-1.2758	+0.0354	+3.1850
3	+0.0429	-2.3881	+0.1895	-2.1550

Table X

Computation of the Magnitude and Phase of E_θ in the E Plane for Constant R

θ°	$\lvert E_\theta \rvert$	$\angle E_\theta^\circ$	Incremental Source db.	Array Factor	Finite Source db.
0	4.7936	0	0.00	1.00	0.00
1	4.7600	69.6	-0.05	1.00-	-0.05
2	4.6800	132.0	-0.10	1.00-	-0.10
3	4.7000	207.3	-0.10	1.00-	-0.10

These values are plotted on Figure XXX.

The Exterior-Sound Electric Potential of Spheroidal Type B Plane Polarized E Plane Field Pattern

Substitute $\psi = \psi_0^e$ and $\psi^0 = \frac{1}{2}\psi_0^e$ in Equations (8). The $A(\alpha,\beta_0^1)$ and the $B(\beta,\alpha)$ radial laws already been computed.

Table VIII

Computation of the Real Part of ψ_0^e in the E plane

θ°	$R(\alpha,\beta_0^1)$ $S^1(\beta_0^1,\cos\theta)$	$R(\alpha,\beta_0^3)$ $S^1(\beta_0^3,\cos\theta)$	$R(\alpha,\beta_0^5)$ $S^1(\beta_0^5,\cos\theta)$	$R_e[\psi_0^e]$
0	+4.7936	0.0000	0.0000	+4.7936
1	+4.0980	-1.3491	+0.0230	+2.6819
2	+0.3280	-3.1512	+0.3760	-2.4520
3	-1.7280	-3.1071	+0.9030	-4.1720

Table IX

Computation of the Imaginary Part of ψ_0^e in the E Plane

θ°	$P_1^1(\alpha,\beta_0^1)$ $S^1(\beta_0^1,\cos\theta)$	$R(\alpha,\beta_0^3)$ $S^1(\beta_0^3,\cos\theta)$	$R(\alpha,\beta_0^5)$ $S^1(\beta_0^5,\cos\theta)$	$\psi_{0m}^e[E_\theta]$
0	0.0000	0.0000	0.0000	0.0000
1	+4.0830	-0.4293	+0.0026	+4.6564
2	+4.0734	-1.2758	+0.0254	+3.1230
3	+0.0129	-1.2891	+0.1293	-1.1350

Table X

Computation of the Magnitude and Phase of ψ_0^e in the E plane for Case Number II

θ°	$\lvert E_\theta^e \rvert$	$\frac{E_\theta^e}{E_\theta^o}$	Imaginary Portion $d\theta$.	Error Factor	Finite Increase $\delta\theta$.
0	4.7936	0	0.00	1.00	0.00
1	4.7320	44.0	-0.04	1.03-	-0.03
2	4.6000	136.0	-0.10	1.00-	-0.10
3	4.7320	207.3	-0.10	1.00-	-0.10

These values are plotted on Figure XXX.

BIBLIOGRAPHY

1. "Calculation of the Radiation Properties of Hollow Pipes and Horns", L. J. Chu, Journal of Applied Physics, Vol. 11, September, 1940, pages 603-610.

2. Microwave Antenna Theory and Design, Samuel Silver, McGraw-Hill Book Company, Inc., 1949, page 357.

3. "The Theory of the Electromagnetic Horn", W. L. Barrow and L. J. Chu, Proceedings of the I. R. E., Vol. 27, pages 51-64, January, 1939.

4. "The Sectoral Electromagnetic Horn", W. L. Barrow and F. D. Lewis, Proceedings of the I. R. E., Vol. 27, pages 41-50, January 1939.

5. "Electromagnetic Horn Design", L. J. Chu and W. L. Barrow, Transactions of the A. I. E. E., Vol. 58, pages 333-337, July, 1939.

6. Antennas, J. D. Kraus, McGraw-Hill Book Company, Inc., 1950, pages 375-377.

7. Microwave Antenna Theory and Design, Samuel Silver, McGraw-Hill Book Company, Inc., 1949, page 401.

8. Microwave Antenna Theory and Design, Samuel Silver, McGraw-Hill Book Company, Inc., 1949, page 408.

9. Antennas, J. D. Kraus, McGraw-Hill Book Company, Inc., 1950, The Diagram on page 377.

10. Tables of the Function $\frac{\sin \phi}{\phi}$ and of its First Eleven Derivitives, Staff of the Computation Laboratory of Harvard University, Harvard University Press, Cambridge, Mass., 1949.

11. Tables of the Bessel Functions of the First Kind of Orders Zero and One; Two and Three; Four, Five, and Six, Staff of the Computation Laboratory of Harvard University, Harvard University Press, Cambridge, Mass., 1947.

12. "Transmission between Elliptically Polarized Antennas", V. H. Rumsey, Proceedings of the I. R. E., Vol. 39, No. 5, May, 1951, page 535.

13. Fields and Waves in Modern Radio, Simon Ramo and J. R. Whinnery, John Wiley and Sons, Inc., 1944, pages 294-299.

14. Introduction to Theoretical Physics, J. C. Slater and N. H. Frank, McGraw-Hill Book Co., Inc., New York, 1933, Chapters 26 and 27.

15. Electromagnetic Theory, J. A. Stratton, McGraw-Hill Book Co., Inc., New York, 1941, Chapter 8.

BIBLIOGRAPHY

1. "Calculation of the Radiation Properties of Hollow Pipes and Horns", R. 1. Cox, Journal of Applied Physics, Vol. 11, December, 1940, pages 805-810.

2. Microwave Antenna Theory and Design, Samuel Silver, McGraw-Hill Book Company, Inc., 1949, page 337.

3. "The Theory of the Electromagnetic Horn", W. L. Barrow and L. J. Chu, Proceedings of the I. R. E., Vol. 27, pages 51-64, January, 1939.

4. "The Sectoral Electromagnetic Horn", S. A. Schelkunoff, W. L. Barrow and T. S. Lewis, Proceedings of the I. R. E., Vol. 27, pages 41-50, January 1939.

5. "Electromagnetic Horn Design", R. J. Chu and W. L. Barrow, Transactions of the A. I. E. E., Vol. 59, pages 133-137, July, 1939.

6. Antennas, J. D. Kraus, McGraw-Hill Book Company, Inc., 1950, pages 175-177.

7. Microwave Antenna Theory and Design, Samuel Silver, McGraw-Hill Book Company, Inc., 1949, page 401.

8. Microwave Antenna Theory and Design, Samuel Silver, McGraw-Hill Book Company, Inc., 1949, page 406.

9. Antennas, J. D. Kraus, McGraw-Hill Book Company, Inc., 1950, The Diagram on page 177.

10. Tables of the Function $\int_0^x e^{\frac{\pi}{2}u^2} du$ and of the First Fresnel Integral, Staff of the Computation Laboratory of Harvard University, Harvard University Press, Cambridge, Mass., 1947.

11. Tables of the Fresnel Functions of the First Kind of Orders Zero and One Half Times Pi Over Two, (CCC, 1/2), Staff of the Computation Laboratory of Harvard University, Harvard University Press, Cambridge, Mass., 1947.

12. "Transmission between Circularly Polarized Antennas", V. H. Rumsey, Proceedings of the I. R. E., Vol. 39, No. 5, May, 1951, page 535.

13. Ondas en Varias Dimensiones, Mario Baro and J. R. Pedroarena, John Wiley and Sons, Inc., 1954., pages 401-409.

14. Introduction to Theoretical Physics, L. I. Schiff and H. H. Prum, McGraw-Hill Book Co., Inc., New York, 1937, Chapters 25 and 27.

15. Electromagnetic Waves, S. A. Schelkunoff, McGraw-Hill Book Co., Inc., New York, 1943, Chapter 8.

16. "Some Equivalence Theorems of Electromagnetics and their Applications to Radiation Problems", S. A. Schelkunoff, Bell System Technical Journal, Vol. 15, 1936, pages 92-112.

17. "Diffraction and Radiation of Electromagnetic Waves", S. A. Schelkunoff, Physics Review, Vol. 56, 1939, pages 308-316.

18. Notes on M.I.T. Course No. 6.622, "Antennas", as given by L. J. Chu.

19. "The Diffraction Theory of Electromagnetic Waves", J. A. Stratton and L. J. Chu, Physics Review, Vol. 56, 1939, pages 92-112.

20. Fields and Waves in Modern Radio, S. Ramo and J. R. Whinnery, John Wiley and Sons, New York, 1944, pages 442-457.

21. Electromagnetic Waves, S. A. Schelkunoff, Van Nostrand and Co., 1943, Chapter 8.

22. Principles and Applications of Wave Guide Transmission, George C. Southworth, Van Nostrand and Co., 1950, pages 404-415.

23. "Metal Horns as Directive Receivers of V.H.F. Waves", G. C. Southworth and A. P. King, Proceedings of the I. R. E., Vol. 27, Feb., 1939, pages 95-102.

24. "Radiation Characteristics of Conical Horn Antennas", A. P. King, Proceedings of the I. R. E., March, 1950, pages 249-251.

25. Electromagnetic Waves, S. A. Schelkunoff, Van Nostrand and Co., 1943, pages 360-365.

26. "An Experimental Investigation of the Radiation Patterns of Electromagnetic Horn Antennas", D. R. Rhodes, Proceedings of the I. R. E., Vol. 36, Sept., 1948, pages 1101-1105.

27. "Grating and Screens as Microwave Reflectors", W. D. Hayes, Radiation Laboratory Report No. 54-20, April 1, 1943.

28. A Treatise on the Theory of Bessel Functions, G. N. Watson, Cambridge, London, 1944. Section 2.22.

29. "Characteristics of Horn Feeds on Rectangular Waveguide", J. R. Risser, Radiation Laboratory Report No. 656, December, 1945.

30. Microwave Antenna Theory and Design, S. Silver, McGraw-Hill Book Co., Inc., First Edition, 1949, page 162.

31. Microwave Antenna Theory and Design, S. Silver, McGraw-Hill Book Co., Inc., First Edition, 1949, page 356.

16. "Some Considerations Pertaining to Electromagnetics and Their Application to Radiation Problems", R. E. Schelkunoff, Bell System Technical Journal, Vol. 25, 1946, pages 91-112.

17. "Field Equivalence Principle", S. A. Schelkunoff, Communication Theory, Vol. 36, 1947, pages 308-316.

18. [illegible] Vol. 6, [illegible] "Behavior" as given by L. J. Ryan.

19. "The Diffraction Theory of Electromagnetic Waves", J. A. Stratton and L. J. Chu, Journal of Applied Physics, Vol. 20, 1939, pages 89-133.

20. Fields and Waves in Modern Radio, S. Ramo and J. R. Whinnery, John Wiley and Sons, Inc., 1st Edition, 1944, pages 446-479.

21. Electromagnetic Waves, W. Kraus Crawford, Van Nostrand and Co., 1941, Chapter I.

22. Physics and Applications of Pure Oxide Cathodes, Duncan D. Cockerton, Van Nostrand and Co., 1950, pages 404-415.

23. "Measurements on Directive Receivers at V.H.F.", G. B. Fontenella and A. P. King, Proceedings of the I. R. E., Vol. 27, Feb., 1939, pages 93-104.

24. "Radiating Characteristics of Coupled Open Antennas", A. P. King, Proceedings of the I. R. E., March, 1939, pages 249-252.

25. Electromagnetic Waves, S. A. Schelkunoff, Van Nostrand and Co., 1943, pages 350-355.

26. "An Experimental Investigation of the Radiation Pattern of Microwave Horn Antennas", R. E. Beam, Proceedings of the I. R. E., Vol. 35, Sept., 1944, pages 1141-1165.

27. "Drawing and Forming of Nickel Parts", W. D. Doyle, Radiation Laboratory Report No. 54-48, April 1, 1943.

28. A Treatise on the Theory of Bessel Functions, G. N. Watson, Cambridge, London, 1944. Section 6.22.

29. "Characteristics of Horn Feeds in Paraboloid Antennas", S. W. Adams, Radiation Laboratory Report No. 939, December, 1945.

30. Microwave Antenna Theory and Design, S. Silver, McGraw-Hill Book Co., Inc., First Edition, 1949, page 108.

31. Microwave Antenna Theory and Design, S. Silver, McGraw-Hill Book Co., Inc., First Edition, 1949, page 390.

32. Microwave Antenna Theory and Design, S. Silver, McGraw-Hill Book Co., Inc., First Edition, 1949, page 353.

33. "The Design of Reflectionless Corners", N. Elson, ADRDE Research Report No. 129, January, 1942. Graph titled, "Tuning of a Rectangular Waveguide".

34. Microwave Antenna Theory and Design, S. Silver, McGraw-Hill Book Co., Inc., Section 16-5.

35. Antennas Theory and Practice, S. A. Schelkunoff and H. T. Friis, John Wiley and Sons, Inc., 1952, Section 16.7.

36. Microwave Antenna Theory and Design, S. Silver, McGraw-Hill Book Co., Inc. Section 10.10.

37. Characteristics of Horn Feeds on Rectangular Waveguides, J. R. Risser, R. L. Report 656, December, 1945. Figure 5, Appendix.

38. R. L. Report No. 41, Jan. 1945, Section 60 C.

39. Characteristics of Horn Feeds on Rectangular Waveguides, J. R. Risser, R. L. Report 656, December, 1945. Figure 4, Appendix.

40. Ibid., Section D.

[illegible]

[illegible]

[illegible]

[illegible]

[illegible]

[illegible]

[illegible]

[illegible]

[illegible]